Preparation and Applications of Fluoroalkyl End-Capped Vinyltrimethoxysilane Oligomer/Boric Acid Composites

Doctoral Course
Graduate School of Science and Technology
Hirosaki University

Doctoral Thesis

March 2019

Yuta Aomi

Contents

General Introduction

1. Organofluorine compounds

There has been an increasing interest in the applications of the fluorinated materials into a wide variety of fields, due to their exhibiting unique properties which cannot be achieved by the corresponding non-fluorinated ones. Such unique characteristics are in part ascribed in the physical properties related to fluorine in Table 1.[1 ~ 9)]

Table 1 Physical properties of hydrogen, fluorine and chlorine[1 ~ 9)]

Physical property	Element (X)			Ref.
	H	F	Cl	
van der Waals radius (pm)	120	147	175	4, 8
Electronegativity (Pauling)	2.20	3.98	3.16	3
Ionisation energy (kJ mol^{-1})	1312	1681	1251	7
Electron affinity (kJ mol^{-1})	74.0	332.6	348.5	7
Atom polarizability, α (10^{-24} cm^{-3})	0.667	0.557	2.18	2
Bond lengths of C-X (pm)	109	138	177	1
Bond energies of C-X (kJ mol^{-1})	410	484	323	1
Bond energies of C-X in CX_4 (kJ mol^{-1})	446	546	305	6
Bond energies of X-X (kJ mol^{-1})	434	157	242	9

Table 1 shows that the atomic radius of fluorine is the second smallest following hydrogen, owing to the strong interaction between the electron and nucleus.[1, 4, 7)] Small

atomic radius of fluorine can induce the short bond length and the least atom polarizability in the periodic table.[1, 2, 16] Electronegativity of fluorine has the greatest value among all elements, leading to the high ionization energy and electron affinity.[3, 7] Thus, fluorine has a very strong influence on inter- and intra-molecular forces. [5, 10 ~ 14] In fact, the acidity or basicity of organofluorine compounds is quite different from those of the corresponding non-fluorinated ones (see Table 2). [5, 10 ~ 14]

Table 2 The acidities of fluorinated organic and non-fluorinated compounds[10 ~ 14]

Carboxylic acid	pK_a	Alcohol	pK_a	Amine	pK_a
CH_3CO_2H	4.76[10]	CH_3CH_2OH	15.9[11]	$CH_3CH_2NH_2$	10.7[12]
CH_2FCO_2H	2.66[10]	CF_3CH_2OH	12.4[11]	$CF_3CH_2NH_2$	5.7[12]
CHF_2CO_2H	1.24[10]	$(CH_3)_3COH$	19.2[11]	$C_6H_5NH_2$	4.6[11]
CF_3CO_2H	0.23[10]	$(CF_3)_3COH$	5.1[11]	$C_6F_5NH_2$	-0.36[11]
Sulfamic acid	**pK_a**	**Aromatic acid**	**pK_a**		
$CH_3SO_2NH_2$	10.5[13]	$C_6H_5CO_2H$	4.21[14]	C_6H_5OH	10.0[14]
$CF_3SO_2NH_2$	5.8[13]	$C_6F_5CO_2H$	1.75[14]	C_6F_5OH	5.5[14]

Fluorine gas (F_2) is highly reactive due to the extremely weak F-F bond energy (F-F bond: 157 kJ mol^{-1}), providing the very strong bond formation with other atoms.[9, 15, 17] For example, the bond energy of carbon-fluorine (C-F; 484 kJ mol^{-1}) is stronger than that of the carbon-hydrogen (C-H; 410 kJ mol^{-1}) and the carbon-chlorine (C-Cl; 323 kJ mol^{-1}) as

shown in Table 1.[1, 5] Similarly, the strength of C-F bond in CF_4 (546 kJ mol^{-1}) is superior to that of C-H in CH_4 (446 kJ mol^{-1}) or C-Cl in CCl_4 (305 kJ mol^{-1}).[6] Such bond strength imparted by fluorine atom can supply a high thermal, oxidative and chemical stability toward the organofluorine compounds.[15, 17]

Table 3 Physicochemical properties of *n*-alkanes and perfluorinated alkanes[18 ~ 23]

Property	*n*-Alkane		Perfluorinated alkane	
	C_6H_{14}	C_9H_{20}	C_6F_{14}	C_9F_{20}
Boiling point (°C)	69[18]	157[19]	57[18]	117[19]
Critical temperature, T_c (°C)	235[18]	~310[21]	174[18]	~251[21]
Density, d^{25} (g cm^{-3})	0.655[18]	0.718*[20]	1.672[18]	1.799[20]
Viscosity, η^{25} (mPa·s)	0.29[18]	0.681[22]	0.66[18]	1.78[23]
Surface tension, γ^{25} (mN m^{-1})	17.9[18]	22.8*[19]	11.4[18]	14.4[20]
Refractive index, n_D^{25}	1.372[18]	1.40[19]	1.252[18]	1.28[19]
Dielectric constant, ε	1.89[18]	—	1.69[18]	—

* The value was measured at 20 °C

The introduction of fluorine atom into *n*-hexane can give rise to decrease the boiling point, surface tension, refractive index and dielectric constant. Such effect is due to the combination of the highest electronegativity and the smaller atomic radius derived from fluorine atoms.[18] It can be also observed the similar tendency toward the introduction of fluorine into *n*-nonane.[19 ~ 23]

Heretofore, organofluorine compounds have been applied into a wide variety of fields

such as organic dyes, surfactants, surface modifiers, membranes, conductive polymers, agrochemicals and medicinal chemicals.[12, 16] Because, oraganofluorine compounds can exhibit quite different characteristics such as thermal and chemical stability, low surface tension, low refractive index and low dielectric constant from those of the corresponding non-fluorinated ones.[1, 24, 25]

2. Fluoropolymers

It is well-known that fluoropolymers such as poly(tetrafluoroethylene) [PTFE], poly(vinylidene fluoride) [PVDF], perfluoroethylene-perfluorovinylether copolymer [PFA], and perfluoroethylene-propylene copolymer [FEP] provide high thermal stability, excellent chemical resistance, good mechanical properties, water- and oil-repellency, low flammability and low refractive index, which cannot be achieved by the corresponding non-fluorinated ones.[1, 26 ~ 35] However, these fluoropolymers, in general, give a poor solubility toward organic solvents, affording some difficulties for additional applications in numerous fields.[29, 34, 35] In contrast, perfluoroalkylated (meth)acrylate polymers, of whose fluoroalkyl groups are randomly introduced through the ester or amide bonds on the polymeric side chain (see Figure 1), can exhibit not only the higher solubility toward the organic media including water, but also the higher surface active characteristic than that of

the corresponding non-fluorinated ones. However, the surface active characteristic of the block-type (meth)acrylate copolymers containing longer perfluoroalkyl chains (see Figure 1) is superior to that of the corresponding randomly perfluoroalkylaed ones. Because, the block-type perfluoroalkylated copolymers are likely to form the self-assembled polymeric aggregates like micelle in the aqueous and organic media.[36 ~ 41)]

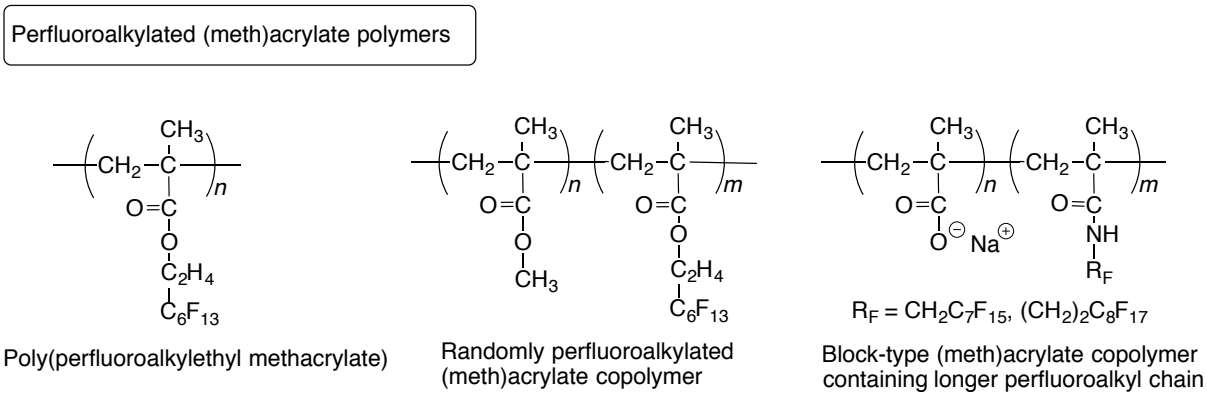

Figure 1 Chemical structure of perfluoroalkylated (meth)acrylate polymers[36 ~ 41)]

These perfluoroalkylated copolymers are in general unstable under acidic or alkaline conditions since the perfluoroalkyl segments are introduced into polymeric main chain through the ester or amide bonds, suffering the hydrolysis to produce the fluorinated alcohols due to the strong electronegativity of fluorine[42)] (see Scheme 1).

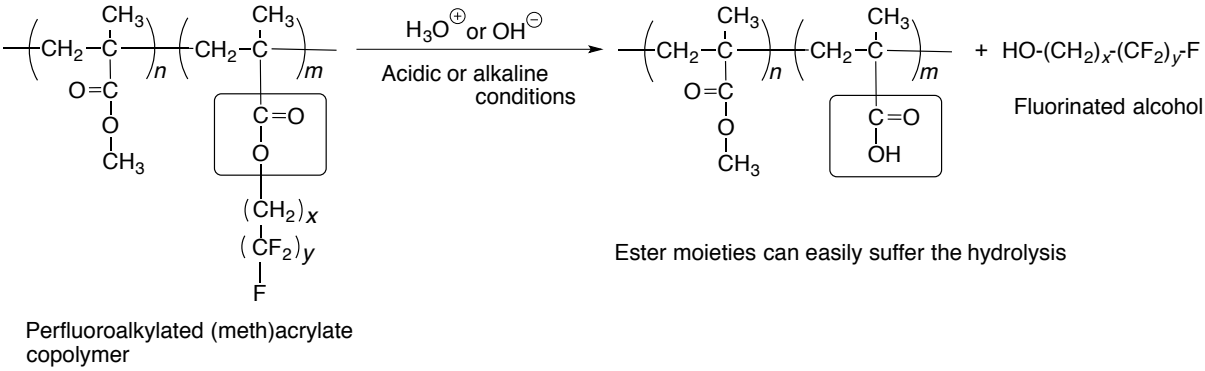

Scheme 1 The hydrolysis of perfluoroalkylated (meth)acrylate copolymer under acidic or alkaline conditions

Therefore, it is of considerable importance to develop the synthetic methods on the introduction of longer perfluoroalkyl segments into polymeric main chain through the carbon-carbon bond formation. From the developmental viewpoint of partially fluoroalkylated polymers through the carbon-carbon bond formation, two fluoroalkyl end-capped oligomers [R_F-$(M)_n$-R_F; R_F = fluoroalkyl groups; M = radical polymerizable monomers], of whose fluoroalkyl segments are directly introduced into polymeric end-sites through the carbon-carbon bond formation, are attractive fluorinated polymeric materials.[42 ~ 45] In fact, two fluoroalkyl end-capped acrylic acid oligomers have been already synthesized by radical oligomerization of acrylic acid monomer using fluoroalkanoyl peroxide as a key intermediate via primary radical termination or radical chain transfer to the peroxides as shown in Scheme 2.[42, 46]

i) Thermal decomposition of fluoroalkanoyl peroxide to produce fluoroalkyl radical

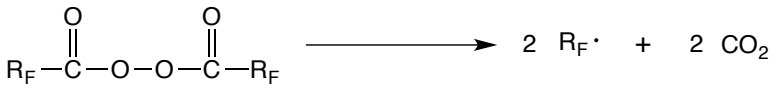

R_F = fluoroalkyl radical

ii) Addition of fluoroalkyl radical to monomer

Acrylic acid monomer

iii) Propagation

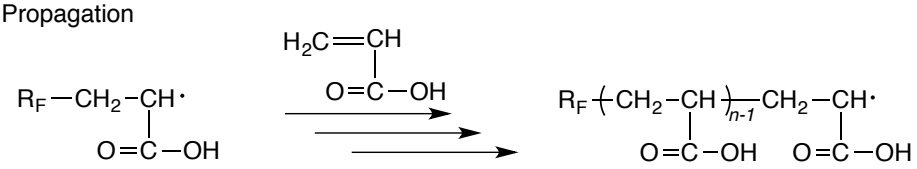

iv) Primary radical termination or radical chain transfer to the peroxide

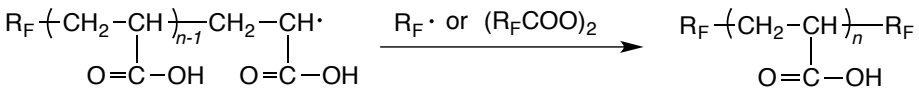

Scheme 2 Synthesis of two fluoroalkyl end-capped acrylic acid oligomer[42, 46)]

These fluoroalkyl end-capped oligomers can exhibit a variety of unique properties such as higher solubility toward aqueous and traditional organic media, excellent surface active properties imparted by two fluoroalkyl groups and nanometer size-controlled molecular aggregates with the aggregation of terminal fluoroalkyl segments in oligomers, quite different from that of the corresponding non-fluorinated polymers or randomly fluoroalkylated polymers.[42 ~ 45)] Therefore, it is of particular interest to develop new fluorinated functional materials by using fluoroalkyl end-capped oligomers.

In fact, it has been already reported that two fluoroalkyl end-capped oligomers can form

the nanometer size-controlled oligomeric aggregates in aqueous and organic media, and these fluorinated aggregates can interact with organic dyes and inorganic fine particles as guest molecules to provide the fluorinated oligomeric aggregates/guest molecules nanocomposites[42, 47] as shown in the following Schematic illustration (see Figure 2).

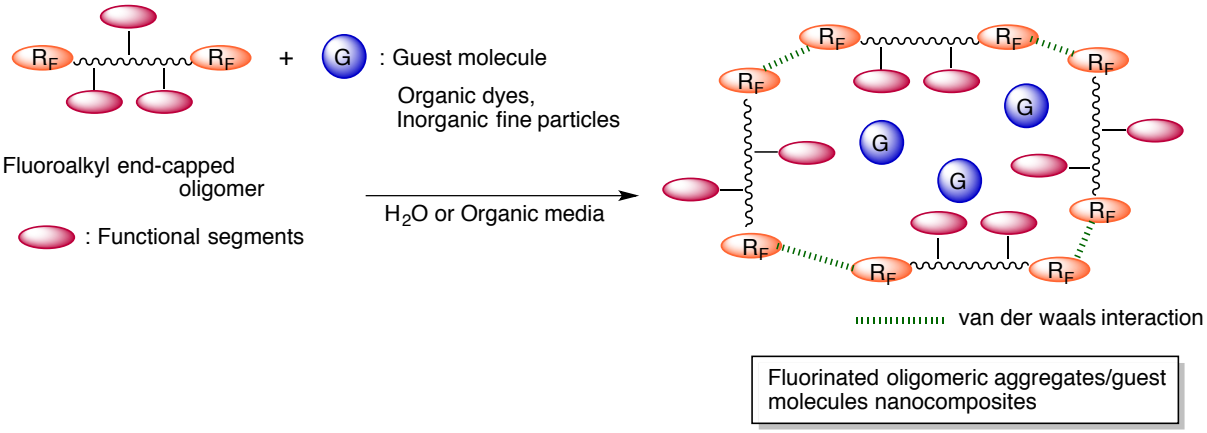

Figure 2 Schematic illustration for the interaction of self-assembled fluoroalkyl end-capped oligomer with guest molecules[42, 47]

These obtained nanocomposites can give not only the surface active characteristic imparted by longer fluoroalkyl groups in oligomers but also the unique properties related to the guest moleculese.[32, 42] In fact, fluoroalkyl end-capped oligomers have been applied to the nanocomposite reactions with silica nanoparticles to afford the corresponding fluorinated oligomer/silica nanocomposite.[42] For example, fluoroalkyl end-capped *N*-(1,1-dimethyl-3-oxobutyl)acrylamide oligomer/silica nanocomposites [R_F-(DOBAA)$_n$-R_F/SiO_2] can be prepared by the sol-gel reactions of tetraethoxysilane in

the presence of the corresponding oligomer under alkaline conditions (see Scheme 3).[48, 49)] The R_F-(DOBAA)$_n$-R_F/SiO_2 nanocomposite thus obtained can supply no weight loss behavior in proportion to the contents of oligomer in the composites even after calcination at 800°C.[48, 49)] Such no weight loss characteristic is due to the formation of ammonium hexafluorosilicate during the nanocomposite reaction, although the PTFE/SiO_2 hybrids provide a clear weight loss corresponding to the contents of PTFE at around 700 °C.[49, 50)]

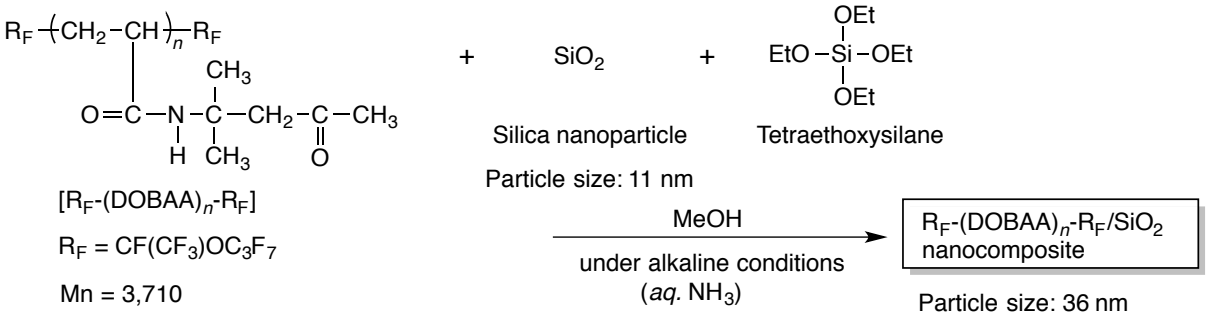

Scheme 3 Preparation of R_F-(DOBAA)$_n$-R_F/SiO_2 nanocomposite[48, 49)]

Thus, it is of particular importance to fabricate the fluorinated nanocomposite materials by using fluoroalkyl end-capped oligomers from the developmental viewpoint of new fluorinated functional materials. In a variety of two fluoroalky end-capped oligomers, especially, two fluoroalkyl end-capped vinyltrimethoxysilane oligomer [R_F-($CH_2CHSi(OMe)_3$)$_n$-R_F; R_F =$CF(CF_3)OC_3F_7$, n = 2, 3] has high potential for the exploration of new fluorinated oligomeric nanocomposites, because this oligomer possesses

not only two flkuoroalkyl end groups but also some trimethoxysilyl segments on the oligomeric side chain.[51] Therefore, this fluorinated oligomer can undergo the sol-gel reactions under alkaline conditions to produce the fluoroalkyl end-capped vinyltrimethoxysilane oligomeric silica nanoparticles [R_F-(CH_2CH-SiO_2)$_n$-R_F], affording the nanometer size-controlled self-assembled molecular aggregates with the aggregation of terminal fluoroalkyl segments as shown in the following Schematic illustration (see Scheme 4).[42, 52]

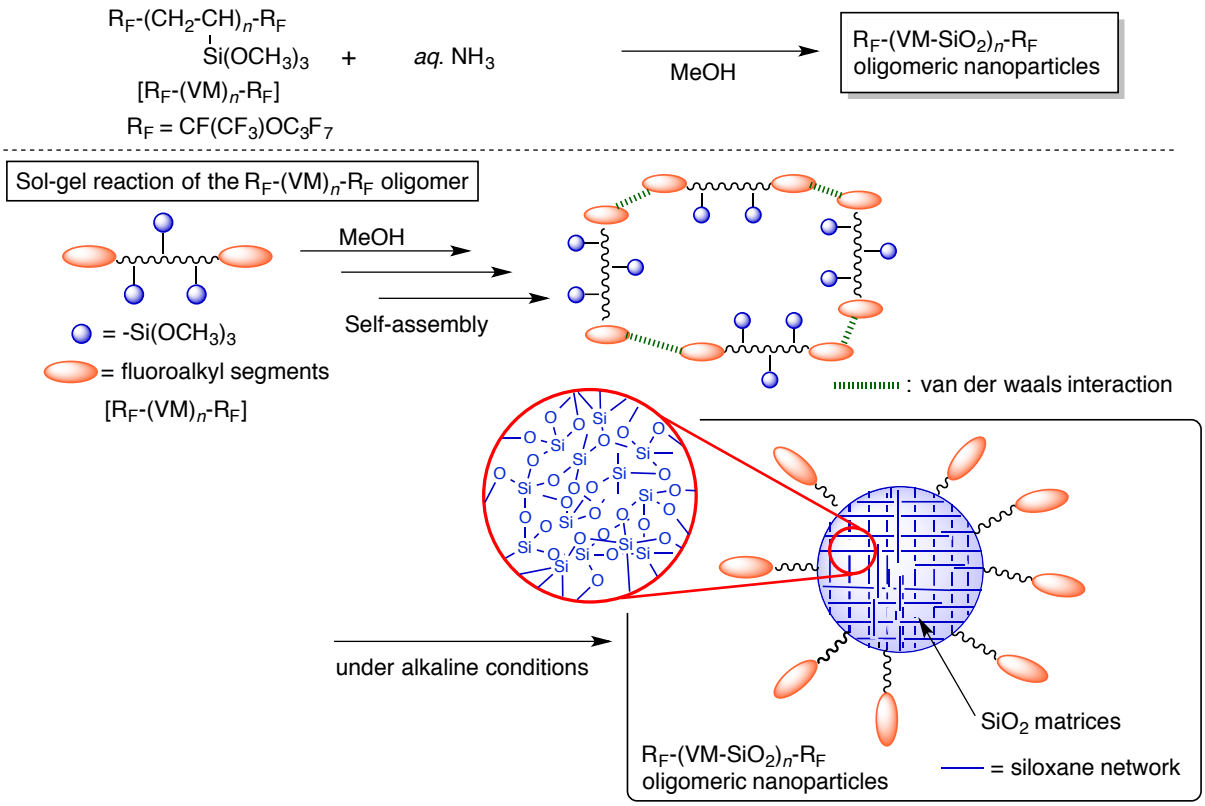

Scheme 4 Preparation of fluoroalkyl end-capped vinyltrimethoxysilane oligomeric silica nanoparticles[42, 52]

Thus, a variety of organic and inorganic guest molecules can be effectively encapsulated into the self-assembled molecular aggregate cores to afford the corresponding fluorinated oligomeric silica/guest molecules nanocomposites through the sol-gel reaction under alkaline conditions.[42] For example, low molecular weight aromatic compounds such as 1,1'-bi-2-naphthol (BINOL) can be effectively encapsulated into the fluorinated vinyltrimethoxysilane oligomeric silica nanoparticle cores to provide the R_F-(VM-SiO_2)$_n$-R_F/BINOL nanocomposites through the sol-gel reaction under alkaline conditions as shown in Scheme 5.[52] Interestingly, the obtained nanocomposites can provide no weight loss behavior corresponding to the contents of BINOL even after calcination at 800 °C.[53]

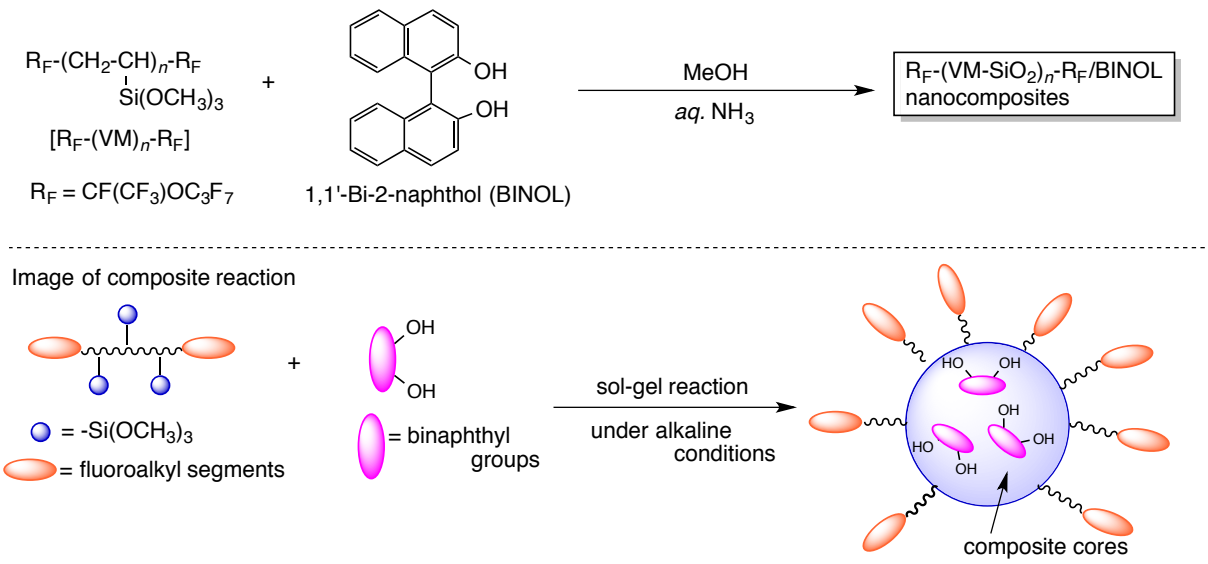

Scheme 5 Preparation of R_F-(VM-SiO_2)$_n$-R_F/BINOL nanocomposites[53]

Furthermore, fluoroalkyl end-capped vinyltrimethoxysilane oligomer has been applied to the encapsulation of not only low molecular weight aromatic compounds but also inorganic particles such as titanium oxide, talc and magnesium carbonate to afford the corresponding fluorinated oligomeric silica/inorganic nanocomposites.[54 ~ 56)] Theses nanocomposites can give the unique surface wettability such as a superhydrophobic characteristic (water contact angle value: 180°) derived from the synergistic effect of end-capped fluoroalkyl units in oligomer and encapsulated inorganic particles.[42, 54 ~ 56)]

In this way, the fluoroalkyl end-capped vinyltrimethoxysilane oligomer will have high potential for a promising material from the developmental viewpoint of new fluorinated nanocomposite materials possessing not only unique surface wettability but also the extremely higher thermal stability.

3. Development of organic/boron hybrid materials

In general, the boron compounds can be classified according to their structures into the following groups: (1) borane, (2) borinic acid, (3) boronic acid, (4) boric acid, (5) boroxine, and (6) the ester (borinic ester, boronic ester or borate ester) (see Figure 3).[57)]

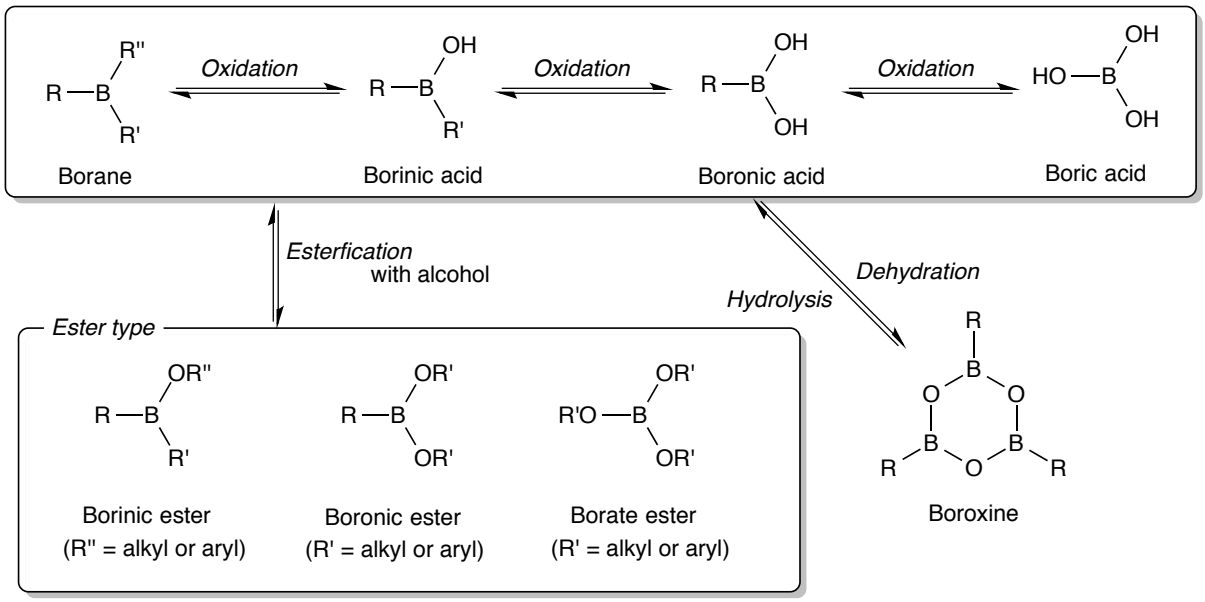

Figure 3 A variety of boron compounds[57)]

In these boron compounds, organoboron compounds, which are derived from the inorganic boric acid, have been widely used as a key intermediate for the organic synthesis.[58)] In contrast, inorganic boric acid is the most widely used in numerous fields, because it is cheaply and readily available.[58)]

Boron has several unique structural and electrical properties: (1) boron compounds, in general, orient to a trigonal planar geometry; (2) boron compounds have high Lewis acidity due to the presence of a vacant p-orbital, of whose orbital is low-energy state and is orthogonal to three substitutes; (3) the vacant p-orbital can interact effectively with π-conjugated compounds.[57, 59, 60)] These unique properties related to boron enables the boron compounds to apply into a variety of fields such as catalyst, cross-coupling reagents,

receptors and sensors for saccharides, biological and medicinal applications, electronic materials, flame retardants and fluorescence sensors.[57, 59, 61 ~ 63] From this point of view, there have been hitherto numerous studies on the preparation of organic/boron hybrid materials by using inorganic boric acid as boron source (see Table 4[64 ~ 69]). The higher thermal stability and good mechanical properties of the boron-containing hybrid materials are due to the strong bond energy related to boron.[68] For example, the bond energy of boron-oxygen (B-O; 514 kJ mol^{-1}) is superior to that of carbon-oxygen (C-O; 358 kJ mol^{-1}) or silicon-oxygen (Si-O; 451 kJ mol^{-1}).[68, 70]

Table 4 Examples of boron-containing hybrid materials using boric acid as boron source[64 ~ 69]

Boron-containig hybrid	Organic compounds	Properties	Ref.
Boron/Fluorine/Silicon hybrid coating	Acrylate resins*	Good thermal stability, mechanical property and hydrophobicity	64
Boron/Silicon hybrid coating	Acrylate resins*	Good thermal stability, mechanical property and high transparency	65
Poly(vinyl alcohol)/boric acid hybrid film	Poly(vinyl alcohol)	Good thermal stability and barrier property	66
Flame retardant polypropylene -containing poly(borosiloxane)	Polypropylene	Good flame retardant effect	67
Boron-doped silicone resin	Silicone resin**	Good thermal stability	68
Wool fabric/boron/silica sol hybrid	Wool fabric	Good flame retardant effect and thermal stability	69

* Acrylate resins contain several kinds of resin possessing different functional groups.

** Silicone resin is composed of oraganic and inornic moieties.

In this way, there have been numerous reports on the preparations of the organic molecules/inorganic hybrid materials containing boron units. However, studies on the preparation of organic molecules/inorganic boron hybrids possessing longer perfluoroalkyl groups have been very limited so far, although such studies are of considerable importance from the developmental viewpoint of new fluorinated functional materials.

As indicated above, fluoroalkyl end-capped vinyltrimethoxysilane oligomer [R_F-$(VM)_n$-R_F], of whose oligomer possesses some trimethoxysilyl groups on the side chain, can form the self-assembled molecular aggregates with the aggregation of terminal fluoroalkyl segments. 1, 1'-Bi-2-naphthol (BINOL) can be effectively encapsulated as guest molecule into such molecular aggregates through the sol-gel reaction under alkaline conditions, affording the fluorinated oligomeric silica/BINOL nanocomposites [R_F-$(VM\text{-}SiO_2)_n$-R_F/BINOL].[42, 53] The encapsulated BINOL into the R_F-$(VM\text{-}SiO_2)_n$-R_F oligomeric nanocomposite cores can exhibit the nonflammable characteristic even after calcination at 800 °C through the formation of rigid silica gel matrices and ammonium hexafluorosilicate during the sol-gel process.[53] Especially, the ammonium hexafluorosilicate would be easily formed through the dehydrofluorination between the fluorine in oligomer and acidic proton in BINOL catalyzed by ammonia in the presence of silica nanoparticles as co-catalyst.[53] The obtained hydrogen fluoride should react with

silica nanoparticles to afford SiF_4, finally ammonium hexafluorosilicate, due to the strong bond energy between silicon and fluorine (Si-F bond energy is 540 kJ mol^{-1}), its value being higher than C-F bond energy: 484 kJ mol^{-1}. [1, 53, 71] On the other hand, boron – fluorine bond energy is much stronger (B-F bonds; 757 kJ mol^{-1}) than that (540 kJ mol^{-1}) of Si-F bond energy.[71, 72] This higher bond energy would enable the fluoroalkyl end-capped oligomer/boron nanocomposite to create the numerous unique properties including the extremely higher thermal stability than that of the fluorinated oligomer/silica nanocomposites.

4. **Thesis outline**

In this study, preparation and properties of the fluoroalkyl end-capped vinyltrimethoxysilane oligomeric silica/boric acid nanocomposites – encapsulated a variety of organic molecules such as low molecular weight compounds and thermoplastic elastomers will be described.

In chapter 1, preparation of fluoroalkyl end-capped vinyltrimethoxysilane oligomer/silica/boric acid nanocomposites is described. In addition, the preparation and thermal stability of the fluoroalkyl end-capped vinyltrimethoxysilane oligomer/silica/boric acid nanocomposite – encapsulated low molecular weight organic compounds are also

described (see Scheme 6).

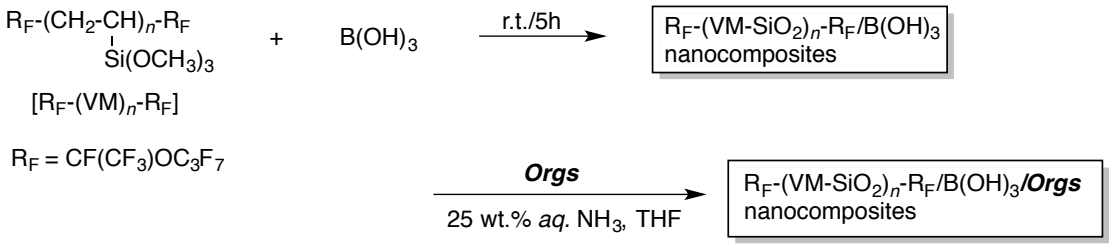

Orgs: diphenylsilanediol (DPSDO), 1, 1'-bi-2-naphthol, 4, 4'-biphenol, bisphenol A (BPA), bisphenol F (BPF), bisphenol AF (BPAF), biphenyl, dibenzyl, and pentaerythritol (PETERL)

Scheme 6 Preparation of R_F-$(VM$-$SiO_2)_n$-$R_F/B(OH)_3$ and R_F-$(VM$-$SiO_2)_n$-$R_F/B(OH)_3$/***Orgs*** nanocomposites

In chapter 2, preparation and thermal stability of fluoroalkyl end-capped vinyltrimethoxysilane oligomeric silica/boric acid nanocomposites – encapsulated a variety of thermoplastic elastomers are described (see Scheme 7).

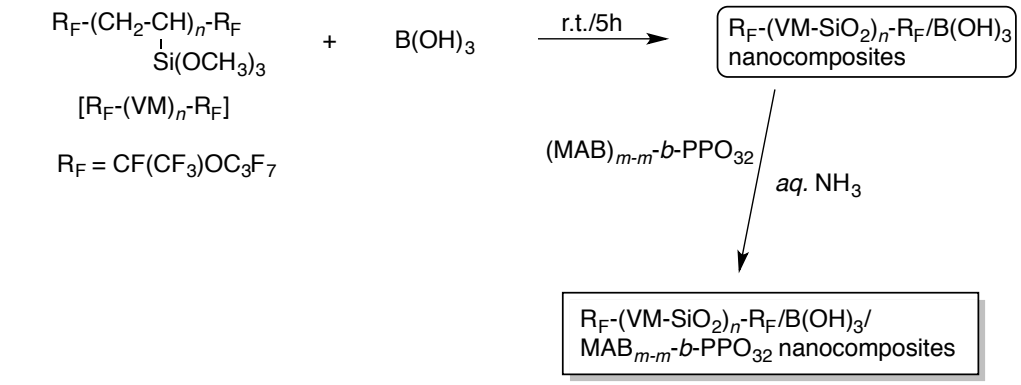

Thermoplastic elastomers

$(MAB)_{m\text{-}m}$-b-PPO_{32}

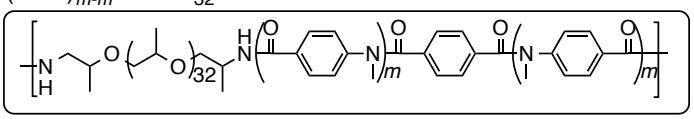

Scheme 7 Preparation of R_F-$(VM$-$SiO_2)_n$-$R_F/B(OH)_3$/thermoplastic elastomers nanocomposites

In chapter 3, preparation of fluoroalkyl end-capped vinyltrimethoxysilane oligomeric silica/boric acid/poly(vinyl alcohol) [PVA] composite films is described (see Scheme 8). In this chapter, the water-resistance ability and thermal stability of the modified PVA film are also described.

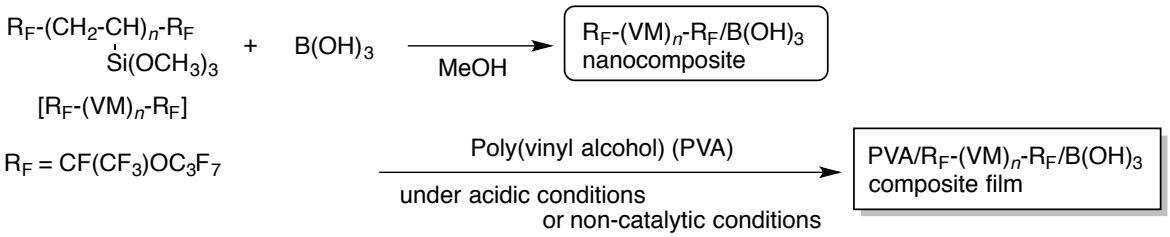

Scheme 8 Preparation of PVA/R_F-(VM)$_n$-R_F/$B(OH)_3$ composite film under non-catalytic or acidic conditions

References

1) P. Kirch, *Modern Fluorooganic Chemistry*, Wiley-VCH, Weinheim, Germany (2004).

2) J. K. Nagel, *J. Am. Chem. Soc.*, **112**, 4740 (1990).

3) K. D. Sen and C. K. Jorgensen, *Electronegativity*, Splinger, New York (1987).

4) A. Bond, *J. Phys. Chem*., **68**, 441 (1964).

5) R. D. Chambers, *Fluorine in Organic Chemistry*, Blackwoll Publishing, Oxford (2000).

6) B. E. Smart, J. F. Liebman, and A. Greenberg (Eds.), *Fluorinated Organic Chemistry*, VCH Publishers, Deerfield Beach (1986).

7) R. E. Banks, B. E. Smart, and J. C. Tallow, *Organofluorine Chemistry: Principles and Commercial Applications*, Plenum, New York (1994).

8) K. Takano and Y. Hashimoto, *DIC Technical Review*, **7**, 13 (2001).

9) N. N. Greenwood and A. Earnshaw, *Chemistry of the Elements*, Pergamon, Oxford (1989).

10) W. K. Hagmann, *J. Med. Chem,*, **51**, 4359 (2008).

11) S. Purser, P. R. Moore, S. Swallow, and V. Gouverneur, *Chem. Soc. Rev.*, **37**, 320 (2008).

12) M. Morgenthaler, E. Schweizer, A. Hoffmann-Roder, F. Benini, R. E. Martin,

G. Jaeschke, B. Wagner, H. Fischer, S. Bendels, D. Zimmerli, J. Schneider, F. Diederich, M. Kansy and K. Muller, *ChemMedChem*, **2**, 1100 (2007).

13) N. V. Grishin, A. L. Osterman, H. B. Brooks, M. A. Phillips, and E. J. Goldsmith, *Biochemistry*, **38**, 15174 (1999).

14) B. E. Smart, *J. Fluorine Chem.*, **109**, 3 (2001).

15) M. G. Campbell and T. Ritter, *Chem. Rev.*, **115**, 612 (2015).

16) R. Berger, G. Resnati, P. Metrangolo, E. Weber, and J. Hulliger, *Chem. Soc, Rev.*, **40**, 3496 (2011).

17) W. R. Dolbier Jr., *J. Fluorine Chem.*, **126**, 157 (2005).

18) M. P. Krafft and J. G. Riess, *Chem. Rev.*, **109**, 1714 (2009).

19) P. L. Nostro, *Adv. Colloid Interface Sci.*, **56**, 245 (1995).

20) T. Sakka and Y. H. Ogata, *J. Fluorine Chem.*, **126**, 371 (2005).

21) V. Vandana, D. J. Rosenthal, and A. S. Teja, *Fluid Phase Equilibria,* **99**, 209 (1994).

22) H. Chi, G. Li, Y. Guo, L. Xu, and W. Fang, *J. Chem. Eng. Data,* **58**, 2224 (2013).

23) M. G. Freire, A. G. M. Ferreira, I. M. A. Fonseca, I. M. Marrucho, and J. A. P. Coutinho, *J. Chem. Eng. Data,* **53**, 538 (2008).

24) T. Imae, *Curr. Opin. Colloid Interface Sci.*, **8**, 307 (2013).

25) S. Ando, T. Matsuura, and S. Sasaki, *Macromolecules*, **25**, 5858 (1992).

26) K. E. Perepelkin, *Fiber Chem.*, **36**, 43 (2004).

27) P. Graham, M. Stone, A. Thorpe, T. G. Nevell, and J. Tsibouklis, *J. Fluorine Chem.*, **104**, 29 (2000).

28) N. M. L. Hansen, K. Jankova, and S. Hvilsted, *Euro. Polym. J.*, **43**, 255 (2007).

29) J. S. Forsythe and D. J. T. Hill, *Prog. Polym. Sci.*, **25**, 101 (2000).

30) S. Lee, J. -S. Park, and T. R. Lee, *Langmuir*, **24**, 4817 (2008).

31) B. Ameduri and H. Sawada (Eds.), *Fluorinated polymers: Volume 1, "Synthesis. Properties, Processing and Simulation"*, Cambridge, RSC, UK (2016).

32) B. Ameduri and H. Sawada (Eds.), *Fluorinated polymers: Volume 2, "Application"*, Cambridge, RSC, UK (2016).

33) K. Johns and G. Stead, *J. Fluorine Chem*., **104**, 5 (2000).

34) J. Gardiner, *Aust. J. Chem.*, **68**, 13 (2015).

35) B. Ameduri, *Chem. Rev.*, **109**, 6632 (2009).

36) B. Jiang, L. Zhang, B. Liao, and H. Pang, *Polymer*, **55**, 5350 (2014).

37) K. Tadano, Y. Tanaka, T. Shimizu, and S. Yano, *Macromolecules*, **32**, 1651 (1999).

38) I. J. Park, S. -B. Lee, and C. K. Choi, *Macromolecules*, **31**, 7555 (1998).

39) M. Krupers and M. Moiler, *Macromol. Chem. Phys.*, **198**, 2163 (1997).

40) T. Imae, H. Tabuchi, K. Funayama, A. Sato, T. Nakamura, and N. Amaya, *Colloids*

Surf., A, **167**, 73 (2000).

41) J. -F. Berret, D. Calvet, A Collet and M. Viguier, *Curr. Opin. Colloid Interface Sci.*, **8**, 296 (2003).

42) H. Sawada, *Polym. Chem.*, **3**, 46 (2012).

43) H. Sawada, *Chem. Rev.*, **96**, 1779 (1996).

44) H. Sawada, *J. Fluorine Chem.*, **105**, 219 (2000).

45) H. Sawada, *Polym. J.*, **39**, 637 (2007).

46) H. Sawada, Y. -F. Gong, Y. Minoshima, T. Matsumoto, M. Nakayama, M. Kosugi, and T. Migita, *J. Chem. Soc., Chem. Commun.*, 537 (1992).

47) H. Sawada, K. Ikeno, and T. Kawase, *Macromolecules*, **35**, 4306 (2002).

48) H. Sawada, T. Narumi, S. Kodama, M. Kamijo, R. Ebara, M. Sugiya, and Y. Iwasaki, *Colloid Polym. Sci.*, **285**, 977 (2007).

49) H. Sawada, T. Tashima, H. Kakehi, T. Nishiyama, M. Kikuchi, M. Miura, Y. Sato, and N. Isu, *Polym. J.*, **42**, 167 (2010).

50) Y. -C. Chen, C. -C. Tsai, and Y. -D. Lee, *J. Polym. Sci., Part A: Polym. Chem.*, **42**, 1789 (2004).

51) T. Kawase, T. Fuji, M. Minagawa, H. Sawada, T. Matsumoto, and M. Nakayama, *J. Adhision Sci. Technol.*, **10**, 1031 (1996)

52) H. Sawada, T. Suzuki, H. Takashima, and K. Takishita, *Colloid Polym. Sci.*,**286**, 1569 (2008).

53) H. Sawada, Y. Matsuki, Y. Goto, S. Kodama, M. Sugiya, and Y. Nishiyama, *Bull Chem. Soc. Jpn*., **83**, 75 (2010).

54) S. Guo, H. Yoshioka, H. Kakehi, Y. Kato, M. Miura, N. Isu, B. Ameduri, and H. Sawada, *J. Colloid Interface Sci.,* **387**, 141 (2012).

55) Y. Oikawa, T. Saito, S. Yamada, M. Sugiya, and H. Sawada, *ACS Appl. Mater. Interfaces.*, **7**, 13782 (2015).

56) Y. Oikawa, T. Saito, S. Idomukai, T. Tanaka, M. Nishida, and H. Sawada, *J. Fluorine Chem.*, **177**, 70 (2015).

57) D. G. Hall (Eds), *Boronic Acids: Preparation, Applications in Organic Synthesis Medicine*, Wiley-VCH, Weinheim, Germany (2005).

58) R. K. Mylavarapu, K. GCM, N. Kolla, R. Veeramalla, P. Koilkonda, A. Bhattacharya, and R. Bandichhor, *Org. Process Res. Dev.*, **11**, 1065 (2007).

59) A. Wakamiya and S. Yamaguchi, *Bull. Chem. Soc. Jpn.*, **88**, 1357 (2015).

60) F. Jakle, *Cood. Chem. Rev.*, **250**, 1107 (2006).

61) Y. Zhu and N. S. Hosmane, *Cood. Chem. Rev.*, **293**, 357 (2015).

62) W. L. A. Brooks and B. S. Sumerlin, *Chem. Rev.*, **116**, 1375 (2016).

63) D. Roy, J. N. Cambre, and B. S. Sumerlin, *Chem. Commun.*, 2477 (2008).

64) B. Zeytuncu, M. V. Kahraman, and O. Yucel, *J. Vinyl Add. Technol.*, **19**, 39 (2013).

65) Y. Mulazim, M. V. Kahraman, N. K. Apohan, S. Kızıltaş, and A. Guong, *J. Appl. Polym. Sci.*, **120**, 2112 (2011).

66) M. Lim, H. Kwon, D. Kim, J. Seo, H. Han, and S. B. Khan, *Prog. Org. Coat.*, **85**, 68 (2015).

67) X. Lai, X. Zeng, H. Li, and H. Zhang, *J. Macromol. Sci. Part B: Phys.*, **53**, 721 (2014).

68) Z. Hao, J. Zhang, Y. Wu, J. Yu, and L. Yu, *J. Appl. Polym. Sci.*, 40934 (2014).

69) Q. Zhang, W. Zhang, J. Huang, Y. Lai, T. Xing, G. Chen, W. Jin, H. Liu, and B. Sun, *Mater. Des.*, **85**, 796 (2015).

70) T. Oh and C. K. Choi, *J. Kor. Phys. Soc.*, **56**, 1150 (2010).

71) R. Walsh, *Acc. Chem. Res.*, **14**, 246 (1981).

72) W. J. Zhang, C. Y. Chan, X. M. Meng, M. K. Fung, I. Bello, Y. Lifshitz, S. T. Lee, and X. Jiang, *Angew. Chem. Int. Ed.*, **44**, 4749 (2005).

CHAPTER 1

Preparation and Thermal Stability of Fluoroalkyl End-Capped Vinyltrimethoxysilane Oligomeric Silica/Boric Acid Nanocomposites - Encapsulated a Variety of Low Molecular Weight Organic Compounds

1.1. Introduction

It is well-known that boric acid is a useful precursor for the preparation of poly(borosiloxanes).[1, 2] For example, the condensation reaction of boric acid with diphenylsilanediol can proceed in *n*-butylether at 300 °C to afford the poly(borodiphenylsiloxane),[3 ~ 6] and these poly(organo-borosiloxanes) are considered to be a cheaply and accessible starting material for ceramics such as boron and silicon oxycarbide (SiBCO) glass fibers.[7] Therefore, the exploration of a variety of the preceramic poly(borosiloxanes) is of particular interest from the developmental viewpoints of novel SiBCO ceramics.[8 ~ 16] Borosilicate glass can exhibit high tolerance to chemicals and solvents, combined with excellent mechanical and thermal stability.[17, 18] Thus, the development of the borosilicate nanoparticles should play an important role in the material science as well as silica nanoparticles. In general, silica nanoparticles can be easily prepared by the traditional Stöber method by the base-catalyzed hydrolytic polycondensation of tetraethoxysilane.[19] However, the formation of borosilicate nanoparticles has not been hitherto achieved due to the high reactivity of boron precursors for water and catalysts in the Stöber method except for the preparation of borosilicate nanoparticles by the sol-gel reaction of

tetraethoxysilane in the presence of trimethoxy boroxine catalyzed by formic acid in dichloromethane and 2-propanol.[20] Hitherto, numerous fluoroalkyl end-capped oligomers [R_F-$(M)_n$-R_F; R_F = fluoroalkyl group, M = radical polymerizable monomers] have been prepared by using a fluoroalkanoyl peroxide [R_F-C(=O)-OO-(O=)C-R_F] as a key intermediate, and their properties have been also studied in detail.[21 ~ 24] For example, fluoroalkyl end-capped cooligomers containing adamantly segments can form the nanometer size-controlled oligomeric nanoparticles,[25] and fullerene and gold nanoparticles can be effectively encapsulated into these nanoparticle cores to provide the corresponding fluorinated cooligomeric nanocomposites - encapsulated these guest molecules, respectively.[26, 27] In this way, it is of particular interest to study on the new fluorinated oligomeric silica/boron nanocomposites, from the developmental view points of new fluorinated functional materials possessing the borosiloxane units. This chapter shows that fluoroalkyl end-capped vinyltrimethoxysilane oligomeric silica/boric acid nanocomposites can be easily prepared by reaction of the corresponding oligomer with boric acid at room temperature. The obtained nanocomposites were also applied to the encapsulation of a variety of guest molecules such as diphenylsilanediol, 1, 1'-bi-2-naphthol, 4, 4'-biphenol, bisphenol A,

bisphenol F, bisphenol AF, biphenyl, dibenzyl, and pentaerythritol into these nanocomposite cores to provide the corresponding fluorinated oligomeric silica/boric acid nanocomposites - encapsulated these guest molecules. Interestingly, these encapsulated nanocomposites thus obtained were found to exhibit no weight loss behavior corresponding to the contents of these guest molecules even after calcination at 800 °C, although the nanocomposites were isolated through no purification process. These results will be described in this chapter.

1.2. Experimental

1.2.1 Measurements

Solid-state ^{11}B NMR spectra were measured on a Varian 600 NMR system spectrometer system spectrometer (Palo Alto, CA) operated at 192.48 MHz for the ^{11}B nuclei with a Varian 3.2 mm Varian $^{1}H/^{31}P$-$^{13}C/^{13}C$-^{15}N BioMASTM probe spun at 15 kHz, and a Varian 400 NMR system spectrometer (Palo Alto, CA) operated at 100.56 MHz for the ^{13}C nuclei with a Varian 4 mm double-resonance T3 solid probe spun at 15 kHz, respectively. Solid-state ^{1}H NMR spectra were measured on a Varian 400 NMR system spectrometer (Palo Alto, CA) operated at 399.88 MHz for the ^{1}H nuclei with a Varian 4 mm double-resonance T3 solid probe spun at 15 kHz. Fourier-transform infrared (FT-IR) spectra were measured with a FT-IR spectrophotometer (FTIR-8400, Shimadzu, Japan). Thermal analyses were recorded by raising the temperature around 800 °C (the heating rate: 10 °C/min) under atmospheric conditions by the use of Bruker axs TG-DTA2000SA differential thermobalance (Kanagawa, Japan). Size [number-average diameter (average hydrodynamic diameter)]

of nanocomposites was measured by using Otsuka Electronics DLS-7000 HL (Tokyo, Japan). Field emission scanning electron micrographs (FE-SEM) were recorded by means of JEOL JSM-7000F (Tokyo, Japan). X-ray diffraction (XRD) measurements were performed by the use of Mac Science M18XHF-SRA (Tokyo, Japan).

1.2.2. Materials

Bisphenol AF (BPAF), diphenylsilanediol (DPSDO), bisphenol A (BPA), bisphenol F (BPF), biphenol, 1, 1'-bi-2-naphthol (BINOL), 4, 4'-biphenol, dibenzyl, biphenyl and pentaerythritol (PETERL) were purchased from Tokyo Kasei Kogyo (Tokyo, Japan). Boric acid and biphenyl were purchased from Wako Pure Chemical Industries (Osaka Japan). Vinyltrimethoxysilane was used as received from Dow Corning Toray (Tokyo, Japan). Fluoroalkyl end-capped vinyltrimethoxysilane oligomer [R_F-(CH_2-$CHSi(OMe)_3)_n$-R_F: the mixture of dimer and trimer; R_F = $CF(CF_3)OC_3F_7$] was synthesized by reaction of fluoroalkanoyl peroxide with the corresponding monomer according to the previously reported method.[28)]

1.2.3. Preparation of fluoroalkyl end-capped vinyltrimethoxsilane oligomeric silica/boric acid nanocomposites

Boric acid powder (62 mg) was added to a liquid fluoroalkyl end-capped vinyltrimethoxysilane oligomer (735 mg). The heterogeneous solution was stirred at room temperature for 5 h to give the transparent viscous colorless solution. After addition of tetrahydrofuran (3 mL), the obtained solution was stirred at room temperature for 1 day, and dried *in vacuo* at 50 °C for 2 days to afford the expected white powdery product nanocomposites (570 mg).

1.2.4. Preparation of fluoroalkyl end-capped vinyltrimethoxysilane oligomeric silica/boric acid nanocomposites - encapsulated a variety of low molecular weight organic guest molecules

Boric acid powder (124 mg) was added to a liquid fluoroalkyl end-capped vinyltrimethoxysilane oligomer (735 mg). The heterogeneous solution was stirred at room temperature for 5 h to give the transparent viscous colorless solution. After

addition of diphenylsilanediol (100 mg), 25 wt% ammonia (0.25 mL), and tetrahydrofuran (3 mL), the obtained solution was stirred at room temperature for 1 day, and dried *in vacuo* at 50 °C for 2 days to afford the expected white powdery product nanocomposites (746 mg). The nanocomposites - encapsulated other guest molecules were prepared under similar conditions.

The fluorinated nanocomposites thus obtained exhibited the following spectra characteristics:

R_F-(VM-SiO_2)$_n$-R_F/$B(OH)_3$/ DPSDO nanocomposites;

IR ν/cm^{-1} 3180 (OH), 1402 (B-O), 1337 (C-F), 1100 (Si-O-Si), 750, 719, 698 (Ph-Si in DPSDO), 698 (Si-O-B).

The spectra characteristics of the other fluorinated nanocomposites are as following:

R_F-(VM-SiO_2)$_n$-R_F/$B(OH)_3$/BINOL nanocomposites;

IR ν/cm^{-1} 3450 (OH), 1618, 1600 (C=C in BINOL), 1402 (B-O), 1337 (C-F), 1103 (Si-O-Si), 696 (Si-O-B).

R_F-(VM-SiO_2)$_n$-R_F/$B(OH)_3$/BPA nanocomposites;

IR ν/cm^{-1} 3380 (OH), 1612, 1600 (C=C in BPA), 1412 (B-O), 1337 (C-F), 1105

(Si-O-Si), 694 (Si-O-B).

R_F-(VM-SiO_2)$_n$-R_F/$B(OH)_3$/BPAF nanocomposites;

IR ν/cm^{-1} 3378 (OH), 1518, 1445 (C=C in BPAF), 1412 (B-O), 1338 (C-F), 1105 (Si-O-Si), 702 (Si-O-B).

R_F-(VM-SiO_2)$_n$-R_F/$B(OH)_3$/BPF nanocomposites;

IR ν/cm^{-1} 3447 (OH), 1603, 1510 (C=C in BPF), 1412 (B-O), 1338 (C-F), 1101 (Si-O-Si), 696 (Si-O-B).

R_F-(VM-SiO_2)$_n$-R_F/$B(OH)_3$/bisphenol nanocomposites;

IR ν/cm^{-1} 3394 (OH), 1611, 1591 (C=C in bisphenol), 1402 (B-O), 1337 (C-F), 1101 (Si-O-Si), 702 (Si-O-B).

R_F-(VM-SiO_2)$_n$-R_F/$B(OH)_3$/biphenyl nanocomposites;

IR ν/cm^{-1} 1402 (B-O), 1337 (C-F), 1101 (Si-O-Si), 698 (Si-O-B).

R_F-(VM-SiO_2)$_n$-R_F/$B(OH)_3$/dibenzyl nanocomposites;

IR ν/cm^{-1} 1402 (B-O), 1337 (C-F), 1101 (Si-O-Si), 698 (Si-O-B).

R_F-(VM-SiO_2)$_n$-R_F/$B(OH)_3$/PETERL nanocomposites;

IR ν/cm^{-1} 1406 (B-O), 1338 (C-F), 1067 (Si-O-Si), 698 (Si-O-B).

1.3. Results and discussion

1.3.1. Preparation of fluoroalkyl end-capped vinyltrimethoxysilane oligomeric silica/boric acid nanocomposites

Boric acid powder was added to a liquid fluoroalkyl end-capped vinyltrimethoxysilane oligomer. The heterogeneous solution was stirred at room temperature for 5 h to give the transparent viscous colorless solution. The obtained viscous solution was dissolved into tetrahydrofuran, and successively stirred at room temperature for 1 day. The solvent was removed under reduced pressure at 80 °C, and then dried *in vacuo* to afford the white-colored powdery product. The results are shown in Scheme 1-1 and Table 1-1.

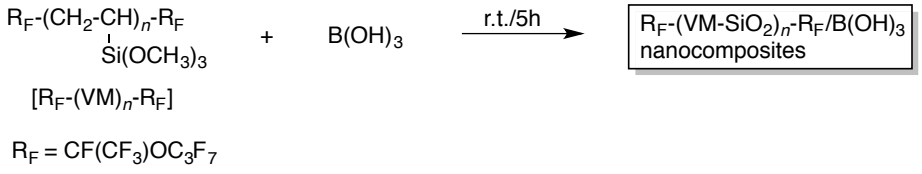

Scheme 1-1 Preparation of R_F-$(VM$-$SiO_2)_n$-$R_F/B(OH)_3$ nanocomposites.

Table 1-1 Preparation of R_F-(VM-SiO_2)$_n$-R_F/$B(OH)_3$ nanocomposites

Run	R_F-(VM)$_n$-R_F (mg)	$B(OH)_3$ (mg)	Yield[a] (%)	Size of composites[b] (nm) ± STD
1	735	31	77	104.5 ± 18.6
2	735	62	71	45.5 ± 10.8
3	735	124	67	88.2 ± 17.3
4	735	155	83	36.0 ± 4.1
5	735	247	72	65.8 ± 12.7
6	735	309	74	79.1 ± 15.9

a) Yields were based on R_F-(VM)$_n$-R_F and $B(OH)_3$.

b) Determined by dynamic light scattering (DLS) measurements.

As shown in Scheme 1-1 and Table 1-1, the expected composites were obtained in 67 ~ 83 % isolated yields. The obtained composites were found to have good dispersibility toward the traditional organic solvents, such as methanol, 1,2-dichloroethane (DE), tetrahydrofuran (THF), dimethyl sulfoxide, *N,N*-dimethylformamide and fluorinated aliphatic solvents (1:1 mixed solvents (AK-225^{TR}) of 1,1-dichloro-2,2,3,3,3-pentafluoropropane and 1,3-dichloro-1,2,2,3,3-pentafluoropropane) except for water. Thus, the average particle size of the R_F-(VM-SiO_2)$_n$-R_F/$B(OH)_3$ composite particles was measured in THF using DLS (dynamic light scattering) measurements at 25 °C, and the results are also shown in Table 1-1.

As shown in Table 1-1, the R_F-(VM-SiO_2)$_n$-R_F/$B(OH)_3$ composites are

nanometer size-controlled fine particles (average particle size: 36.0 ± 4.1 ~ 104.5 ± 18.6 nm).

The field emission scanning electron micrograph (FE-SEM) measurements of the R_F-(VM-SiO_2)$_n$-R_F/$B(OH)_3$ composites (Run 4 in Table 1-1) before and after calcination at 800 °C were also performed in their THF solutions (see Figure 1-1).

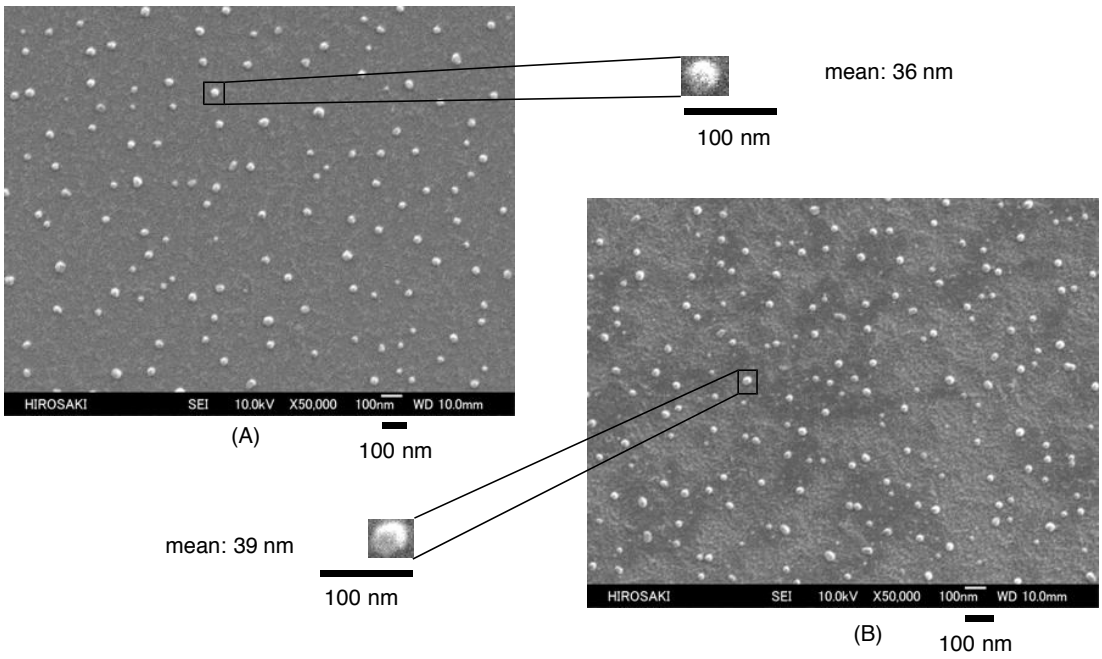

Figure 1-1 FE-SEM (field emission scanning electron microscopy) images of R_F-(VM)$_n$-R_F/$B(OH)_3$ nanocomposite in THF solutions (Run 4 in Table 1-1). (A): before calcination at 800 ºC, (B): after calcination at 800 ºC.

Figure 1-1 shows that the obtained composites are very fine spherical particles with mean diameter: 36 nm before calcination [Figure 1-1 (A)], and the similar spherical fine particles with mean diameter 39 nm were also observed even after

calcination at 800 °C [Figure 1-1 (B)]. Especially, the same particle size of the composites as that (36 nm) by DLS measurements can be obtained as shown in Run 4 (in Table 1-1).

To verify the structure of the present nanocomposites, ^{11}B Magic-angle spinning (MAS) NMR spectra of the R_F-(VM-SiO_2)$_n$-R_F/$B(OH)_3$ nanocomposites illustrated in Table 1-1 have been studied, and the results are shown in Figure 1-2.

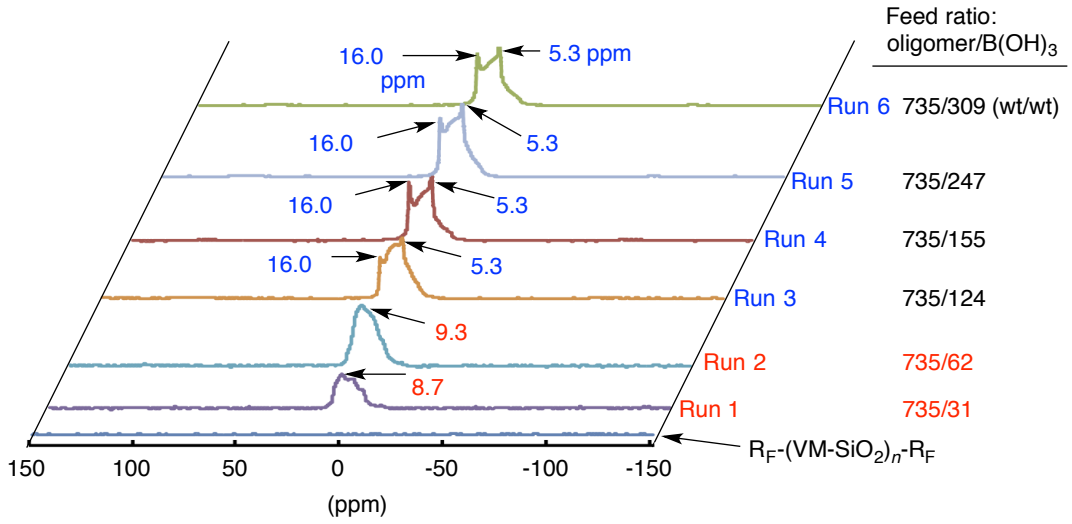

Figure 1-2 ^{11}B Magic-angle spinning (MAS) NMR spectra of R_F-(VM-SiO_2)$_n$-R_F/$B(OH)_3$ nanocomposites: Runs 1 ~ 6 in Table 1-1 determined by Varian 400 NMR system with a Varian 4 mm double-resonance T3 solid probe spun at 15 kHz.

As shown in Figure 1-2, a clear ^{11}B NMR signal was observed at around 9 ppm in the cases of the lower feed amounts of boric acid: 31 ~ 62 mg (Runs 1 and 2). On the other hand, two ^{11}B NMR signals were observed at around 5 ~ 16 ppm levels in the

cases of the higher feed amounts of boric acid: 124 ~ 309 mg (Runs 3 ~ 6). 9 ppm signal would be attributed to the trigonal boron units and 5 ~ 16 ppm signals are due to the borate network including the unreacted boric acid as shown in the following Schematic illustration (see Scheme 1-2).

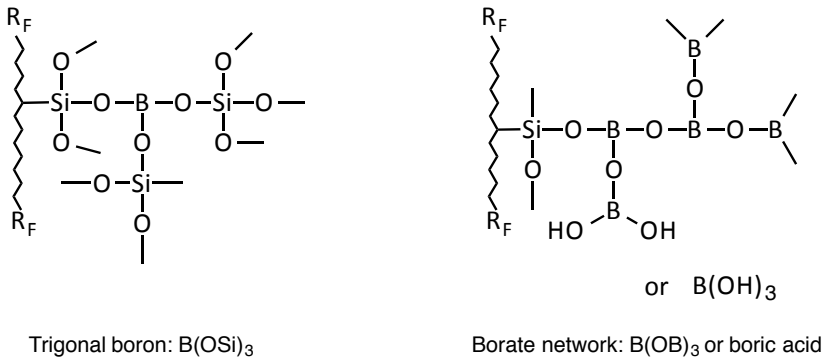

Scheme 1-2 Schematic illustration of the proposal structure of the R_F-(VM-SiO_2)$_n$-R_F/$B(OH)_3$ nanocomposites.

In fact, it has been already reported that the peaks at around 14 ~ 15 ppm are associated to the trigonal borosiloxane [$B(OSiR_3)_3$] units and the peaks at around 19 ppm are characteristic of boric acid or borate [$B(OB)_3$] networks, respectively, by ^{11}B MAS NMR spectral measurements.[4, 17, 18] FT-IR spectra also show that the R_F-(VM-SiO_2)$_n$-R_F/$B(OH)_3$ nanocomposites (Runs 1 and 2), which were prepared under the lower feed amounts (31 ~ 62 mg) of boric acid, can afford no absorption

peak related to boric acid; however, the nanocomposites (Runs 3 ~ 6), which were prepared under the higher feed amounts of boric acid, can supply the clear absorption peaks: 3200, 2260, and 1472 cm^{-1} related to the parent boric acid (see Figure 1-3). A similar result was obtained in the XRD (X-ray diffraction) measurements, and it can be observed the clear diffraction patterns related to the original boric acid in the composites (Runs 3 ~ 6) (see Figure 1-4). These findings suggest that the present nanocomposites consist of the trigonal boron units and borate networks including the parent boric acid illustrated in Scheme 1-2.

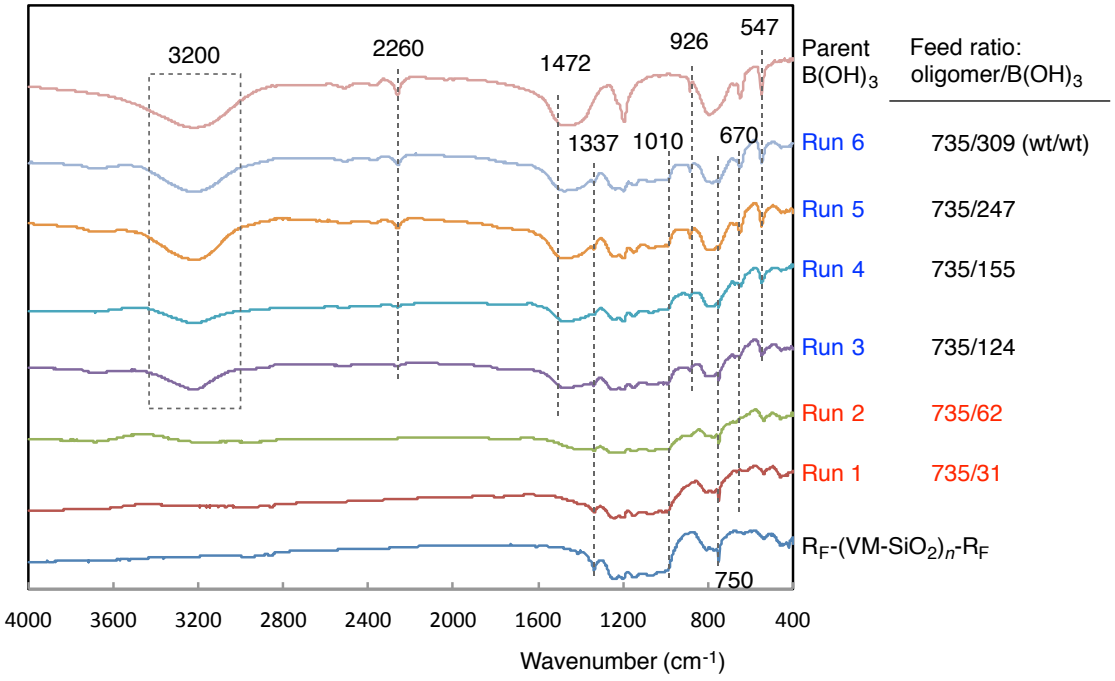

Figure 1-3 FT-IR spectra of R_F-(VM-SiO_2)$_n$-R_F/$B(OH)_3$ nanocomposites: Runs 1 ~ 6 in Table 1-1

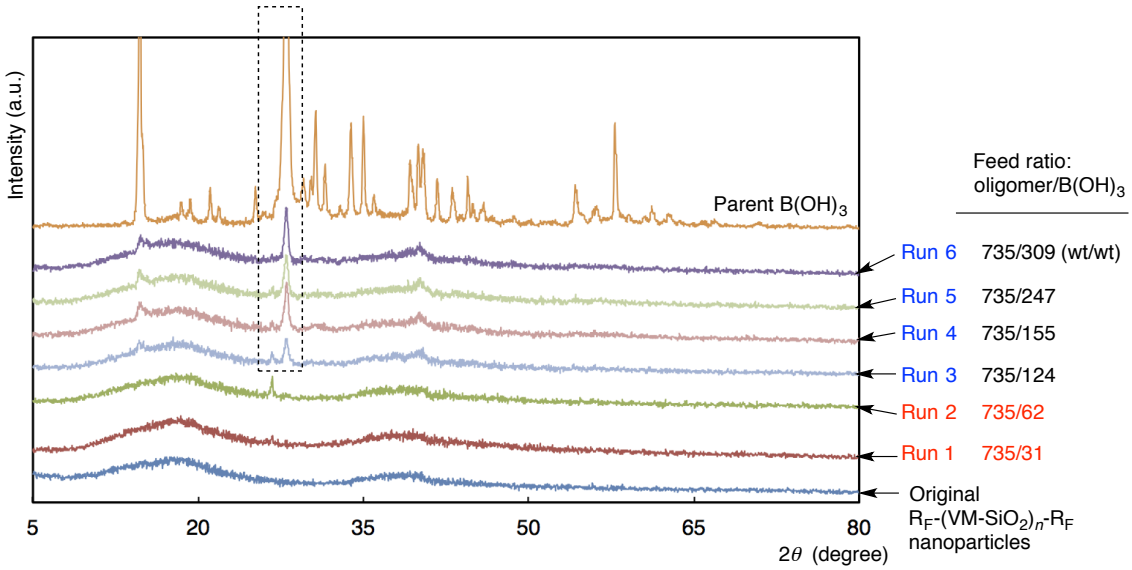

Figure 1-4 X-ray diffraction (XRD) patterns of R_F-(VM-SiO_2)$_n$-R_F/$B(OH)_3$ nanocomposites (Runs 1 ~ 6 in Table 1-1)

1.3.2. Thermal stability of the R_F-(VM-SiO_2)$_n$-R_F/$B(OH)_3$ nanocomposites

The thermal stability of the R_F-(VM-SiO_2)$_n$-R_F/$B(OH)_3$ nanocomposites illustrated in Table 1-1 have been studied by the use of thermogravimetric analyses (TGA), in which the weight loss of these nanocomposites was measured by raising the temperature around 800 °C at a 10 °C/min heating rate under air atmospheric conditions, and the results are shown in Figures 1-5 and 1-6.

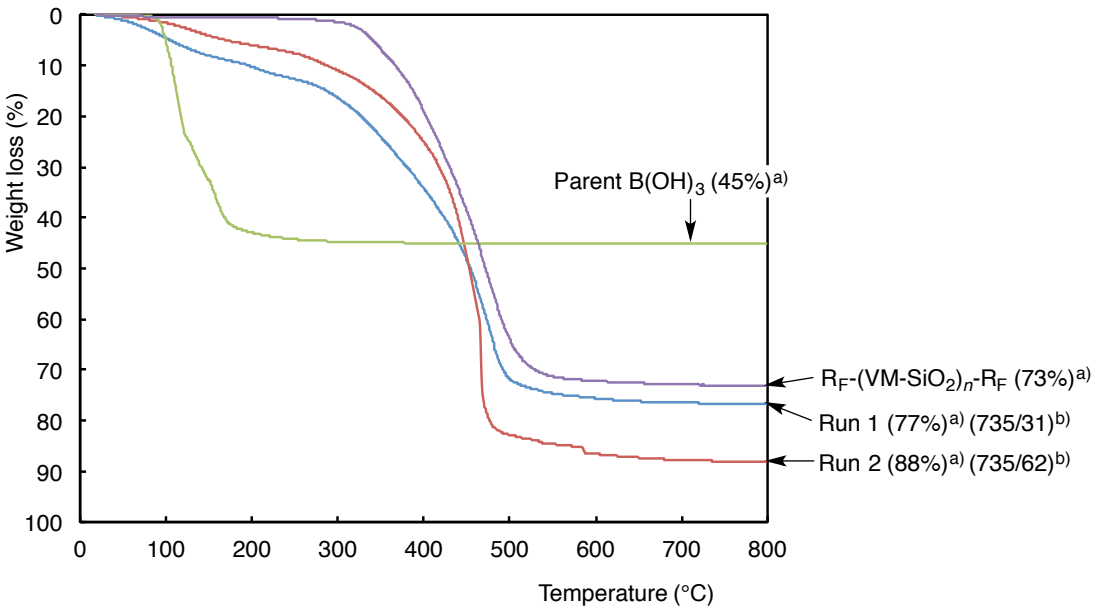

Figure 1-5 Thermogravimetric analyses (TGA) of R_F-(VM-SiO_2)$_n$-R_F/$B(OH)_3$ nanocomposites (Runs 1 and 2 in Table 1-1). (a) Weight loss (%) at 800 °C, (b) feed ratio of R_F-(VM)$_n$-R_F/$B(OH)_3$ (wt/wt).

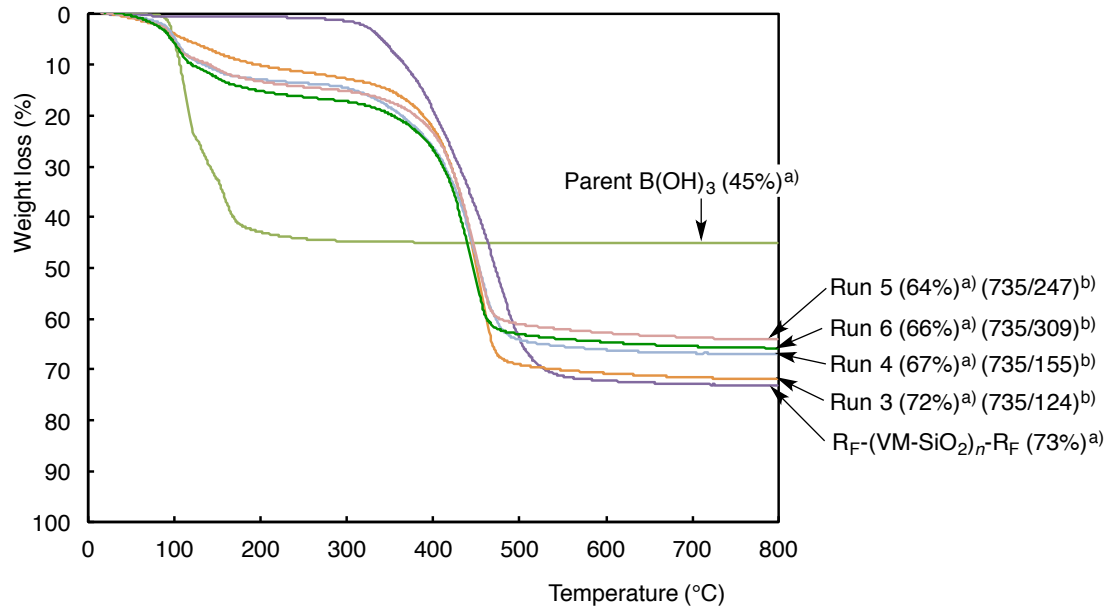

Figure 1-6 Thermogravimetric analyses (TGA) of R_F-(VM-SiO_2)$_n$-R_F/$B(OH)_3$ nanocomposites (Runs 3– 6 in Table 1-1). (a) Weight loss (%) at 800 °C, (b) feed ratio of R_F-(VM)$_n$-R_F/$B(OH)_3$ (wt/wt).

As shown in Figure 1-5, the nanocomposites, which were prepared under the

lower feed amounts of boric acid (31 ~ 62 mg: Runs 1 and 2 in Table 1-1), can afford the higher weight loss at 800 °C than that of the original R_F-(VM-SiO_2)$_n$-R_F nanoparticles, indicating that these nanocomposites consist of the trigonal boron units illustrated in Scheme 1-2. On the other hand, the nanocomposites, which were prepared under the higher feed amounts of boric acid: 124 ~ 309 mg: Runs 3 ~ 6, were found to provide the lower weight loss at 800 °C than that of the original nanoparticles. This finding suggests that these nanocomposites consist of the borate network structures including the parent boric acid (see Scheme 1-2). Original boric acid [$B(OH)_3$] can afford the metaboric acid (HBO_2) at 118 °C and boron trioxide (B_2O_3) at 160 °C by the dehydration under similar calcination process (see Figures 1-5 and 1-6). The formation of inorganic molecules such as boron trioxide during the calcination would decrease the weight loss of these nanocomposites as shown in Figure 1-6.

1.3.3. Preparation and thermal stability of the R_F-(VM-SiO_2)$_n$-R_F/$B(OH)_3$ nanocomposites - encapsulated a variety of low molecular weight organic compounds

It is well known that R_F-($CH_2CHSi(OMe_3)$)$_n$-R_F oligomer can undergo the sol–gel reaction under alkaline conditions in the presence of low molecular weight aromatic compounds, such as 1, 1'-bi-2-naphthol (BINOL) and 4, 4'-biphenol to afford the corresponding fluorinated oligomeric silica nanocomposites - encapsulated these aromatic compounds after purification process.[29 ~ 31] These encapsulated compounds can give no weight loss behavior in the fluorinated nanocomposites even after calcination at 800 °C.[29 ~ 31] This no weight loss behavior would be due to the formation of hexafluorosilicate anion, which should be obtained through the dehydrofluorination between the phenol-type acidic hydroxy protons in the organic compounds and fluorines in the oligomer under alkaline conditions.[29 ~ 31] Thus, the R_F-(VM-SiO_2)$_n$-R_F/$B(OH)_3$ nanocomposites - encapsulated diphenylsilanediol (DPSDO) have been prepared, and the results are shown in Scheme 1-3 and Table 1-2. The R_F-(VM-SiO_2)$_n$-R_F/$B(OH)_3$ nanocomposites - encapsulated other low molecular weight organic compounds such as 1, 1'-bi-2-naphthol (BINOL), 4, 4'-biphenol, bisphenol A (BPA), bisphenol F (BPF), bisphenol AF (BPAF), biphenyl, dibenzyl, and pentaerythritol (PETERL) under similar conditions have been also prepared, and the results are shown in Scheme 1-3 and Table 1-3.

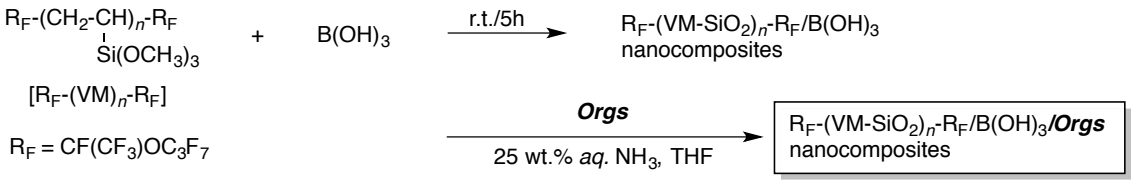

***Orgs*:** diphenylsilanediol (DPSDO), 1, 1'-bi-2-naphthol (BINOL), 4, 4'-biphenol, bisphenol A (BPA), bisphenol F (BPF), bisphenol AF (BPAF), biphenyl, dibenzyl, and pentaerythritol (PETERL)

Scheme 1-3 Preparation of R_F-$(VM$-$SiO_2)_n$-$R_F/B(OH)_3$/***Orgs*** nanocomposites.

Table 1-2 Preparation of R_F-$(VM$-$SiO_2)_n$-$R_F/B(OH)_3$/DPSDO nanocomposites

Run	R_F-$(VM)_n$-R_F (mg)	$B(OH)_3$ (mg)	DPSDO (mg)	Yield[a)] (%)	Size of composites[b)] (nm) ± STD
1	735	124	50	71	65.1 ± 7.4
1'	735	0	50	71	56.3 ± 7.2
2	735	124	100	77	48.2 ± 10.7
2'	735	0	100	77	56.3 ± 7.2
3	735	124	200	75	27.7 ± 2.4
3'	735	0	200	80	55.1 ± 5.4
4	735	124	300	80	50.3 ± 6.0
4'	735	0	300	79	63.7 ± 6.4
5	735	124	400	80	79.9 ± 4.9
5'	735	0	400	81	82.6 ± 8.3
6	735	124	500	82	53.9 ± 3.6
6'	735	0	500	82	63.3 ± 6.4
7	735	124	600	82	55.6 ± 11.7
8	735	124	700	82	56.1 ± 8.1
9	735	124	800	83	56.3 ± 11.3
9'	735	0	800	85	42.0 ± 4.1
10	735	124	1000	85	63.2 ± 6.3
10'	735	0	1000	87	49.2 ± 4.1
11	735	124	1500	87	69.0 ± 8.4

a) Yields were based on R_F-$(VM)_n$-R_F, $B(OH)_3$ and DPSDO (or R_F-$(VM)_n$-R_F and DPSDO).
b) Determined by dynamic light scattering (DLS) measurements.

Table 1-3 Preparation of R_F-(VM-SiO_2)$_n$-R_F/$B(OH)_3$/***Orgs*** nanocomposites

Run	R_F-(VM)$_n$-R_F (mg)	$B(OH)_3$ (mg)	***Orgs*** (mg)	Yield[a)] (%)	Size of composites[b)] (nm) ± STD
			BINOL		
12	735	124	50	77	43.7 ± 5.1
12'	735	0	50	75	53.2 ± 3.2
13	735	124	100	79	38.9 ± 5.0
13'	735	0	100	75	82.3 ± 7.8
14	735	124	200	80	51.2 ± 6.2
14'	735	0	200	80	84.2 ± 15.6
15	735	124	300	79	63.8 ± 6.4
15'	735	0	300	83	89.7 ± 14.1
16	735	124	600	83	65.0 ± 7.6
16'	735	0	600	84	68.8 ± 8.2
			BPA		
17	735	124	50	77	78.5 ± 13.4
17'	735	0	50	75	84.2 ± 9.2
18	735	124	100	78	73.2 ± 7.3
18'	735	0	100	76	82.6 ± 8.0
19	735	124	200	82	71.8 ± 6.7
19'	735	0	200	80	67.1 ± 8.2
20	735	124	300	82	43.0 ± 4.8
20'	735	0	300	83	85.4 ± 13.9
21	735	124	600	83	55.2 ± 5.5
21'	735	0	600	83	73.4 ± 7.3

			BPAF		
22	735	124	50	76	42.1 ± 4.2
22'	735	0	50	76	72.6 ± 7.2
23	735	124	100	79	62.7 ± 5.6
23'	735	0	100	75	92.3 ± 11.2
24	735	124	200	80	41.1 ± 2.7
24'	735	0	200	80	80.0 ± 8.9
25	735	124	300	78	83.0 ± 13.5
25'	735	0	300	82	73.6 ± 7.2
26	735	124	600	83	83.4 ± 8.4
26'	735	0	600	82	99.7 ± 12.1
			BPF		
27	735	124	50	76	57.0 ± 6.6
27'	735	0	50	75	83.9 ± 9.0
28	735	124	100	78	45.9 ± 4.9
28'	735	0	100	78	71.4 ± 12.7
29	735	124	200	79	48.3 ± 4.6
29'	735	0	200	78	84.5 ± 9.6
30	735	124	300	80	52.4 ± 6.3
30'	735	0	300	83	55.3 ± 5.2
31	735	124	400	81	40.9 ± 2.7
31'	735	0	400	84	87.3 ± 10.7
32	735	124	500	80	67.4 ± 9.4
32'	735	0	500	85	83.3 ± 8.3
33	735	124	800	88	74.9 ± 8.3
33'	735	0	800	89	70.2 ± 4.5

			Biphenol		
34	735	124	50	78	42.0 ± 4.3
34'	735	0	50	74	55.1 ± 5.5
35	735	124	100	78	67.2 ± 9.7
35'	735	0	100	78	55.4 ± 5.5
36	735	124	200	77	41.7 ± 3.8
36'	735	0	200	79	43.8 ± 5.9
37	735	124	300	81	42.3 ± 4.1
37'	735	0	300	79	67.2 ± 8.4
38	735	124	400	84	66.3 ± 8.1
38'	735	0	400	83	50.6 ± 5.9
39	735	124	500	84	54.5 ± 5.0
39'	735	0	500	84	54.9 ± 5.2
			Biphenyl		
40	735	124	50	80	42.3 ± 4.4
40'	735	0	50	72	51.9 ± 8.2
41	735	124	100	82	58.5 ± 7.1
41'	735	0	100	71	56.8 ± 6.6
42	735	124	200	70	41.6 ± 2.8
42'	735	0	200	70	43.8 ± 6.8
43	735	124	300	76	63.5 ± 6.3
43'	735	0	300	72	49.1 ± 5.3
44	735	124	400	78	54.7 ± 5.1
44'	735	0	400	75	55.3 ± 5.5
45	735	124	500	79	66.9 ± 8.2
45'	735	0	500	75	82.9 ± 8.2

			Dibenzyl		
46	735	124	50	77	32.5 ± 3.6
46'	735	0	50	72	63.4 ± 6.3
47	735	124	100	79	31.9 ± 3.1
47'	735	0	100	75	54.1 ± 4.5
48	735	124	200	79	45.5 ± 5.5
48'	735	0	200	75	52.8± 3.0
49	735	124	300	82	49.7 ± 5.4
49'	735	0	300	78	83.1 ± 8.3
50	735	124	400	83	65.3 ± 7.8
50'	735	0	400	80	54.9 ± 5.4
51	735	124	500	82	56.1 ± 5.9
51'	735	0	500	82	83.4 ± 8.5
			PETERL		
52	735	124	50	76	55.0 ± 6.8
52'	735	0	50	78	41.0 ± 4.5
53	735	124	100	62	42.1 ± 4.0
53'	735	0	100	77	53.1 ± 3.2
54	735	124	200	87	43.7 ± 5.1
54'	735	0	200	80	83.2 ± 9.6
55	735	124	300	75	61.5 ± 9.7
55'	735	0	300	81	22.8 ± 9.6

a) Yields were based on R_F-$(VM)_n$-R_F, $B(OH)_3$ and ***Orgs*** (or R_F-$(VM)_n$-R_F and ***Orgs***).
b) Determined by dynamic light scattering (DLS) measurements.

As shown in Scheme 1-3, Tables 1-2 and 1-3, the R_F-$(VM\text{-}SiO_2)_n$-R_F/$B(OH)_3$ composites - encapsulated not only DPSDO but also other low molecular weight organic compounds (***Orgs***) were obtained in 71 ~ 87 and 76 ~ 88 % isolated yields, respectively. These obtained composites were found to have the similar dispersibility

to that of the R_F-(VM-SiO_2)$_n$-R_F/$B(OH)_3$ nanocomposites illustrated in Scheme 1-1 and Table 1-1. Thus, the average particle size of these composites in THF are measured by the use of DLS measurements, and the results are also shown in Tables 1-2 and 1-3.

The average particle size of these composites was nanometer size-controlled particles with mean diameter: 28 ~ 83 nm. In addition, the corresponding fluorinated oligomeric silica nanocomposites - encapsulated these organic compounds [R_F-(VM-SiO_2)$_n$-R_F/***Orgs***] were prepared under similar conditions with no use of boric acid, for comparison. The results are also shown in Tables 1-2 and 1-3.

The expected R_F-(VM-SiO_2)$_n$-R_F/***Orgs*** composites were obtained in 70 ~ 89 % isolated yields through no purification process and the average particles size of these composites in THF determined by using DLS measurements were nanometer size-controlled: 23 ~ 100 nm as illustrated in Tables 1-2 and 1-3.

FE-SEM pictures of the R_F-(VM-SiO_2)$_n$-R_F/$B(OH)_3$/DPSDO nanocomposites and the R_F-(VM-SiO_2)$_n$-R_F/DPSDO nanocomposites (Runs 2 and 20 in Table 1-2) before and after calcination at 800 °C show the formation of very fine nanoparticles with mean diameters: 56 and 60 nm before calcination, and 45 and 50 nm after calcination,

respectively (see Figures 1-7 and 1-8). Thus, the similar size of the composites before and after calcination was observed, respectively.

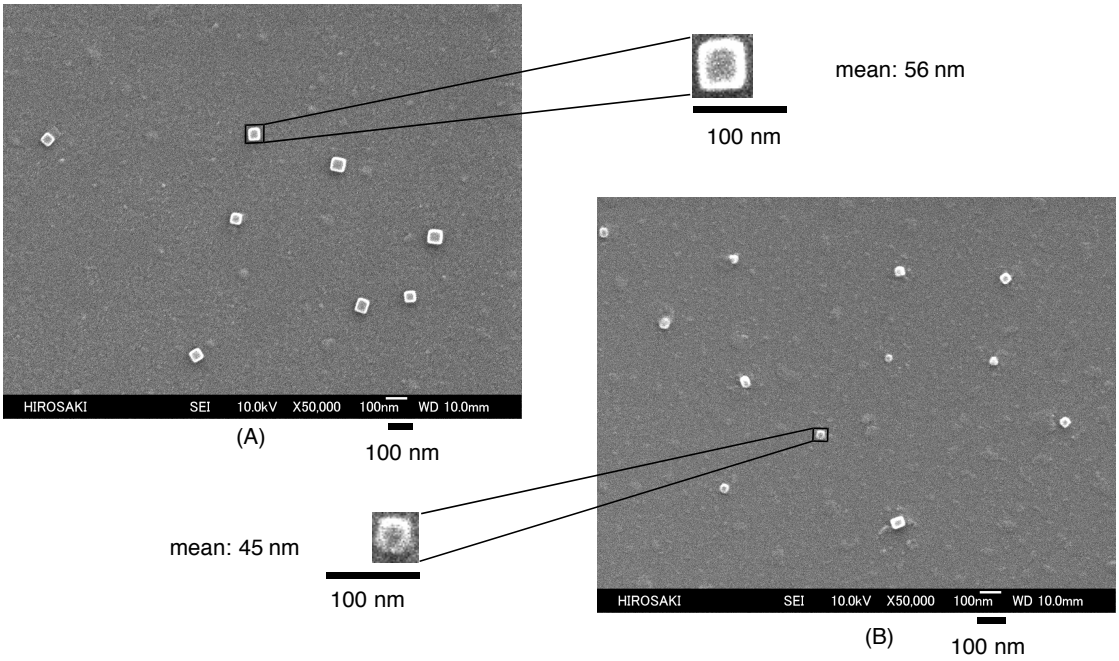

Figure 1-7 FE-SEM (field emission scanning electron microscopy) images of R_F-(VM-SiO_2)$_n$-R_F/$B(OH)_3$/DPSDO nanocomposite in THF solutions (Run 2 in Table 1-2). (A): before calcination at 800 ºC, (B): after calcination at 800 ºC.

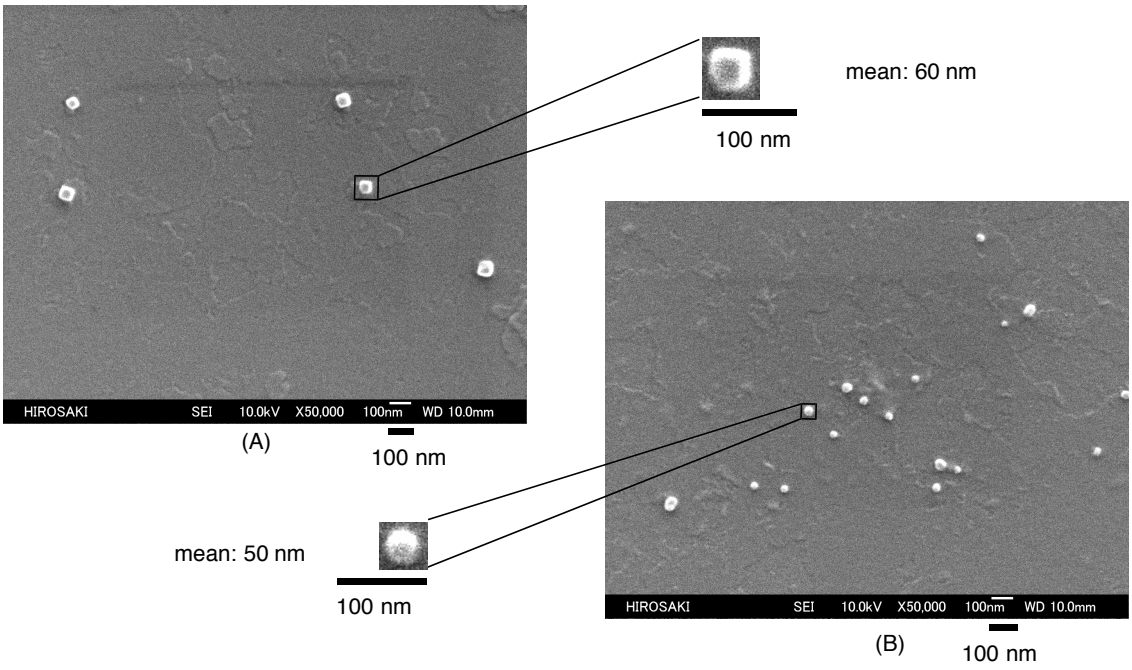

Figure 1-8 FE-SEM (field emission scanning electron microscopy) images of R_F-(VM-SiO_2)$_n$-R_F/DPSDO nanocomposite in THF solutions (Run 2' in Table 1-2). (A): before calcination at 800 ºC, (B): after calcination at 800 ºC.

Thermal stability of these obtained nanocomposites was studied by the use of TGA measurements, and the results are shown in Figure 1-9.

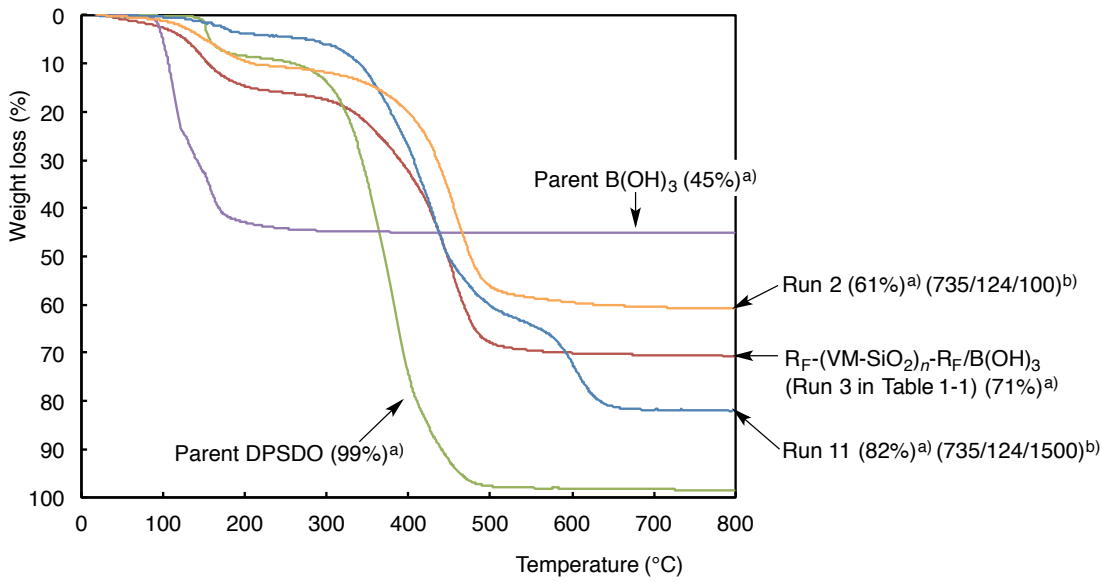

Figure 1-9 Thermogravimetric analyses (TGA) of R_F-(VM-SiO_2)$_n$-R_F/$B(OH)_3$/DPSDO nanocomposites (Runs 2 and 11 in Table 1-2). (a) Weight loss (%) at 800 °C, (b) feed ratio of R_F-(VM)$_n$-R_F/$B(OH)_3$/DPSDO (wt/wt/wt).

Figure 1-9 shows that the R_F-(VM-SiO_2)$_n$-R_F/$B(OH)_3$/DPSDO nanocomposites (Run 2 in Table 1-2: feed amount of DPSDO: 100 mg) can give the lower weight loss than that of the R_F-(VM-SiO_2)$_n$-R_F/$B(OH)_3$ nanocomposites (Run 3 in Table 1-1) even after calcination at 800 °C, although the R_F-(VM-SiO_2)$_n$-R_F/$B(OH)_3$/DPSDO nanocomposites were isolated through no purification process. This finding suggests that the encapsulated DPSDO should afford no weight loss characteristic in the nanocomposite cores even after calcination. On the other hand, the R_F-(VM-SiO_2)$_n$-R_F/$B(OH)_3$/DPSDO nanocomposites (Run 11 in Table 1-2), which were prepared under a higher feed amount (1500 mg) of DPSDO, were found to give a

clear weight loss (82 %) after calcination at 800 °C, compared with that of the R_F-(VM-SiO_2)$_n$-R_F/$B(OH)_3$ nanocomposites (Run 3 in Table 1-1) (see Run 11 in Figure 1-9). In addition, the thermal stability of the other nanocomposites in Table 1-2 was studied under similar conditions, and the weight loss at 800 °C are summarized in Figure 1-10.

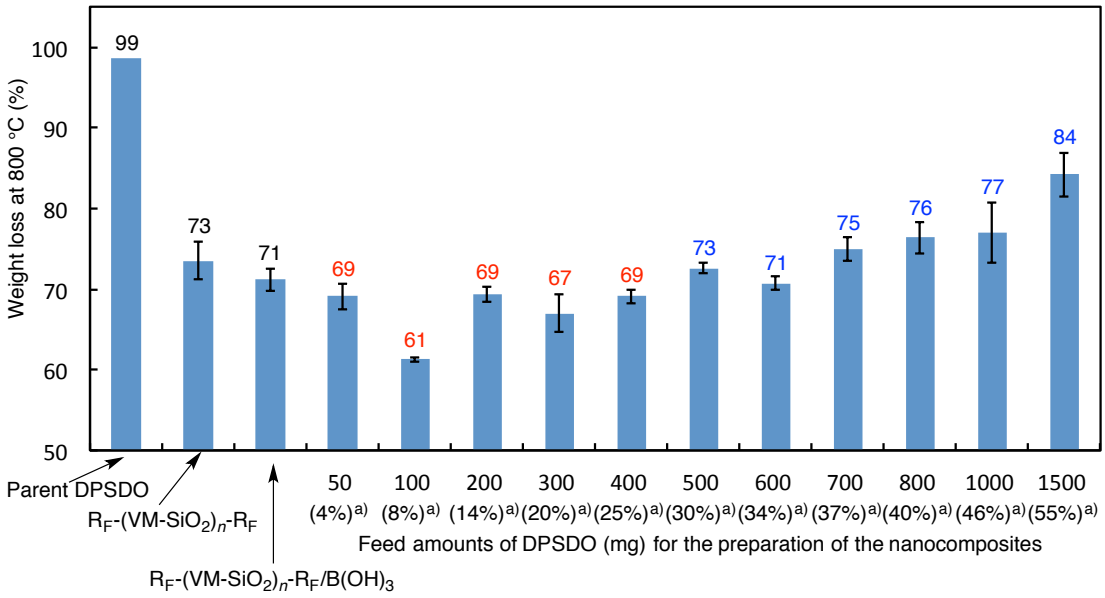

Figure 1-10 Weight loss of R_F-(VM-SiO_2)$_n$-R_F/$B(OH)_3$/DPSDO nanocomposites after calcination at 800 °C.
a) Theoretical contents of DPSDO in nanocomposite (%)

As shown in Figure 1-10, the parent DPSDO, the R_F-(VM-SiO_2)$_n$-R_F oligomeric nanoparticles and the R_F-(VM-SiO_2)$_n$-R_F/$B(OH)_3$ nanocomposites were found to provide the 98, 73, and 71 % weight loss at 800 °C, respectively. In contrast, the

R_F-(VM-SiO_2)$_n$-R_F/$B(OH)_3$/DPSDO nanocomposites (Runs 1 ~ 5 in Table 1-2), which were prepared under the feed amounts: 50 ~ 400 mg of DPSDO, can provide the weight loss of 61 ~ 69 %, of whose values are smaller than that (71 %) of the R_F-(VM-SiO_2)$_n$-R_F/$B(OH)_3$ nanocomposites (Run 3 in Table 1-1), indicating that the encapsulated DPSDO should afford no weight loss characteristic in the composite cores even after calcination at 800 °C. However, it was demonstrated that the R_F-(VM-SiO_2)$_n$-R_F/$B(OH)_3$/DPSDO nanocomposites (Runs 6 ~ 11 in Table 1-2), which were prepared under higher feed amounts: 500 ~ 1500 mg of DPSDO, supply the clear weight loss (71 ~ 84 %) corresponding to the contents of DPSDO in the composites after calcination. From these findings, the DPSDO can be effectively encapsulated into the R_F-(VM-SiO_2)$_n$-R_F/$B(OH)_3$ nanocomposite cores to afford no weight loss characteristic in the composites, and the saturated amounts of the encapsulated DPSDO to afford no weight loss behavior are within 500 mg, and the feed amounts of DPSDO greater than 500 mg can provide the usual weight loss corresponding to the contents of DPSDO.

The thermal stability of the R_F-(VM-SiO_2)$_n$-R_F/DPSDO nanocomposites illustrated in Table 1-2 was studied, and the results for the weight loss at 800 °C of

these nanocomposites are shown in Figure 1-11.

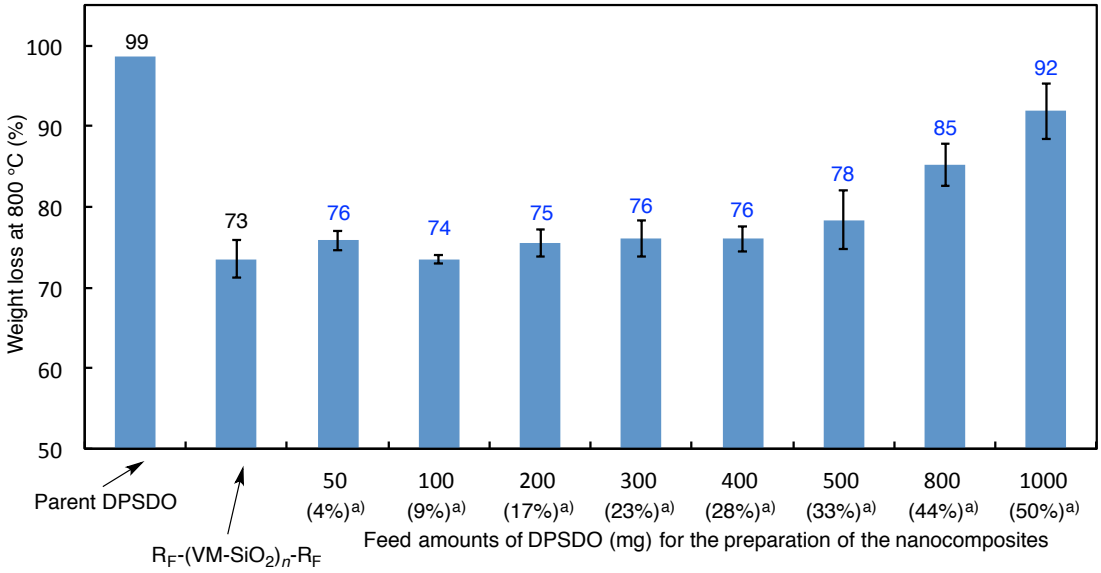

Figure 1-11 Weight loss of R_F-(VM-SiO_2)$_n$-R_F/DPSDO nanocomposites illustrated in Table 1-2 after calcination at 800 °C
a) Theoretical contents of DPSDO in nanocomposite (%)

As shown in Figure 1-11, the R_F-(VM-SiO_2)$_n$-R_F/DPSDO nanocomposites (see Runs 1' ~ 10' in Table 1-2), which were prepared under the feed amounts: 50 ~ 1000 mg of DPSDO, were found to give a clear weight loss from 74 to 92 % at 800 °C, compared with that (73 %) of the R_F-(VM-SiO_2)$_n$-R_F oligomeric nanoparticles. This finding suggests that the DPSDO in these nanocomposites should afford the usual weight loss behavior during the calcination process. Therefore, it was clarified that the introduction of the boric acid units into the nanocomposites are essential for affording

no weight loss behavior toward the encapsulated DPSDO.

Table 1-4 shows the thermal stability of the R_F-(VM-SiO_2)$_n$-R_F/$B(OH)_3$/BINOL, BPA, BPAF, BPF, biphenol, PETERL, biphenyl, and dibenzyl nanocomposites. The thermal stability of the corresponding nanocomposites possessing no boric acid units was also shown in Table 1-4, for comparison. Especially, the results for the weight loss values at 800 °C of these nanocomposites are summarized in Table 1-4.

Table 1-4 Relationship between the weight loss values of the R_F-(VM-SiO_2)$_n$-R_F/$B(OH)_3$/***Orgs*** nanocomposites (including the R_F-(VM-SiO_2)$_n$-R_F/***Orgs*** nanocomposites) at 800 °C and the feed amounts of ***Orgs*** for the preparation of the corresponding nanocomposites

Feed amounts of ***Orgs*** (mg)	0	50	100	200	300	400	500	600	800
R_F-(VM-SiO_2)$_n$-R_F/$B(OH)_3$/BINOL (%)*	71	70	73	78	78			85	
R_F-(VM-SiO_2)$_n$-R_F/BINOL (%)*	73	81	79	80	84			90	
R_F-(VM-SiO_2)$_n$-R_F/$B(OH)_3$/BPA (%)*	71	71	72	72	81			86	
R_F-(VM-SiO_2)$_n$-R_F/BPA (%)*	73	77	80	80	84			90	
R_F-(VM-SiO_2)$_n$-R_F/$B(OH)_3$/BPAF (%)*	71	71	70	72	80			87	
R_F-(VM-SiO_2)$_n$-R_F/BPAF (%)*	73	77	82	85	84			87	
R_F-(VM-SiO_2)$_n$-R_F/$B(OH)_3$/BPF (%)*	71	67	68	74	78	80	83		84
R_F-(VM-SiO_2)$_n$-R_F/BPF (%)*	73	76	77	84	79	88	84		88
R_F-(VM-SiO_2)$_n$-R_F/$B(OH)_3$/biphenol (%)*	71	70	73	76	79	81	83		
R_F-(VM-SiO_2)$_n$-R_F/biphenol (%)*	73	77	81	80	82	85	87		
R_F-(VM-SiO_2)$_n$-R_F/$B(OH)_3$/PETERL (%)*	71	68	70	75	80				
R_F-(VM-SiO_2)$_n$-R_F/PETERL (%)*	73	76	79	86	86				
R_F-(VM-SiO_2)$_n$-R_F/$B(OH)_3$/biphenyl (%)*	71	72	74	75	79	80	84		
R_F-(VM-SiO_2)$_n$-R_F/biphenyl (%)*	73	74	76	78	80	85	85		
R_F-(VM-SiO_2)$_n$-R_F/$B(OH)_3$/dibenzyl (%)*	71	71	74	76	77	78	82		
R_F-(VM-SiO_2)$_n$-R_F/dibenzyl (%)*	73	75	79	81	83	85	87		

* Weight loss (%) at 800 °C

Table 1-4 shows that the boric acid units enable the encapsulated ***Orgs*** to afford

the higher thermal stability in the fluorinated nancomposite cores. The R_F-(VM-SiO_2)$_n$-R_F/$B(OH)_3$/***Orgs*** nanocomposites, which were prepared under the feed amounts: 50 ~ 100 mg of ***Orgs*** except for biphenyl and dibenzyl, can supply the 62 ~ 73 % weight loss, indicating that the encapsulated ***Orgs*** would afford the perfect or partially no weight loss behavior in the nanocomposite cores. On the other hand, encapsulated ***Orgs***, such as biphenyl and dibenzyl afforded slightly higher weight loss: 73 ~ 74 %, suggesting that the encapsulated these guest molecules should exhibit the partially weight loss behavior during their calcination process.

To verify the presence of ***Orgs*** in the nanocomposites after calcination at 800 °C, ^{1}H MAS NMR spectra of the R_F-(VM-SiO_2)$_n$-R_F/$B(OH)_3$/biphenyl nanocomposites (Run 41 in Table 1-3) before and after calcination at 800 °C have been studied, and the results are shown in Figure 1-12.

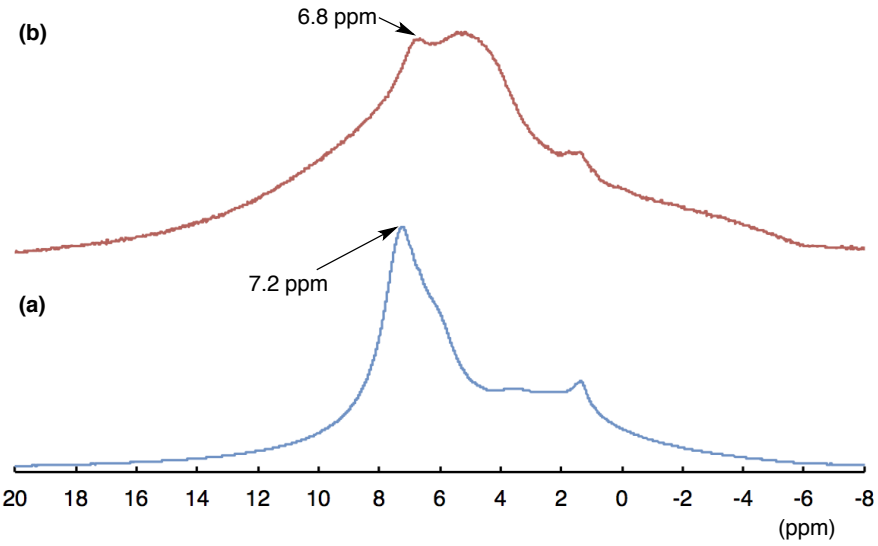

Figure 1-12 ^{1}H Magic-angle spinning (MAS) NMR spectra of R_F-(VM-SiO_2)$_n$-R_F/$B(OH)_3$/biphenyl nanocomposites (Run 41 in Table 1-3) before **(a)** and after **(b)** calcination at 800 °C determined by Varian 400 NMR system with a Varian 4 nm double-resonance T3 solid probe spun at 15 kHz.

As shown in Figure 1-12, the relatively sharp aromatic proton signals at around 7 ppm levels related to the encapsulated biphenyl was observed before **(a)** and even after calcination **(b)**, respectively. Especially, the aromatic signal at around 7 ppm after calcination reveals the presence of biphenyl in the nanocomposites.

Similarly, ^{1}H MAS NMR spectra of the R_F-(VM-SiO_2)$_n$-R_F/biphenyl nanocomposites possessing no boric acid units (Run 41' in Table 1-3) before calcination can exhibit the clear aromatic signal at around 7 ppm levels related to the presence of biphenyl in the nanocomposites [see Figure 1-13-**(a)**]. However, proton NMR signals at around 7 ppm have been completely disappeared during the

calcination process [see Figure 1-13-**(b)**], indicating that the encapsulated biphenyl can afford the usual weight loss characteristic.

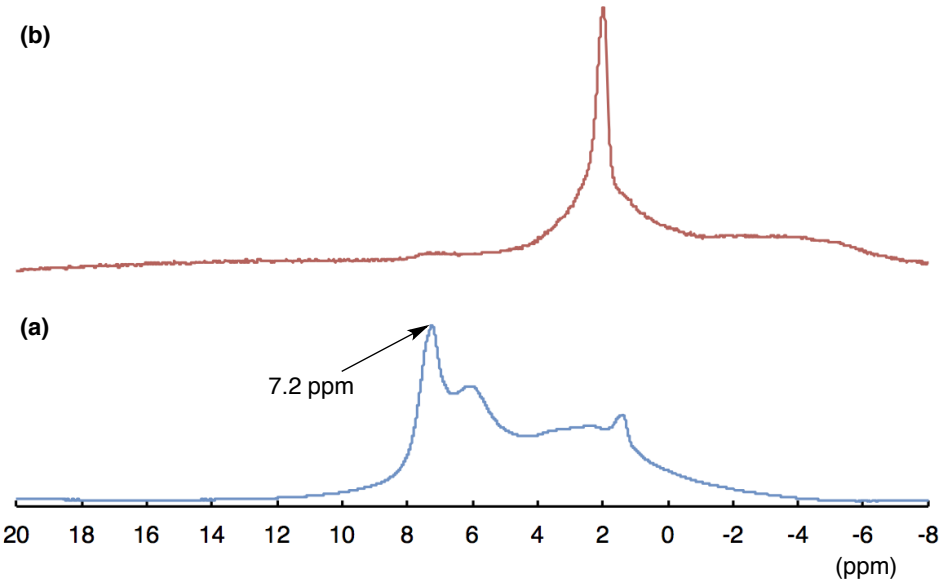

Figure 1-13 ^{1}H Magic-angle spinning (MAS) NMR spectra of R_F-(VM-SiO_2)$_n$-R_F/biphenyl nanocomposites (Run 41' in Table 1-3) before **(a)** and after **(b)** calcination at 800 °C determined by Varian 400 NMR system with a Varian 4 nm double-resonance T3 solid probe spun at 15 kHz.

These findings suggest that the incorporation of boric acid units into the fluorinated oligomeric silica nanocomposite cores is essential for providing no weight loss behavior for the encapsulated organic molecules such as biphenyl.

It was previously reported that fluoroalkyl end-capped acrylic acid oligomer [R_F-($CH_2CHCOOH$)$_n$-R_F]/silica nanocomposites - encapsulated bisphenol AF, which

were prepared by the sol-gel reactions of tetraethoxysilane and silica nanoparticles in the presence of the corresponding oligomer and bisphenol AF under alkaline conditions, can give no weight loss corresponding to the contents of bisphenol AF in the composites even after calcination at 800 °C.[32] This no weight loss behavior is due to the formation of ammonium hexafluorosilicate, which would be formed by the smooth dehydrofluorination of phenol-type acidic hydroxy protons in bisphenol AF with fluorines in oligomers catalyzed by both ammonia and silica nanoparticles.[32] The present R_F-(VM-SiO_2)$_n$-R_F/$B(OH)_3$/biphenyl nanocomposites - encapsulated biphenyl has no phenol-type acidic protons. However, the encapsulated biphenyl can afford no weight loss behavior in the nanocomposite cores even after calcination at 800 °C. In contrast, as mentioned above, the encapsulated biphenyl in the R_F-(VM-SiO_2)$_n$-R_F nanocomposite cores can supply the usual weight loss characteristic. These findings suggest that boric acid units in the composites should afford no weight loss characteristic toward the encapsulated biphenyl. In order to clarify such unique no weight loss property, ^{11}B Magic-angle spinning (MAS) NMR spectra of the R_F-(VM-SiO_2)$_n$-R_F/$B(OH)_3$/DPSDO nanocomposites (Run 2 in Table 1-2) and the R_F-(VM-SiO_2)$_n$-R_F/$B(OH)_3$/biphenyl nanocomposites (Run 42 in Table 1-3) before

and after calcination at 800 °C were studied, and the results are shown in Figures 1-14 and 1-15.

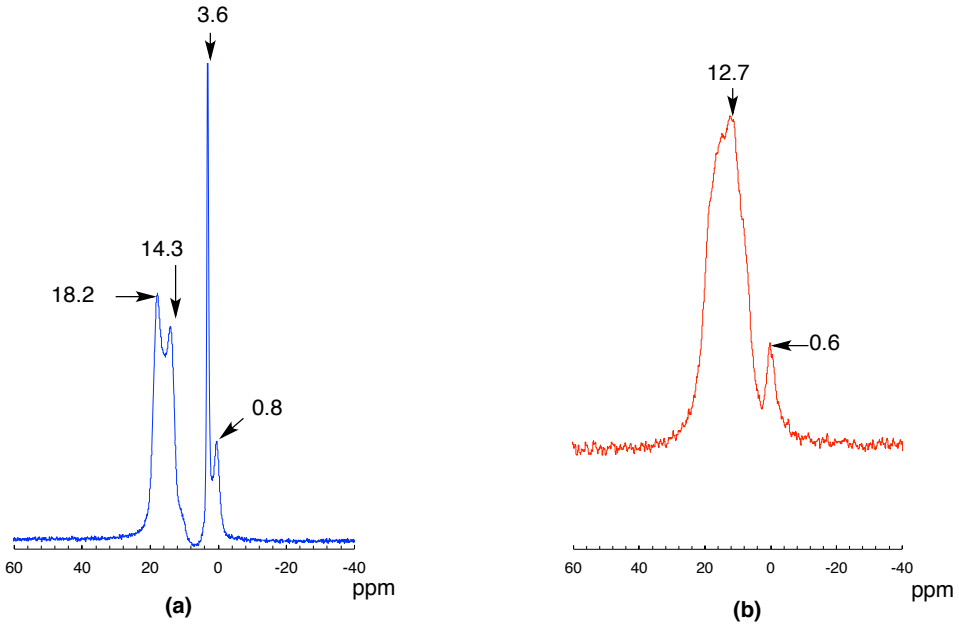

Figure 1-14 ^{11}B Magic-angle spinning (MAS) NMR spectra of R_F-(VM-SiO_2)$_n$-R_F/$B(OH)_3$/DPSDO nanocomposites (Run 2 in Table 1-2) before **(a)** and after **(b)** calcination at 800 °C determined by Varian 600 NMR system with a Varian 3.2 nm Varian $^{1}H/^{31}P$-$^{13}C/^{13}C$-^{15}N BioMASTM probe spun at 15 kHz.

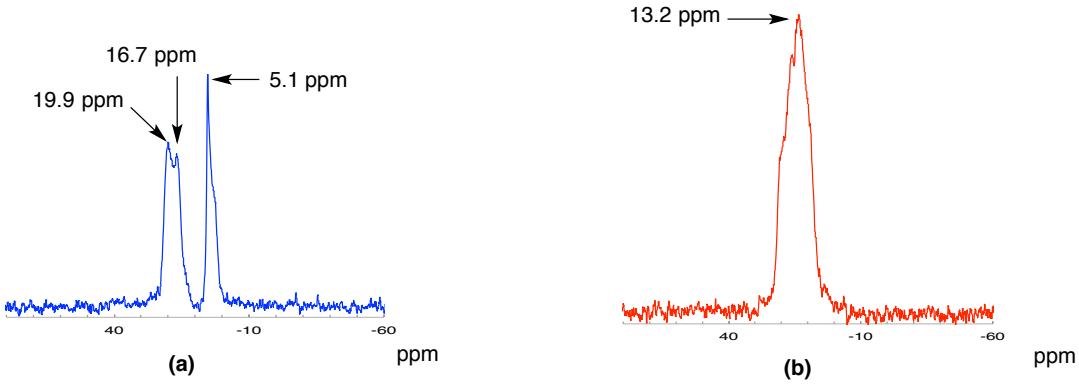

Figure 1-15 ^{11}B Magic-angle spinning (MAS) NMR spectra of R_F-(VM-SiO_2)$_n$-R_F/$B(OH)_3$/biphenyl nanocomposites (Run 42 in Table 1-3) before **(a)** and after **(b)** calcination at 800 °C determined by Varian 600 NMR system with a Varian 3.2 nm Varian $^{1}H/^{31}P$-$^{13}C/^{13}C$-^{15}N BioMASTM probe spun at 15 kHz.

^{11}B MAS NMR spectra for the R_F-(VM-SiO_2)$_n$-R_F/$B(OH)_3$/DPSDO and the R_F-(VM-SiO_2)$_n$-R_F/$B(OH)_3$/biphenyl nanocomposites before calcination show the two clear signals at around 14.3 ~ 19.9 ppm and 0.8 ~ 5.1 ppm levels, of whose peaks are associated with the presence of the trigonal boron units (>B–)[4, 17, 18] and the tetragonal boron units (>B<),[33 ~ 36] respectively. The DPSDO nanocomposites after calcination can exhibit the similar two signals at around 12.7 and 0.6 ppm, which correspond to the trigonal and tetragonal boron units, respectively [see Figure 1-14-**(b)**]. The biphenyl nanocomposites were found to exhibit the only one signal at around 13.2 ppm related to the trigonal boron units [see Figure 1-15-**(b)**], indicating that the tetragonal boron units in the nanocomposites would be consumed during the calcination process. On the other hand, the hydroxy units in the DPSDO nanocomposites should interact effectively with the boron moieties to keep the tetragonal boron units even after calcination process as shown in Scheme 1-4.

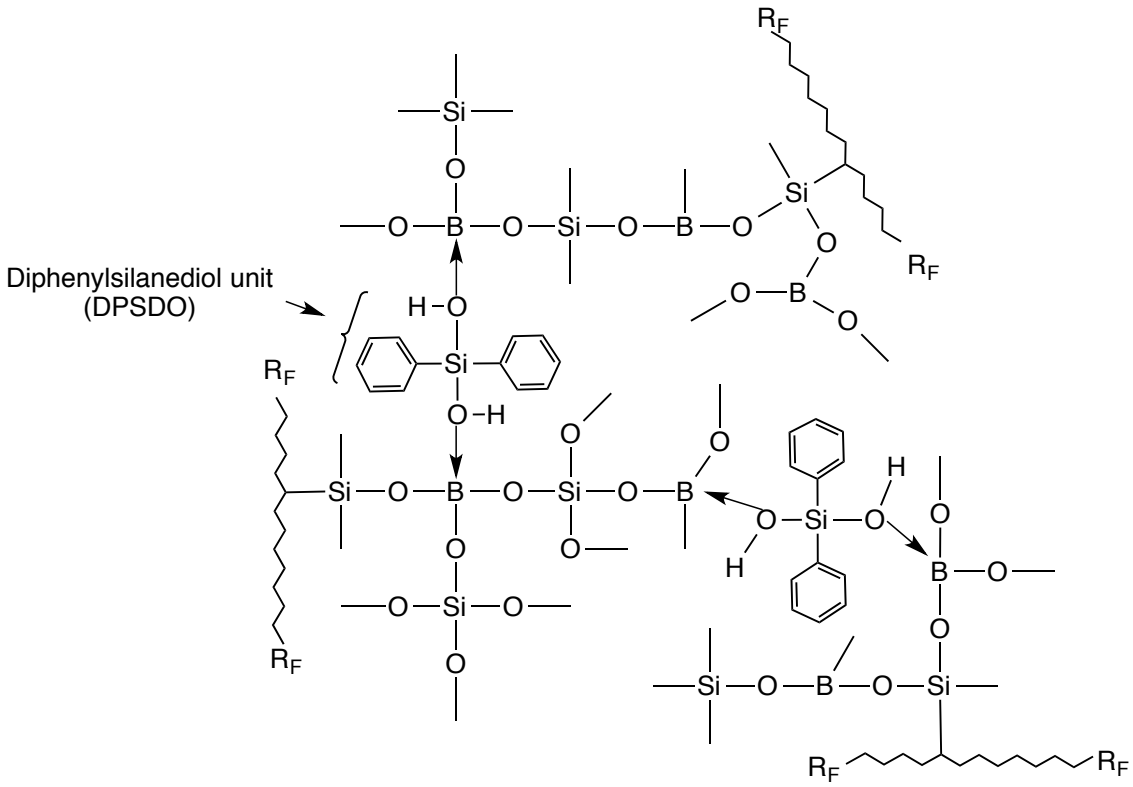

Scheme 1-4 Plausible structures of R_F-(VM-SiO_2)$_n$-R_F/$B(OH)_3$/DPSDO nanocomposites

In this way, it was verified that the formation of the tetragonal boron units in the composites can afford no weight loss characteristic toward the encapsulated organic molecules in the nanocomposite cores even after calcination at 800 °C.

1.4. Conclusion

It was demonstrated that fluoroalkyl end-capped vinyltrimethoxysilane oligomer [R_F-$(VM)_n$-R_F] can react with boric acid to afford the corresponding fluorinated oligomer/silica/boric acid nanocomposites [R_F-$(VM\text{-}SiO_2)_n$-$R_F/B(OH)_3$]. ^{11}B MAS NMR spectra show that these obtained nanocomposites consist of the trigonal boron units and the borate network or unreacted boric acid. The R_F-$(VM\text{-}SiO_2)_n$-$R_F/B(OH)_3$ nanocomposites are effective for the encapsulation of a variety of guest molecules (***Orgs***) such as diphenylsilanediol (DPSDO), 1, 1'-bi-2-naphthol (BINOL), 4, 4'-biphenol, bisphenol A (BPA), bisphenol F (BPF), bisphenol AF (BPAF), biphenyl, dibenzyl, and pentaerythritol (PETERL) into these nanocomposite cores to afford the corresponding fluorinated nanocomposites - encapsulated ***Orgs***. The R_F-$(VM\text{-}SiO_2)_n$-R_F nanocomposites - encapsulated ***Orgs*** were also prepared under similar conditions, for comparison. The R_F-$(VM\text{-}SiO_2)_n$-$R_F/B(OH)_3$ nanocomposites - encapsulated ***Orgs*** were found to exhibit no weight loss behavior corresponding to the contents of the ***Orgs*** in the composites even after calcination at 800 °C; although these nanocomposites were isolated through no purification process. On the other hand,

encapsulated ***Orgs*** in the R_F-(VM-SiO_2)$_n$-R_F nanocomposite cores were found to afford the usual weight loss through the calcination process. ^{11}B MAS NMR spectra of the R_F-(VM-SiO_2)$_n$-R_F/$B(OH)_3$ nanocomposites - encapsulated ***Orgs*** before calcination show the clear signal at around 1 ~ 5 ppm levels which corresponds to the tetragonal boron units formation. The formation of such tetragonal boron units enables the encapsulated ***Orgs*** to afford no weight loss in the nanocomposite cores even after calcination. Therefore, the present R_F-(VM-SiO_2)$_n$-R_F/$B(OH)_3$ nanocomposites may develop as new fluorinated functional materials possessing boron units for providing extremely higher thermal stability for a variety of low molecular weight organic compounds.

References

1) S. Yajima, Y. Hasegawa, K. Okamura, and T. Matsuzawa, *Nature*, **273**, 527 (1978).

2) J. Yajima, K. Hayashi, and K. Okamura, *Nature*, **266**, 521 (1977).

3) D. Devapal, S. Packirisamy, K. J. Sreejith, P. V. Ravindran, and B. K. George, *J. Inorg. Organomet. Polym.*, **20**, 666 (2010).

4) M. A. Schiavon, N. A. Armelin, and I. V. P. Yoshida, *Mater. Chem. Phys.*, **112**, 1047 (2008).

5) J. Pola, N. Herlin-Boime, J. Brus, Z. Bastl, K. Vacek, J. Subrt, and V. Vorlicek, *Solid State Sci.*, **7**, 123 (2005).

6) W. Zhou, Y. Chen, X. Wang, and J. Zhang, *CIESC J.*, **63**, 3365 (2012).

7) A. Klonczynski, G. Scheneider, R. Riedel, and R. Theissmann, *Adv. Eng. Mater.*, **6**, 64 (2004).

8) S. Hoshi, A. Kojima, and S. Otani, *J. Mater. Res.*, **11**, 2536 (1996).

9) R. L. Siqueira, I. V. P. Yoshida, L. C. Pardini, and M. A. Schiavon, *J. Mater. Res.*, **10**, 147 (2007).

10) H. W. Bai, G. Wen, X. X. Huang, Z. X. Han, B. Zhong, Z. X. Hu, and X. D. Zhang, *J. Eur. Ceram. Soc.*, **31**, 931 (2011).

11) R. Pena-Alonso and G. D. Soraru, *J. Sol-Gel Sci. Technol.*, **43**, 313 (2007).

12) H. M. Williams, E. A. Dawson, P. A. Barnes, B. Rand, and R. M. D. Brydson, *Microporous Mesoporus Mater.*, **99**, 261 (2007).

13) S. Hoshii, A. Kojima, H. Endou, S. Otani, T. Satou, Y. Nakaido, and Y. Hasegawa, *Tanso*, 29 (1993).

14) S. Hoshii, A. Kojima, M. Shimoda, S. Otani, T. Satou, Y. Nakaido, and Y. Hasegawa, *Tanso*, 23 (1994).

15) Q. Wang, L. Fu, X. Hu, Z. Zhang, and Z. Xie, *J. Appl. Polym. Sci.*, **99**, 719 (2006).

16) G. D. Soraru, F. Babonneau, C. Gervais, and N. Dallabona, *J. Sol-Gel Sci. Technol.*, **18**, 11 (2000).

17) C. Gervais, F. Babonneau, N. Dallabonna, and G. D. Soraru, *J. Am. Ceram. Soc.*, **84**, 2160 (2001).

18) G. D. Soraru, F. Babonneau, S. Maurina, and J. Vicens, *J. Non-Crystallogr. Solids*, **224**, 173 (1998).

19) W. Stöber, A. Fink, and E. Bohn, *J. Colloid Interface Sci.*, **26**, 62 (1968).

20) V. K. Parashar, J. B. Orham, A. Sayah, M. Cantoni, and M. A. M. Gijs, *Nat. Nanotechnol.*, **3**, 589 (2008).

21) H. Sawada, *Chem. Rev.*, **96**, 1779 (1996).

22) H. Sawada, *Prog. Polym. Sci.*, **32**, 509 (2007).

23) H. Sawada, *Polym. Chem.*, **3**, 46 (2012).

24) H. Sawada, *J. Fluorine Chem.*, **121**, 111 (2003).

25) M. Mugisawa, K. Ohnishi, and H. Sawada, *Langmuir*, **23**, 5848 (2007).

26) M. Mugisawa, R. Kasai, and H. Sawada, *Langmuir*, **25**, 415 (2009).

27) M. Mugisawa and H. Sawada, *Langmuir*, **24**, 9215 (2008).

28) H. Sawada and M. Nakayama, *J. Chem. Soc. Chem. Commun.*, 677 (1991).

29) H. Sawada, Y. Matsuki, Y. Goto, S. Kodama, M. Sugiya, and Y. Nishiyama, *Bull. Chem. Soc. Jpn.*, **83**, 75 (2010).

30) Y. Goto, H. Takashima, K. Takishita, and H. Sawada, *J. Colloid Interface Sci.*, **362**, 375 (2011).

31) Y. Goto, Y. Matsuki, M. Nishida, S. Oyama, K. Chikama, and H. Sawada, *Colloid Polym. Sci.*, **290**, 11 (2011).

32) H. Sawada, M. Kikuchi, and M. Nishida, *J. Polym. Sci. A: Polym. Chem.*, **49**, 1070 (2011).

33) K. Yamada, T. Shimizu, K. Deguchi, S. Ando, H. Kamada, and T. Kobayashi, *Polym. Preprints Jpn.*, **60**, 2D26 (2011).

34) L. S. Du and J. F. Stebbins, *J. Non-Crystallogr. Solids*, **351**, 3508 (2005).

35) S. Sen, Z. Xu, and J. F. Stebbins, *J. Non-Crystallogr. Solids*, **226**, 29 (1998).

36) G. L. Turner, K. A. Smith, R. J. Kirkpatrick, and E. Oldfield, *J. Magn. Res.*, **67**, 544 (1986).

CHAPTER 2

Preparation of Fluoroalkyl End-Capped Vinyltrimethoxysilane Oligomeric Silica/Boric Acid/Poly(*N*-methyl benzamide)-*b*-Poly(propylene oxide) Block Copolymer Nanocomposites – No Weight Loss Behavior of the Block Copolymer in the Nanocomposites even after Calcination at 800 °C

2.1. Introduction

Much attention has been hitherto focused on the polyborosiloxanes, due to their wide applications such as modifiers for thermosetting resins to improve the thermal stability, heat-resistance painting, halogen-free flame retardants, and ceramic precursors.[1 ~ 8] Such higher thermal stability can be attributed to the presence of higher bond energy of B-O and Si-O bonds.[9] In general, polyborosiloxanes can be easily synthesized by the reactions of boric acid with diarylsilanediols or diaryldichlorosilanes.[10 ~ 20] Alkoxysilanes, vinylalkoxysilanes and hydrosilanes are also useful for the synthesis of polyborosiloxanes by using boric acid as a key intermediate.[8, 9, 14, 17] This synthetic method has high potential from the practical applicable point of view, because boric acid is the cheapest source of boron for the synthesis of polyborosiloxanes. A considerable interest has been also devoted to fluorinated polymers, especially, block copolymers containing longer perfluoroalkyl groups, because these fluorinated block copolymers can exhibit a wide variety of unique properties such as surface active characteristic and the self-assembled polymeric aggregates in aqueous and organic media, which cannot be achieved by the corresponding randomly fluoroalkylated polymers.[21, 22] In fact, ABA triblock-type

two fluoroalkyl end-capped oligomers [R_F-$(M)_n$-R_F; R_F = fluoroalkyl groups; M = radical polymerizable hydrocarbon monomers] can form the nanometer size-controlled self-assembled molecular aggregates through the aggregation of the terminal fluoroalkyl segments in aqueous and organic media.[23 ~ 25] These fluorinated oligomeric aggregates can interact with a variety of guest molecules such as silica, titanium oxide, magnetite, hydroxyapatite, gold, silver, copper, zinc oxide, organic dyes, fullerene, and carbon nanotube to afford the corresponding fluorinated oligomeric aggregates/guest molecules nanocomposites.[26 ~ 35] Therefore, it is of particular interest to develop new organoborosiloxanes/fluoroalkyl end-capped oligomeric nanocomposites possessing not only the unique characteristics imparted by the organoborosiloxanes but also the surface active property related to the longer fluoroalkyl groups. However, such studies have been hitherto very limited except for the report on the surface modification of polycarbonate by using cross-linked bisphenol A-based epoxy acrylate resins/polyborosiloxane hybrids containing longer fluoroalkyl chain[36] and our recent work on the preparation of fluoroalkyl end-capped oligomeric silica/boric acid nanocomposites.[37] Low molecular weight aromatic compounds such as diphenylsilanediol, 1, 1'-bi-2-naphthol, bisphenol F, bisphenol AF

and bisphenol A can be encapsulated into these fluoroalkylated composite cores to afford the corresponding fluorinated oligomeric silica/boric acid nanocomposites - encapsulated these aromatic compounds.[37] This chapter shows that thermoplastic aromatic elastomers such as poly(*N*-methyl benzamide)-*b*-polypropylene oxide block copolymers [$(MAB)_{m\text{-}m}$-*b*-PPO_{32}; $m = 5 \sim 8$] can interact with fluoroalkyl end-capped vinyltrimethoxysilane oligomeric silica/boric acid nanocomposites under alkaline conditions to provide the corresponding fluorinated oligomeric silica/boric acid/$(MAB)_{m\text{-}m}$-*b*-PPO_{32} nanocomposites. Interestingly, these obtained nanocomposites were found to exhibit no weight loss behavior corresponding to the contents of the block copolymers in the nanocomposites even after calcination at 800 °C, although the expected nanocomposites were isolated without the purification process. These results will be described in this chapter.

2.2. Experimental

2.2.1 Measurements

Dynamic light scattering (DLS) measurements were measured by using Otsuka Electronics DLS-7000 HL (Tokyo, Japan). Field emission scanning electron micrographs (FE-SEM) were recorded using JEOL JSM-7000F (Tokyo, Japan). Thermal analyses were recorded by raising the temperature around 800 °C (the heating rate: 10 °C/min) under atmospheric conditions by the use of Bruker axs TG-DTA2000SA differential thermobalance (Kanagawa, Japan). Solid state ^{11}B MAS NMR spectra were measured on a Varian 400 NMR system spectrometer (Palo Alto, CA) operated at 100.56 MHz for the ^{13}C nuclei with a Varian 4 mm double-resonance T3 solid probe spun at 15 kHz. Solid state ^{1}H NMR spectra were measured on a Varian 400 NMR system spectrometer (Palo Alto, CA) operated at 399.88 MHz for the ^{1}H nuclei with a Varian 4 mm double-resonance T3 solid probe spun at 15 kHz.

2.2.2. Materials

Boric acid was purchased from Wako Pure Chemical Industries (Osaka, Japan). Vinyltrimethoxysilane was used as received from Dow Corning Toray Co., Ltd. (Tokyo, Japan). Fluoroalkyl end-capped vinyltrimethoxysilane oligomer [R_F-(CH_2-$CHSi(OMe)_3)_n$-R_F: the mixture of dimer and trimer; R_F = $CF(CF_3)OC_3F_7$] was synthesized by the reaction of fluoroalkanoyl peroxide with the corresponding monomer according to the previously reported method.[38] Poly(*N*-methyl benzamide)-*b*-poly(propylene oxide) block copolymers [$(MAB)_{m\text{-}m}$-*b*-PPO_{32}: m = 5 ~ 8] were synthesized according to the procedure reported by Shibasaki et al.[39] Poly(ethersulfone)-*b*-poly(tetrahydrofuran)-*b*-poly(ethersulfone) triblock copolymer (PES-*b*-PTHF-*b*-PES) was synthesized according to the procedure previously reported by Jikei et al..[40]

2.2.3. Preparation of fluoroalkyl end-capped vinyltrimethoxysilane oligomeric silica/boric acid/$(MAB)_{m\text{-}m}$-*b*-PPO_{32} nanocomposites

To a liquid fluoroalkyl end-capped vinyltrimethoxysilane oligomer (735 mg) was added boric acid powder (124 mg). The mixture solution was stirred at room temperature for 5 h to give the transparent viscous colorless solution. The homogeneous tetrahydrofuran solution (3 mL) containing $(MAB)_{5\text{-}5}$-*b*-PPO_{32} (100 mg) and 25 wt% aqueous ammonia solution (0.25 mL) was added to this transparent solution, and was successively stirred at room temperature for 1 day. After the solvent was evaporated off, the obtained product was then dried *in vacuo* at 50 °C for 2 days to afford the expected nanocomposites powders (750 mg). Other fluoroalkyl end-capped vinyltrimethoxysilane oligomeric silica/boric acid/$(MAB)_{m\text{-}m}$-*b*-PPO_{32} (m = 6 ~ 8) nanocomposites were also prepared under similar conditions.

Fluoroalkyl end-capped vinyltrimethoxysilane oligomeric silica/$(MAB)_{m\text{-}m}$-*b*-PPO_{32} nanocomposites were also prepared by the reactions of the corresponding oligomer (735 mg) with the $(MAB)_{m\text{-}m}$-*b*-PPO_{32} block copolymer (100 mg) in tetrahydrofuran (3 mL) in the presence of 25 wt% aqueous ammonia (0.25 mL) under similar conditions.

2.3. Results and discussion

The parent poly(*N*-methyl benzamide)-*b*-poly(propylene oxide) block copolymer [$(MAB)_{m\text{-}m}$-*b*-PPO_{32}; $m = 5$] is a brown-colored film-like polymer at room temperature as illustrated in Scheme 2-1, and this film has a good solubility toward tetrahydrofuran (THF). Thus, the fluoroalkyl end-capped vinyltrimethoxysilane oligomeric silica/boric acid nanocomposites [R_F-$(VM\text{-}SiO_2)_n$-$R_F/B(OH)_3$], which were prepared by the reaction of the corresponding oligomer [R_F-$(CH_2CHSi(OMe)_3)_n$-R_F: R_F-$(VM)_n$-R_F] with boric acid[37], were tried to interact with poly(*N*-methyl benzamide)-*b*-poly(propylene oxide) block copolymer [$(MAB)_{m\text{-}m}$-*b*-PPO_{32}] in THF under alkaline conditions at room temperature as shown in Scheme 2-1.

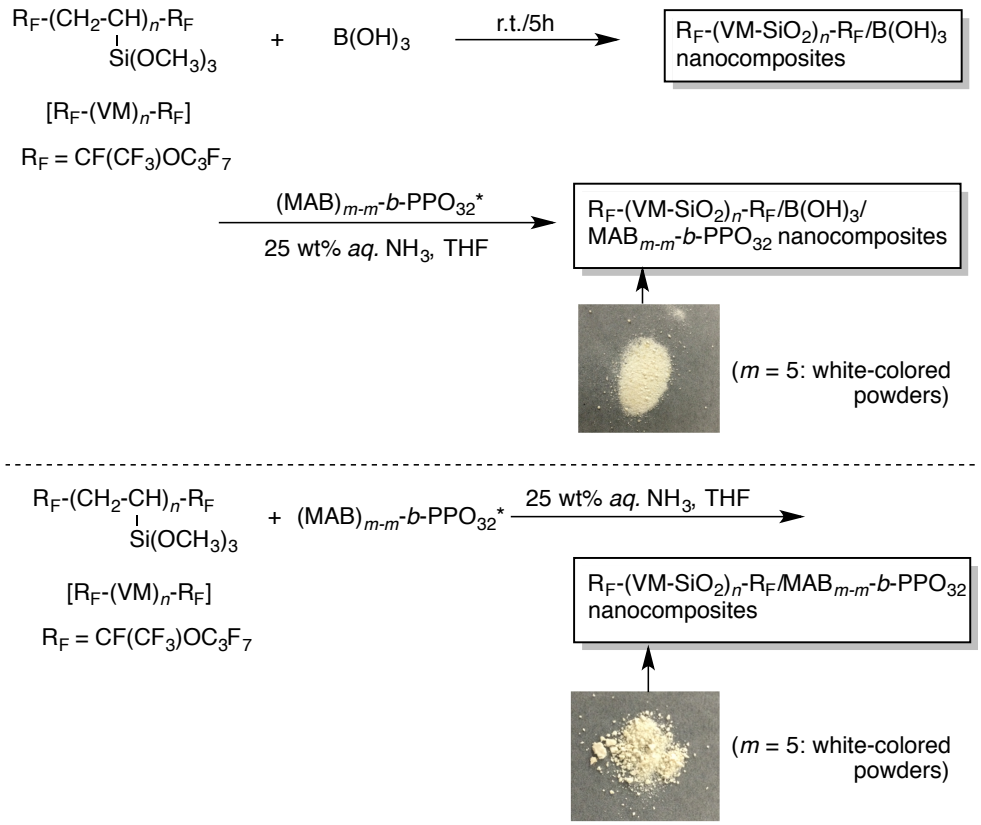

*Poly(*N*-methyl benzamide)-*b*-poly(propylene oxide) block copolymer [$MAB_{m\text{-}m}$-*b*-PPO_{32}]

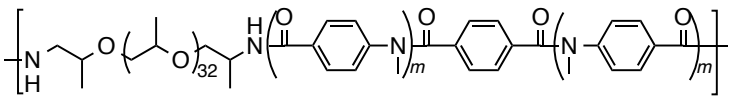

m = 5; Mn = 10,000; *m* = 6; Mn = 9,000; *m* = 7; Mn = 9,400; *m* = 8; Mn = 9,000;

(Brown-colored film)

Scheme 2-1 Preparation of the R_F-$(VM$-$SiO_2)_n$-$R_F/B(OH)_3/(MAB)_{m\text{-}m}$-*b*-$PPO_{32}$ nanocomposites, R_F-$(VM$-$SiO_2)_n$-$R_F/(MAB)_{m\text{-}m}$-*b*-PPO_{32} nanocomposites, and $(MAB)_{m\text{-}m}$-*b*-PPO_{32} block copolymer and each obtained nanocomposites

To the homogenous THF solutions of the $(MAB)_{m\text{-}m}$-*b*-PPO_{32} block copolymer containing 25 wt% ammonia solution was added the viscous R_F-$(VM$-$SiO_2)_n$-$R_F/B(OH)_3$ nanocomposite solution, and were successively stirred at

room temperature for 1 day. After removal of the solvent under reduced pressure at 80 °C, and then dried *in vacuo* to provide the expected white-colored powdery R_F-(VM-SiO_2)$_n$-R_F/$B(OH)_3$/(MAB)$_{m\text{-}m}$-*b*-PPO_{32} composite products (see Scheme 2-1).

As shown in Scheme 2-1 and Table 2-1, the expected R_F-(VM-SiO_2)$_n$-R_F/$B(OH)_3$/(MAB)$_{m\text{-}m}$-*b*-PPO_{32} composites were obtained in 76 ~ 78% isolated yields as white-colored powders. The R_F-(VM-SiO_2)$_n$-R_F/(MAB)$_{m\text{-}m}$-*b*-PPO_{32} composites were also obtained as the white-colored composite powders in similar isolated yields (72 ~ 74 %) (see Scheme 2-1).

Table 2-1 Preparation of R_F-(VM-SiO_2)$_n$-R_F/$B(OH)_3$/$MAB_{m\text{-}m}$-*b*-PPO_{32} nanocomposites

Run	R_F-(VM)$_n$-R_F (mg)	$B(OH)_3$ (mg)	$MAB_{m\text{-}m}$-*b*-PPO_{32} (mg)		Yield[a] (%)	Size of composites[b] (nm) ± STD
1	735	124	*m* = 5	100	78	172.1 ± 20.0
2	735	–		100	72	81.3 ± 9.1
3	735	124	*m* = 6	100	77	89.0 ± 11.6
4	735	–		100	72	36.9 ± 3.8
5	735	124	*m* = 7	100	76	133.0 ± 18.4
6	735	–		100	74	125.7 ± 12.9
7	735	124	*m* = 8	100	76	98.6 ± 14.0
8	735	–		100	73	82.6 ± 7.8
9	735	124		–	77	43.2 ± 7.7

a) Yields are based on R_F-(VM)$_n$-R_F , $B(OH)_3$ and $MAB_{m\text{-}m}$-*b*-PPO_{32} (*m* = 5 ~ 8)
b) Determined by dynamic light scattering (DLS) measurements

The R_F-(VM-SiO_2)$_n$-R_F/$B(OH)_3$/(MAB)$_{m\text{-}m}$-*b*-PPO_{32} composites and the

R_F-(VM-SiO_2)$_n$-R_F/(MAB)$_{m\text{-}m}$-*b*-PPO_{32} composites were found to have good dispersibility toward the traditional organic media such as methanol, THF, 1, 2-dichloroethane, 2-propanol, fluorinated aliphatic solvents (1: 1 mixed solvents (AK-225^{TR}) of 1, 1-dichloro-2, 2, 3, 3, 3-pentafluoropropane and 1, 3-dichloro-1, 2, 2, 3, 3-pentafluoropropane), dimethyl sulfoxide and *N, N*-dimethylformamide except for water. Thus, the average particle size of these composites in THF has been measured, and the results are also shown in Table 2-1.

As shown in Table 2-1, the sizes of the R_F-(VM-SiO_2)$_n$-R_F/(MAB)$_{m\text{-}m}$-*b*-PPO_{32} composites are nanometer size-controlled fine particles from 36.9 (± 3.8) to 126 nm, affording higher values than that (19.6 ± 3.2 nm) of the original R_F-(VM-SiO_2)$_n$-R_F oligomeric nanoparticles, which were prepared by the sol–gel reaction of the corresponding R_F-(VM)$_n$-R_F oligomer under alkaline conditions.[41] Furthermore, an additional increase of the sizes of the R_F-(VM-SiO_2)$_n$-R_F/$B(OH)_3$/(MAB)$_{m\text{-}m}$-*b*-PPO_{32} composites can be observed, compared to the corresponding R_F-(VM-SiO_2)$_n$-R_F/(MAB)$_{m\text{-}m}$-*b*-PPO_{32} composites, suggesting that the composite reactions of the R_F-(VM-SiO_2)$_n$-R_F/$B(OH)_3$ nanocomposites with the block copolymers can proceed smoothly under very mild condition to provide the expected

nanocomposites.

The field emission scanning electron micrographs (FE-SEM) of well-dispersed THF solutions of the R_F-(VM-SiO_2)$_n$-R_F/$B(OH)_3$/(MAB)$_{m\text{-}m}$-*b*-PPO_{32} nanocomposites (Run 1 in Table 2-1) before and after calcination at 800 °C have been measured to clarify the formation of the nanocomposite particles, and the results are shown in Figure 2-1.

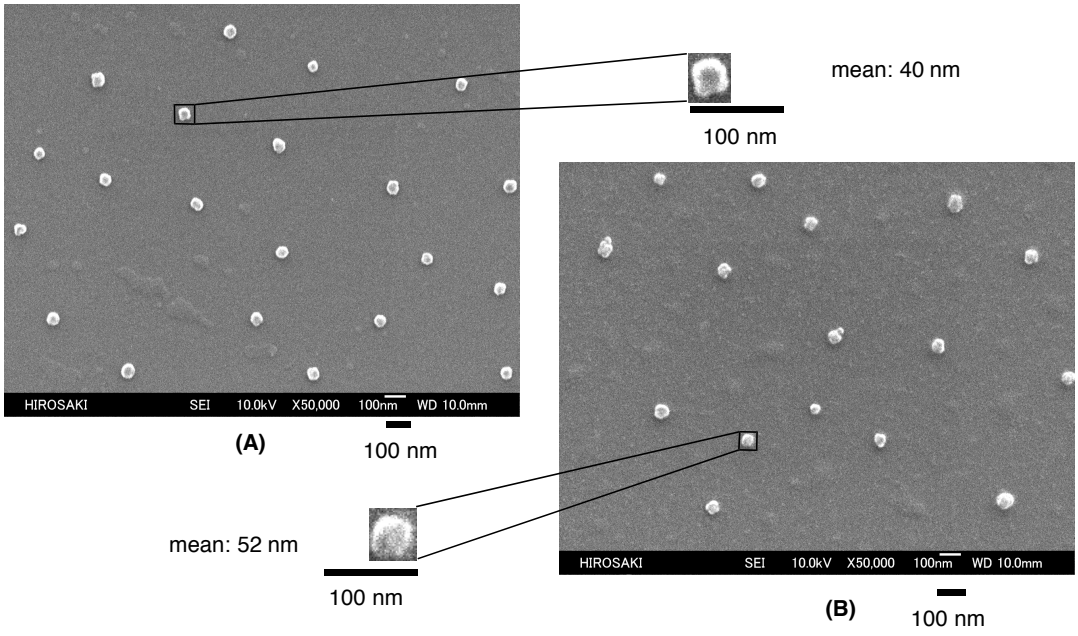

Figure 2-1 FE-SEM (field emission scanning electron microscopy) images of R_F-(VM-SiO_2)$_n$-R_F/$B(OH)_3$/$MAB_{5\text{-}5}$-*b*-PPO_{32} nanocomposites (Run 1 in Table 2-1) in THF solutions (Run 1). **(A)** before calcination at 800 ºC, **(B)** after calcination at 800 ºC.

Electron micrographs also showed the formation of fluorinated very fine

nanoparticles with a mean diameter of 40 nm before calcination (see Figure 2-1-(**A**)), and the similar size value (52 nm) was also observed even after calcination at 800 °C (see Figure 2-1-(**B**)). This finding suggests that the present nanocomposites would have a good thermal stability. Thus, the thermal stability of the nanocomposites illustrated in Table 1 was tried to study by the use of thermogravimetric analyses (TGA), in which the weight loss of the nanocomposites was measured by raising the temperature at around 800 °C at a 10 °C/min heating rate under air atmospheric conditions, and the results are shown in Figure 2-2.

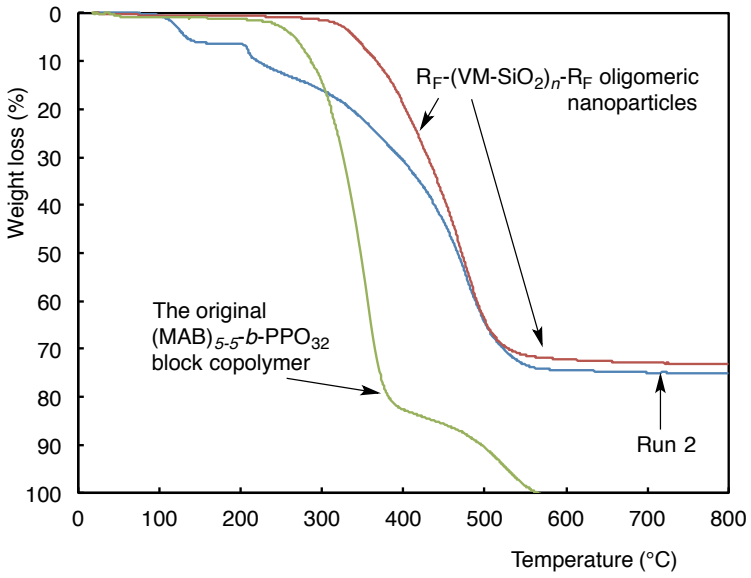

Figure 2-2 Thermogravimetric analyses (TGA) of the R_F-(VM-SiO_2)$_n$-R_F/(MAB)$_{5\text{-}5}$-*b*-PPO_{32} nanocomposites (Run 2 in Table 2-1), the R_F-(VM-SiO_2)$_n$-R_F oligomeric nanoparticles, and the original (MAB)$_{5\text{-}5}$-*b*-PPO_{32} block copolymer.

Figure 2-2 shows the TGA curves of the R_F-(VM-SiO_2)$_n$-R_F oligomeric nanoparticles, the original (MAB)$_{5\text{-}5}$-*b*-PPO_{32} block copolymer and the R_F-(VM-SiO_2)$_n$-R_F/(MAB)$_{5\text{-}5}$-*b*-PPO_{32} nanocomposites (Run 2 in Table 2-1), respectively.

The weight of the parent (MAB)$_{5\text{-}5}$-*b*-PPO_{32} block copolymer markedly dropped around 250 °C and decomposed gradually, reaching 100 % weight loss at around 560 °C. The R_F-(VM-SiO_2)$_n$-R_F oligomeric nanoparticles can start the weight loss from around 400 °C to afford the 73 % weight loss at 800 °C in proportion to the content of the organic moieties in the nanoparticles. The R_F-(VM-SiO_2)$_n$-R_F/(MAB)$_{5\text{-}5}$-*b*-PPO_{32} nanocomposites (Run 2 in Table 2-1) have been isolated without purification process; however, this nanocomposite cannot afford the clear weight loss corresponding to the content of the copolymer in the composites even after calcination at 800 °C. Because, the similar weight loss value (75 %) to that (73 %) of the original R_F-(VM-SiO_2)$_n$-R_F oligomeric nanoparticles was observed as shown in Figure 2-2. DTA (differential thermal analyses) curve of the R_F-(VM-SiO_2)$_n$-R_F/(MAB)$_{5\text{-}5}$-*b*-PPO_{32} nanocomposites shows a clear exothermic peak at around 210 °C (see Figure 2-3), which would be attributed to the dehydration or the

demethanolification related to the ≡Si–OH or ≡Si–OMe units in the composites to form the additional siloxane networks in the nanocomposites during the calcination process. This exothermic peak corresponds to the weight loss at around 210 °C, of whose value would be in proportion to the relatively higher weight loss (75 %) at 800 °C than that (73 %) of the original R_F-(VM-SiO_2)$_n$-R_F oligomeric nanoparticles. In addition, such weight loss at around 110 ~ 210 °C is not observed at all in the parent (MAB)$_{5\text{-}5}$-*b*-PPO_{32} block copolymer, indicating that the corresponding block copolymer should exhibit no weight loss behavior in the fluorinated oligomeric silica nanocomposite cores.

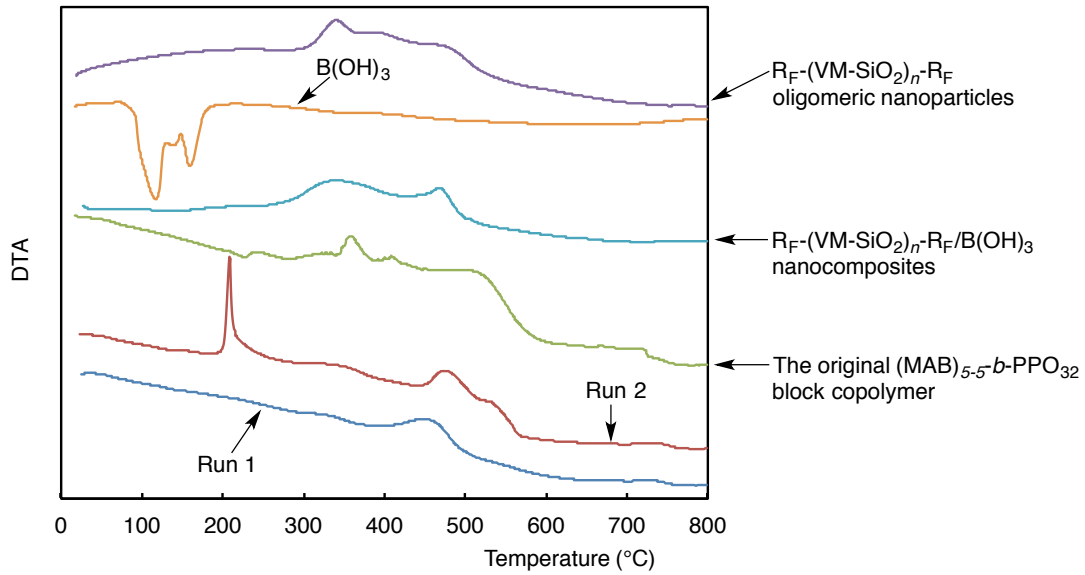

Figure 2-3 Differential thermal analyses (DTA) of the R_F-(VM-SiO_2)$_n$-R_F/$B(OH)_3$/(MAB)$_{5\text{-}5}$-*b*-PPO_{32} nanocomposites (Run 1 in Table 2-1), the R_F-(VM-SiO_2)$_n$-R_F/(MAB)$_{5\text{-}5}$-*b*-PPO_{32} nanocomposites (Run 2 in Table 2-1), the original (MAB)$_{5\text{-}5}$-*b*-PPO_{32} block copolymer, the R_F-(VM-SiO_2)$_n$-R_F/$B(OH)_3$ nanocomposites (Run 9 in Table 2-1), the R_F-(VM-SiO_2)$_n$-R_F oligomeric nanoparticles, and original $B(OH)_3$

The thermal stability of the R_F-(VM-SiO_2)$_n$-R_F/$B(OH)_3$/(MAB)$_{5\text{-}5}$-*b*-PPO_{32} nanocomposites (Run 1 in Table 2-1) have been also studied under similar conditions. Thermal stability of the R_F-(VM-SiO_2)$_n$-R_F/$B(OH)_3$ nanocomposites (Run 9 in Table 2-1), the original (MAB)$_{5\text{-}5}$-*b*-PPO_{32} block copolymer and the parent boric acid were also studied, for comparison. These TGA curves are illustrated in Figure 2-4.

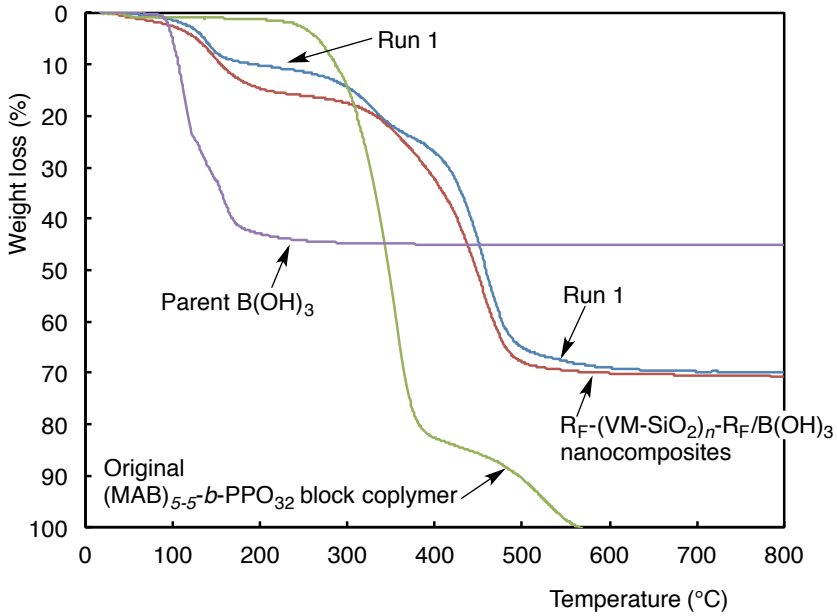

Figure 2-4 Thermogravimetric analyses (TGA) of the R_F-(VM-SiO_2)$_n$-R_F/$B(OH)_3$/(MAB)$_{5\text{-}5}$-*b*-PPO_{32} nanocomposites (Run 1 in Table 2-1), the R_F-(VM-SiO_2)$_n$-R_F/$B(OH)_3$ nanocomposites (Run 9 in Table 2-1), the parent $B(OH)_3$, and the original (MAB)$_{5\text{-}5}$-*b*-PPO_{32} block copolymer.

Of particular interest, the R_F-(VM-SiO_2)$_n$-R_F/$B(OH)_3$/(MAB)$_{5\text{-}5}$-*b*-PPO_{32} nanocomposites (Run 1 in Table 2-1) were found to exhibit no weight loss behavior corresponding to the content of the block copolymer even after calcination at 800 °C, although this nanocomposite was isolated without purification process. This weight loss value (70 %) is quite similar to that (71 %) of the R_F-(VM-SiO_2)$_n$-R_F/$B(OH)_3$ nanocomposites at 800 °C. The clear weight loss at around 100 ~ 200 °C was observed in the R_F-(VM-SiO_2)$_n$-R_F/$B(OH)_3$/(MAB)$_{5\text{-}5}$-*b*-PPO_{32} nanocomposites and the R_F-(VM-SiO_2)$_n$-R_F/$B(OH)_3$ nanocomposites (see Figure 2-4). TGA curve of the original boric acid [$B(OH)_3$] in Figure 2-4 shows the clear weight loss related to the

formation of the metaboric acid (HBO_2) and boron trioxide (B_2O_3) by the dehydration during the calcination process. This dehydration corresponds to the clear endothermic peaks at around 100 ~ 200 °C illustrated in Figure 2-3. Thus, such weight loss behavior in these nanocomposites would be attributed to dehydration related to the boric acid moieties [~$B(OH)_n$; n = 1 or 2] in the nanocomposites.

To confirm the presence of the block copolymers in the R_F-$(VM\text{-}SiO_2)_n$-R_F/$(MAB)_{5\text{-}5}$-*b*-PPO_{32} nanocomposites (Run 2 in Table 2-1) before and after calcination at 800 °C, ^{1}H MAS NMR spectra of these nanocomposites have been studied. The results are shown in Figure 2-5.

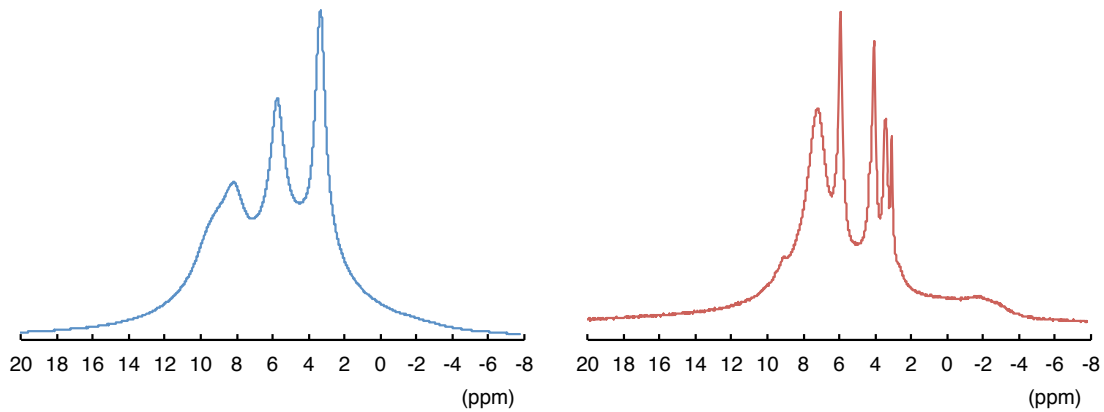

(**A**): Before calcination at 800 °C

(**B**): After calcination at 800 °C

Figure 2-5 ^{1}H Magic-angle spinning (MAS) NMR spectra of the R_F-$(VM\text{-}SiO_2)_n$-R_F/$(MAB)_{5\text{-}5}$-*b*-PPO_{32} nanocomposites (Run 2 in Table 2-1) before (**A**) and after (**B**) calcination at 800 °C.

As shown in Figure 2-5-(**A**), the clear peaks around 3 ~ 8 ppm related to the block copolymer in the nanocomposites before calcination were observed. Interestingly, similar NMR signals to those before calcination were also observed at around 3 ~ 7 ppm related to the copolymer in the nanocomposites even after calcination at 800 °C (see Figure 2-5-(**B**)). These findings suggest that the $(MAB)_{5\text{-}5}$-*b*-PPO_{32} block copolymer should afford no weight loss behavior in the R_F-$(VM\text{-}SiO_2)_n$-R_F nanocomposite cores.

The thermal stability of the other nanocomposites illustrated in Table 2-1 have been studied, and the weight loss values of these composites at 800 °C are shown in Figure 2-6. The weight loss values of the original $(MAB)_{m\text{-}m}$-*b*-PPO_{32} copolymers (*m* = 6, 7, and 8) and the R_F-$(VM\text{-}SiO_2)_n$-R_F oligomeric nanoparticles at 800 °C are also shown in Figure 2-6, for comparison.

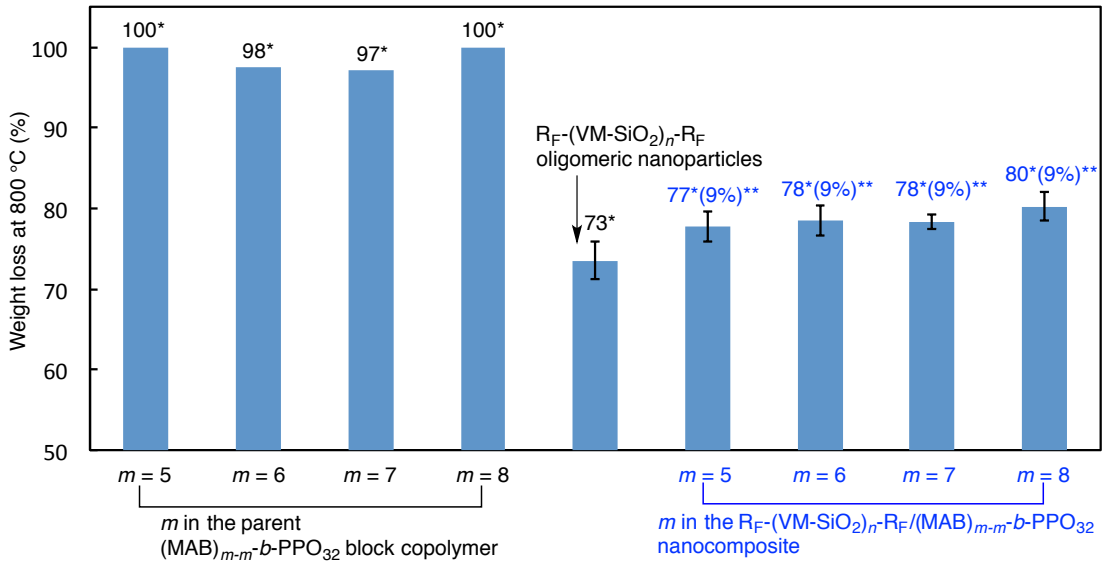

Figure 2-6 Weight loss values at 800 °C of the R_F-(VM-SiO_2)$_n$-R_F/(MAB)$_{m\text{-}m}$-*b*-PPO_{32} nanocomposites, the parent (MAB)$_{m\text{-}m}$-*b*-PPO_{32} block copolymer, and the R_F-(VM-SiO_2)$_n$-R_F oligomeric nanoparticles after calcination at 800 °C. *Weight loss value at 800 °C. **Theoretical contents of (MAB)$_{m\text{-}m}$-*b*-PPO_{32} in nanocomposite (%).

Figure 2-6 shows that the original (MAB)$_{m\text{-}m}$-*b*-PPO_{32} copolymers (*m* = 5, 6, 7, and 8) have 97 ~ 100 % weight loss values at 800 °C, and the weight loss value of the parent R_F-(VM-SiO_2)$_n$-R_F oligomeric nanoparticles is 73 %. As indicated before, the R_F-(VM-SiO_2)$_n$-R_F/(MAB)$_{5\text{-}5}$-*b*-PPO_{32} nanocomposites have a similar weight loss value (77 %) to that (73 %) of the original R_F-(VM-SiO_2)$_n$-R_F nanoparticles, providing no weight loss behavior toward the corresponding block copolymer. However, the weight loss values were found to increase from 77 to 80 % with the increase of the ratios: *m* of the poly(*N*-methyl benzamide) units in block copolymer from 6 to 8, although the molecular weight (M_n) of these block copolymers is almost the same

(9000 ~ 10000) illustrated in Scheme 2-1. Thus, it is suggested that higher ratios of the poly(*N*-methyl benzamide) units could increase slightly the weight loss values corresponding to the block copolymers in the nanocomposite cores. The present $(MAB)_{m\text{-}m}$-*b*-PPO_{32} block copolymers have hard and soft segments in the same polymer chain, and hard segment corresponds to the poly(*N*-methyl benzamide) units. Thus, the block copolymers possessing higher ratios: $m = 6 \sim 8$ of hard segments are not likely to interact with the R_F-$(VM\text{-}SiO_2)_n$-R_F nanocomposite cores in the nanocomposite reactions illustrated in Scheme 2-1, affording higher weight loss values than that of the block copolymer ($m = 5$). From these findings, it is strongly suggested that the introduction of the reinforcing filler such as boric acid into the R_F-$(VM\text{-}SiO_2)_n$-R_F nanocomposite cores should improve the thermal stability of the nanocomposites through the effective interaction of the hard segment in the block copolymers with the nanocomposites.

In fact, as shown in Figures 2-4 and 2-7, it was demonstrated that the R_F-$(VM\text{-}SiO_2)_n$-R_F/$B(OH)_3$/$(MAB)_{m\text{-}m}$-*b*-PPO_{32} nanocomposites ($m = 5 \sim 8$) can give no weight loss behavior corresponding to the block copolymers in the composites, although these nanocomposites were isolated without purification process. Because it

can be observed the lower weight loss values (70 %) except for m = 6 or 8 at 800 °C to that (71 %) of the original R_F-(VM-SiO_2)$_n$-R_F/$B(OH)_3$ nanocomposites in each case. In this way, it was clarified that boric acid units can afford no weight loss characteristic toward the block copolymers in the fluorinated oligomeric silica nanocomposite cores.

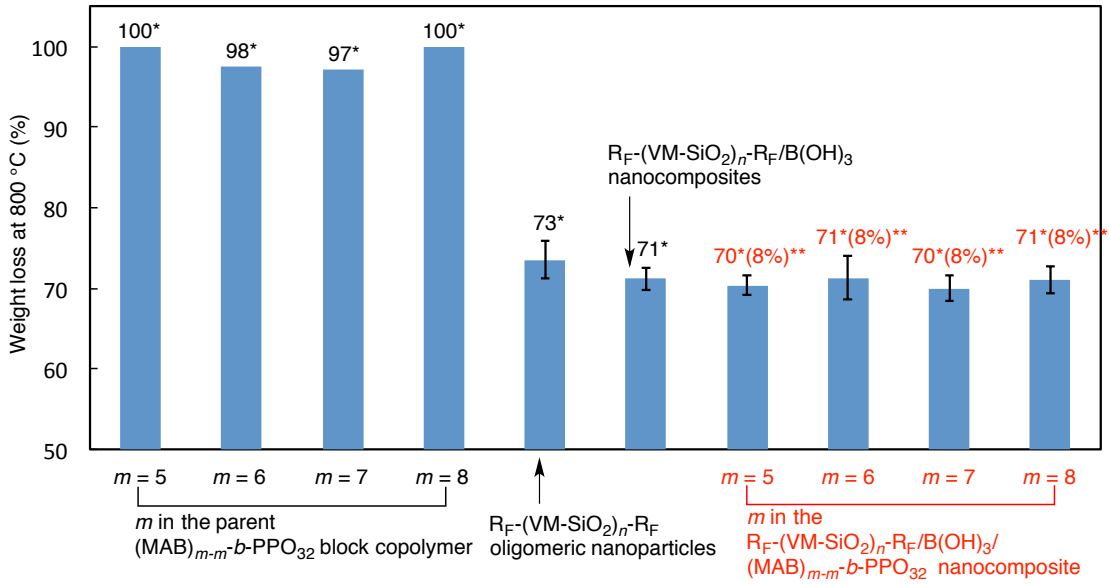

Figure 2-7 Weight loss values at 800 °C of the R_F-(VM-SiO_2)$_n$-R_F/$B(OH)_3$/(MAB)$_{m\text{-}m}$-*b*-PPO_{32} nanocomposites, the parent (MAB)$_{m\text{-}m}$-*b*-PPO_{32} block copolymer, the original R_F-(VM-SiO_2)$_n$-R_F/$B(OH)_3$ nanocomposites, and the R_F-(VM-SiO_2)$_n$-R_F oligomeric nanoparticles after calcination at 800 °C. *Weight loss value at 800 °C. **Theoretical contents of (MAB)$_{m\text{-}m}$-*b*-PPO_{32} in nanocomposite.

In order to clarify such no weigh loss characteristic toward the block copolymers, ^{1}H MAS NMR spectra of the R_F-(VM-SiO_2)$_n$-R_F/$B(OH)_3$/(MAB)$_{5\text{-}5}$-*b*-PPO_{32} nanocomposites before and after calcination at 800 °C have been studied, and these results are shown in Figure 2-8.

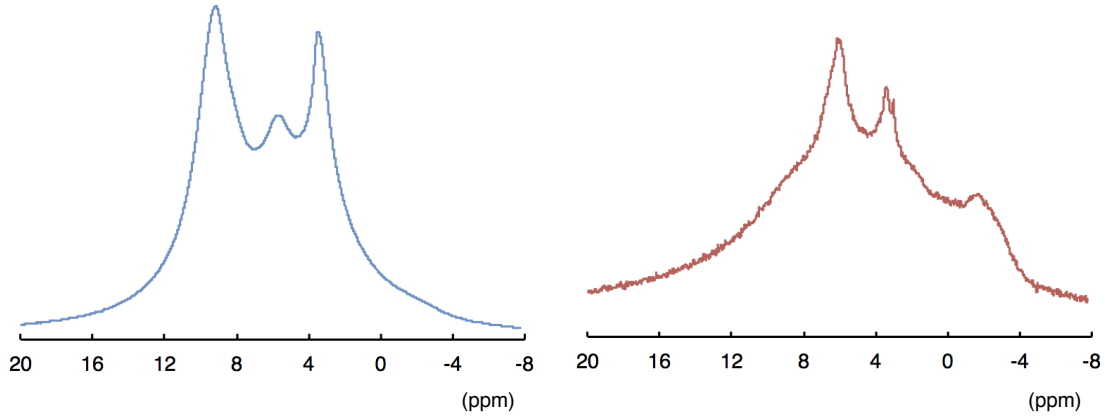

(**A**) Before calcination at 800 °C (**B**) After calcination at 800 °C

Figure 2-8 ^{1}H Magic-angle spinning (MAS) NMR spectra of the R_F-(VM-SiO_2)$_n$-R_F/$B(OH)_3$/$MAB_{5\text{-}5}$-*b*-PPO_{32} nanocomposites (Run 1 in Table 2-1) before (**A**) and after (**B**) calcination at 800 °C.

As shown in Figures 2-8-(**A**) and -(**B**), the similar ^{1}H NMR signals related to the presence of the block copolymer before and even after calcination at 800 °C can be observed, indicating that the block copolymer can supply no weight loss property even after calcination in the nanocomposite cores.

Furthermore, ^{11}B MAS NMR spectra of the R_F-(VM-SiO_2)$_n$-R_F/$B(OH)_3$/ $(MAB)_{5\text{-}5}$-*b*-PPO_{32} nanocomposites before and after calcination at 800 °C have been studied, and the results are shown in Figure 2-9.

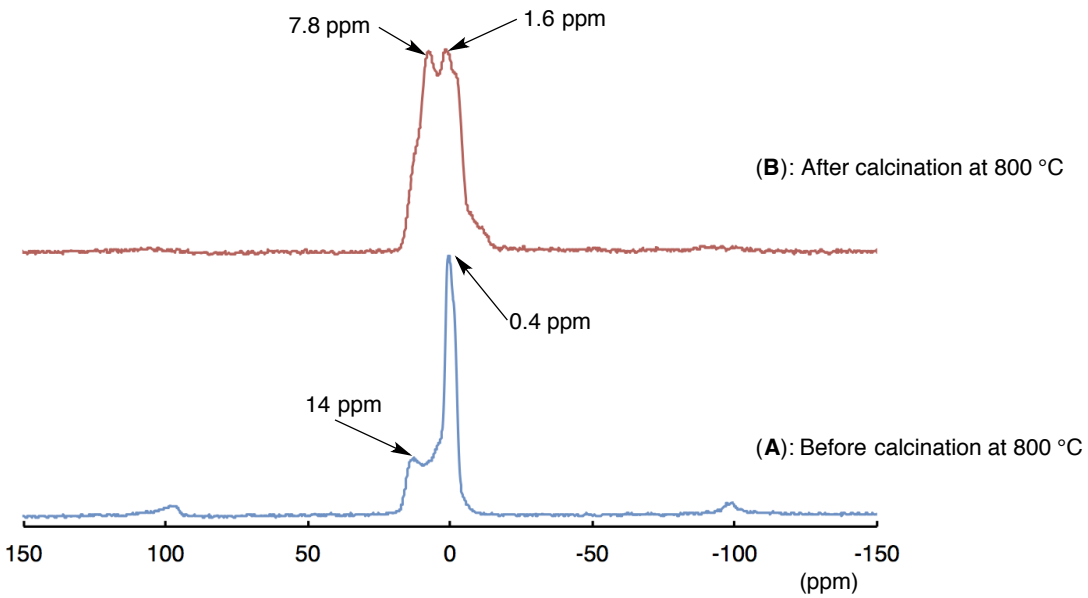

Figure 2-9 ^{11}B Magic-angle spinning (MAS) NMR spectra of the R_F-(VM-SiO_2)$_n$-R_F/$B(OH)_3$/(MAB)$_{5\text{-}5}$-*b*-PPO_{32} nanocomposites (Run 1 in Table 2-1) before (**A**) and after (**B**) calcination at 800 °C

^{11}B MAS NMR spectra show that the R_F-(VM-SiO_2)$_n$-R_F/$B(OH)_3$/(MAB)$_{5\text{-}5}$-*b*-PPO_{32} nanocomposites before calcination show two clear signals at 14 ppm and 0.4 ppm, of whose peaks are attributed to the presence of the trigonal boron units (> B-)[14, 42, 43] and the tetrahedral boron units (> B <)[44 ~ 47], respectively (see Figure 2-9-(A)). Especially, the formation of the tetrahedral boron units in the nanocomposites could induce no weight loss characteristic toward the block copolymers through the interaction of the boron units with the amide moieties corresponding to the hard segments in the block copolymer. Such effective interaction would lead the tetrahedral boron units to give no weight loss behavior toward the

block copolymers. However, the relatively broad doublet peak at 4.7 ppm related to the trigonal boron units after calcination can be observed as shown in Figure 2-9-(**B**), suggesting that the tetrahedral boron units in the composites will be consumed during the calcination process.

Poly(*N*-methyl benzamide)-*b*-poly(propylene oxide) block copolymers compose of hard and soft segments, of whose hard segment corresponds to the poly(*N*-methyl benzamide) units in copolymers. Especially, it was demonstrated that the poly(*N*-methyl benzamide) units in block copolymer (m = 5) should interact with the fluorinated oligomeric silica nanocomposites to afford no weight loss characteristic even after calcination. It is well known that fluoroalkyl end-capped oligomers possessing amide protons such as fluoroalkyl end-capped *N*-(1,1-dimethyl-3-oxobutyl)acrylamide oligomer [R_F-($CH_2CHC(=O)NHCMe_2CH_2C(=O)Me)_n$-$R_F$: R_F = $CF(CF_3)OC_3F_7$] and fluoroalkyl end-capped *N*-isopropylacrylamide oligomer [R_F-($CH_2CHC(=O)NHiPr)_n$-R_F] can undergo the sol–gel reaction in the presence of silica nanoparticles and tetraethoxysilane under alkaline conditions to afford the corresponding fluorinated oligomers/silica nanocomposites.[48 ~ 55] These fluorinated oligomeric silica nanocomposites were also reported to provide no weight loss

behavior corresponding to the contents of oligomers even after calcination at 800 °C.[48 ~ 55] In contrast, fluoroalkyl end-capped oligomers possessing no amide protons such as fluoroalkyl end-capped *N, N*-dimethylacrylamide oligomer [R_F-($CH_2CHC(=O)NMe_2)_n$-R_F] can give a usual weight loss corresponding to the oligomers in the silica nanocomposite cores.[55] Therefore, the present $(MAB)_{m\text{-}m}$-*b*-PPO_{32} block copolymers have high potential for providing the good thermal stability in the fluorinated silica nanocomposite, especially, in the fluorinated silica/boric acid nanocomposite cores, owing to their possessing amide protons as a useful functional units in the block polymers.

To confirm such unique characteristic of the block copolymers in the R_F-($VM\text{-}SiO_2)_n$-R_F nanocomposite cores or in the R_F-($VM\text{-}SiO_2)_n$-R_F/$B(OH)_3$ nanocomposite cores, the other block copolymer which consists of poly(ether sulfone) and poly(tetrahydrofuran) as hard and soft segments, respectively, has been applied to the similar composite reactions.

In fact, as shown in Scheme 2-2, the composite reactions of the R_F-($VM\text{-}SiO_2)_n$-R_F/$B(OH)_3$ nanocomposites with the poly(ether sulfone)-*b*-poly(tetrahydrofuran)-*b*-poly(ether sulfone) triblock copolymer (PES-*b*-PTHF-*b*-PES)

have been tried under similar conditions to that of Scheme 2-1.

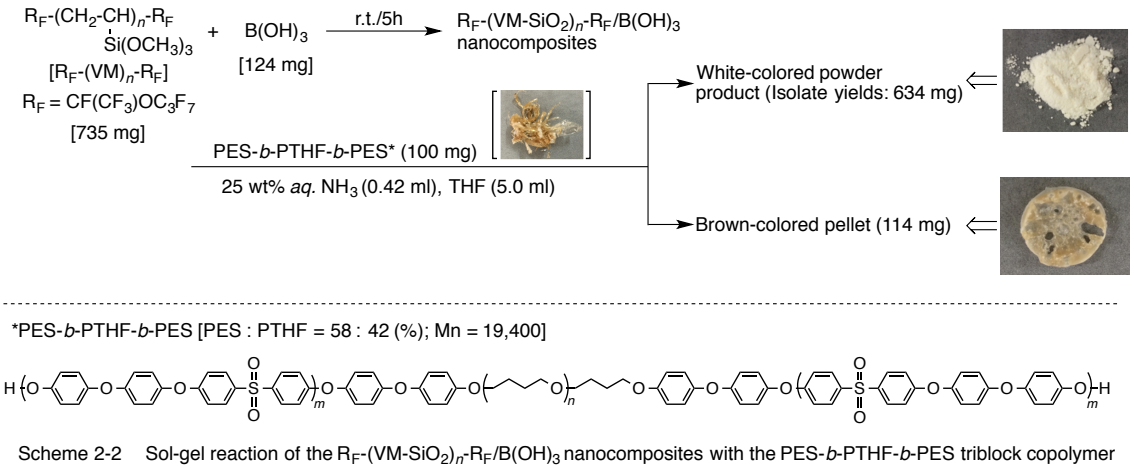

*PES-*b*-PTHF-*b*-PES [PES : PTHF = 58 : 42 (%); Mn = 19,400]

Scheme 2-2 Sol-gel reaction of the R_F-(VM-SiO_2)$_n$-R_F/$B(OH)_3$ nanocomposites with the PES-*b*-PTHF-*b*-PES triblock copolymer under alkaline conditions and the photograph of the isolated two-kinds of phase-separated composites.

The original PES-*b*-PTHF-*b*-PES triblock copolymer has a good solubility toward THF. Thus, the homogeneous THF solution containing PES-*b*-PTHF-*b*-PES triblock copolymer and aqueous ammonia was added to the R_F-(VM-SiO_2)$_n$-R_F/ $B(OH)_3$ nanocomposite viscous colorless THF solution to cause the sol-gel reaction. After stirring the solution at room temperature for 1 day, the solvent was evaporated off, and the obtained product was dried *in vacuo* at 50 °C for 2 days to afford the two kinds of phase-separated composites: one is white-colored powders and the other is brown-colored pellet as illustrated in Scheme 2-2. In order to clarify these two-kinds of composites, the TG-DTA measurements of these composites have been studied, and

the results are shown in Figures 2-10 and 2-11.

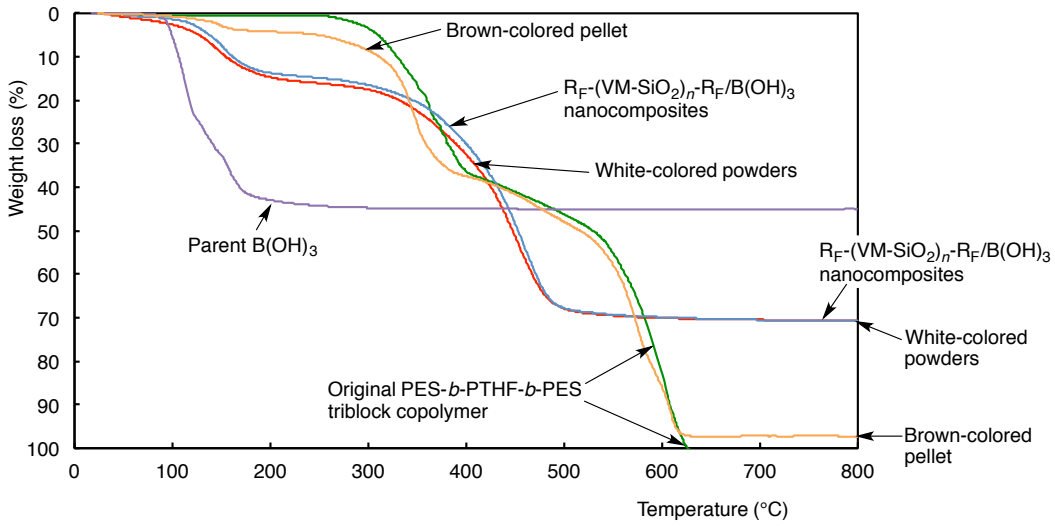

Figure 2-10 Thermogravimetric analyses (TGA) of the isolated products (brown-colored pellet and white colored powders) by the reaction of the R_F-(VM-SiO_2)$_n$-R_F/$B(OH)_3$ nanocomposites with the PES-*b*-PTHF-*b*-PES triblock copolymer, the R_F-(VM-SiO_2)$_n$-R_F/$B(OH)_3$, the parent $B(OH)_3$, and the original PES-*b*-PTHF-*b*-PES triblock copolymer.

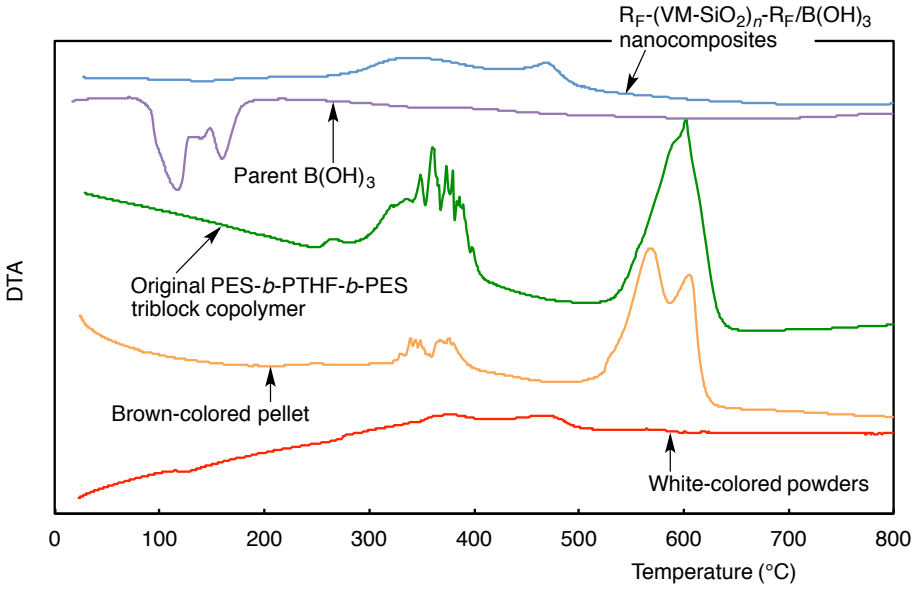

Figure 2-11 Differential thermal analyses (DTA) of the isolated products (brown-colored pellet and white-colored powders) by the reaction of the R_F-(VM-SiO_2)$_n$-R_F/$B(OH)_3$ nanocomposites with the PES-*b*-PTHF-*b*-PES triblock copolymer, the R_F-(VM-SiO_2)$_n$-R_F/$B(OH)_3$ nanocomposites, the parent $B(OH)_3$, and the original PES-*b*-PTHF-*b*-PES triblock copolymer.

The original PES-*b*-PTHF-*b*-PES triblock copolymer has a perfect weight loss at around 620 °C, and the isolated brown-colored pellet, which were derived from the interaction of the triblock copolymer with the R_F-(VM-SiO_2)$_n$-R_F/$B(OH)_3$ nanocomposites, shows the quite similar TGA and DTA curves to those of the original triblock copolymer (see Figures 2-10 and 2-11). In addition, the isolated white-colored powders also have the quite similar TGA and DTA curves to those of the R_F-(VM-SiO_2)$_n$-R_F/$B(OH)_3$ nanocomposites.

A similar result was observed in the case of the composite reaction of R_F-(VM)$_n$-R_F oligomer with the triblock copolymer under alkaline conditions as shown in Scheme 2-3. The isolated pellet and white colored powders afforded the similar TGA and DTA curves to those of the parent triblock copolymers and the R_F-(VM-SiO_2)$_n$-R_F oligomeric nanoparticles, respectively (see Figures 2-12 and 2-13). Lower weight loss value (87 %) of the pellet at 800 °C than that of the original triblock copolymer would be due to the presence of the R_F-(VM-SiO_2)$_n$-R_F oligomeric nanoparticles in the pellet. The higher weight loss value (79 %) of the isolated powders, compared to that (73 %) of the R_F-(VM-SiO_2)$_n$-R_F oligomeric nanoparticles, would be attributed to the dehydration or the demethanolification related to the

residual ≡Si–OH or ≡Si–OMe in the fluorinated oligomeric silica nanoparticles as illustrated in the TGA curve in Run 2 in Figure 2-3.

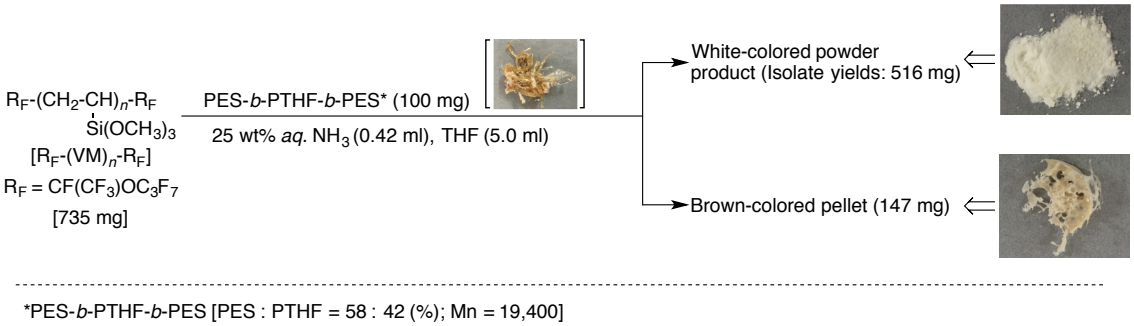

Scheme 2-3 Sol-gel reaction of the R_F-$(VM)_n$-R_F oligomer with the PES-*b*-PTHF-*b*-PES triblock copolymer under alkaline conditions and the isolated two-kinds of phase-separated composites.

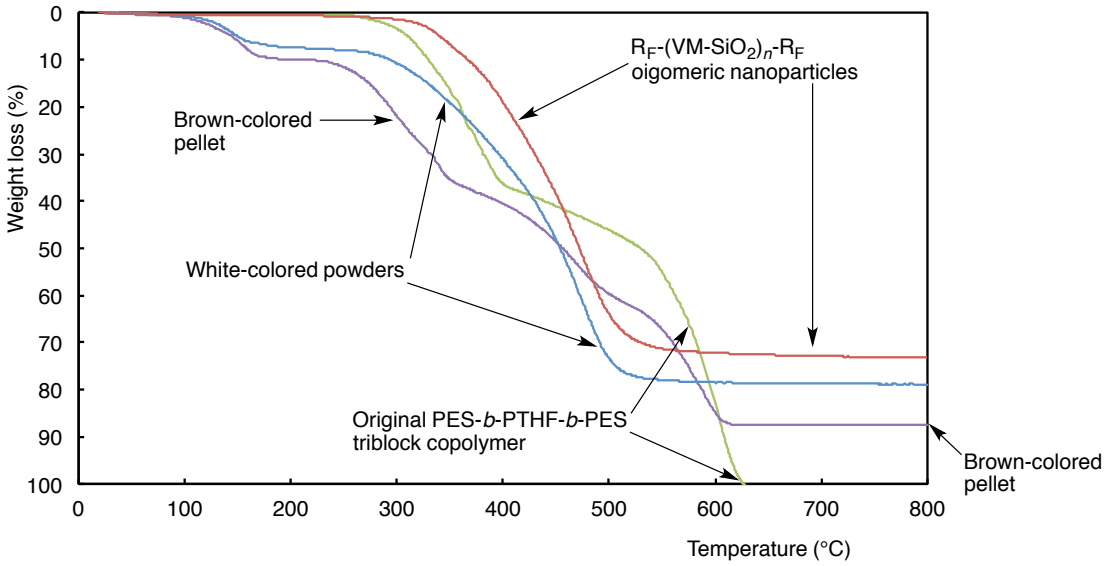

Figure 2-12 Thermogravimetric analyses (TGA) of the isolated products (brown-colored pellet and white colored powders) by the reaction of the R_F-$(VM)_n$-R_F oligomer with the PES-*b*-PTHF-*b*-PES triblock copolymer, the R_F-$(VM\text{-}SiO_2)_n$-R_F oligomeric nanoparticles, and the original PES-*b*-PTHF-*b*-PES triblock copolymer.

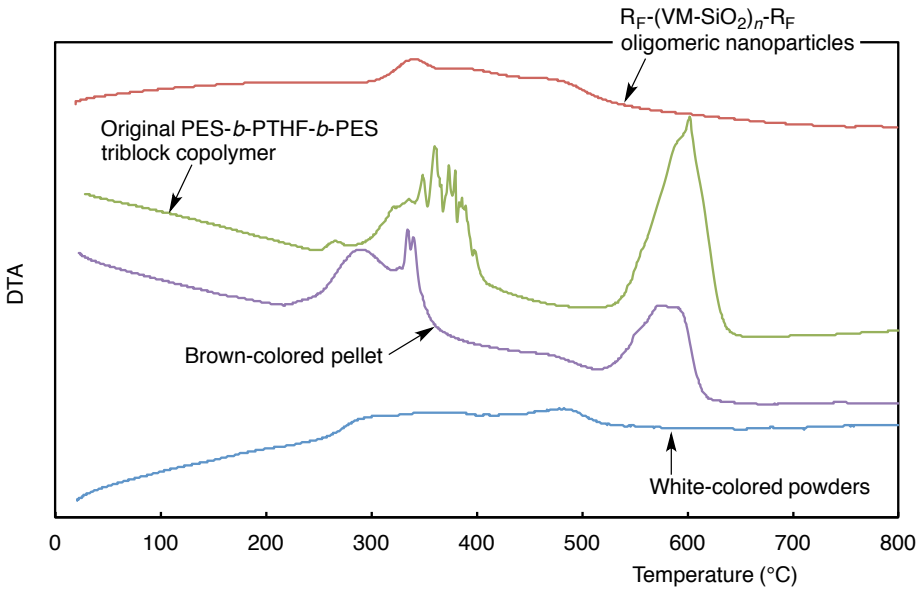

Figure 2-13 Differential thermal analyses (DTA) of the isolated products (brown-colored pellet and white-colored powders) by the reaction of the R_F-(VM)$_n$-R_F oligomer with the PES-*b*-PTHF-*b*-PES triblock copolymer, the R_F-(VM-SiO_2)$_n$-R_F oligomeric nanoparticles, and the original PES-*b*-PTHF-*b*-PES triblock copolymer.

These finding suggest that since the PES-*b*-PTHF-*b*-PES triblock copolymer has no amide protons, quite different from the (MAB)$_{m\text{-}m$-*b*-PPO_{32} block copolymers, this triblock block copolymer is not likely to interact with the R_F-(VM-SiO_2)$_n$-R_F/$B(OH)_3$ nanocomposites or the R_F-(VM-SiO_2)$_n$-R_F nanocomposites during their sol-gel reactions to produce the expected fluoroalkylated oligomeric silica/boric acid/triblock copolymer nanocomposites or the fluorinated oligomeric silica/triblock copolymer nanocomposites.

2.4. Conclusion

Fluoroalkyl end-capped vinyltrimethoxysilane oligomeric silica/boric acid/$(MAB)_{m\text{-}m}$-*b*-PPO_{32} nanocomposites [R_F-$(VM\text{-}SiO_2)_n$-R_F/$B(OH)_3$/$(MAB)_{m\text{-}m}$-*b*-PPO_{32}; m = 5 ~ 8] were prepared by the sol–gel reaction of the corresponding nanocomposites [R_F-$(VM\text{-}SiO_2)_n$-R_F/$B(OH)_3$] with the $(MAB)_{m\text{-}m}$-*b*-PPO_{32} block copolymers [poly(*N*-methyl benzamide)-*b*-poly(propylene oxide) block copolymers] under alkaline conditions. Similarly, the fluoroalkyl end-capped vinyltrimethoxysilane oligomeric silica/$(MAB)_{m\text{-}m}$-*b*-PPO_{32} nanocomposites [R_F-$(VM\text{-}SiO_2)_n$-R_F/$(MAB)_{m\text{-}m}$-*b*-PPO_{32}] were also prepared by the sol–gel reactions of fluoroalkyl end-capped vinyltrimethoxysilane oligomer [R_F-$(VM)_n$-R_F oligomer] with the $(MAB)_{m\text{-}m}$-*b*-PPO_{32} block copolymers under alkaline conditions, for comparison. These two kinds of nanocomposites were isolated without purification process. In the R_F-$(VM\text{-}SiO_2)_n$-R_F/$(MAB)_{m\text{-}m}$-*b*-PPO_{32} nanocomposites (m = 5, 6, 7, and 8) thus obtained, only R_F-$(VM\text{-}SiO_2)_n$-R_F/$(MAB)_{5\text{-}5}$-*b*-PPO_{32} nanocomposites were found to exhibit no weight loss corresponding to the content of the block copolymer in the composites after calcination at 800 °C. However, the R_F-$(VM\text{-}SiO_2)_n$-R_F/$B(OH)_3$/

$(MAB)_{m\text{-}m}$-*b*-PPO_{32} (*m* = 5 ~ 8) nanocomposites were able to provide no weight loss behavior corresponding to the contents of these block copolymers in the nanocomposites even after calcination at 800 °C. ^{1}H MAS NMR spectra showed the clear NMR signals related to the presence of the block copolymer in the R_F-$(VM\text{-}SiO_2)_n$-R_F nanocomposites and the R_F-$(VM\text{-}SiO_2)_n$-R_F/$B(OH)_3$ nanocomposites before and even after calcination at 800 °C, respectively. On the other hand, the other block copolymer such as triblock copolymer: poly(ether sulfone)-*b*-poly(tetrahydrofuran)-*b*-poly(ether sulfone) triblock copolymer [PES-*b*-PTHF-*b*-PES], which consists of poly(ether sulfone) and poly(tetrahydrofuran) as hard and soft segments, quite different structures from $(MAB)_{m\text{-}m}$-*b*-PPO_{32} block copolymer, were not applied to the sol-gel reaction with the R_F-$(VM\text{-}SiO_2)_n$-R_F/$B(OH)_3$ nanocomposites or the R_F-$(VM)_n$-R_F oligomer to give the expected nanocomposites. This finding would be due to the quite different structures between the $(MAB)_{m\text{-}m}$-*b*-PPO_{32} block copolymers and the PES-*b*-PTHF-*b*-PES triblock copolymer, and such triblock copolymer is not likely to interact with the R_F-$(VM\text{-}SiO_2)_n$-R_F/$B(OH)_3$ nanocomposites or the R_F-$(VM)_n$-R_F oligomer to supply the expected nanocomposites owing to its possessing no amide protons in the polymer

chain. In fact, it has been already reported that fluoroalkyl end-capped oligomers possessing no amide protons in the oligomer side chain can afford a usual weight loss in the silica nanocomposite cores after calcination at 800 °C.[56] In this way, the present R_F-(VM-SiO_2)$_n$-R_F/$B(OH)_3$ nanocomposites have high potential for providing an extremely higher thermal stability for the specific polymers possessing amide proton moieties in the polymer chain through the interactions between fluorine, silicon, and boron units in the composites.

References

1) J. J. Chrusciel, G. Janowska, and M. Fejdys, *J. Therm. Anal. Calorim.*, **109**, 1049 (2012).

2) N. Liao, W. Xue, H. Zhou, and M. Zhang, *J. Alloy. Compd.*, **610**, 45 (2014).

3) K. J. Sreejith, P. V. Prabhakaran, K. P. Laly, R. Dimple, and S. Packirisamy, *Ceram. Int.*, **42**, 15285 (2016).

4) G. D. Soraru, F. Babonneau, S. Maurina, and J. Vicens, *J. Non-Cryst. Solids*, **224**, 173 (1998).

5) A. Y. Lu and I. Hamerton, *Prog. Polym. Sci.*, **27**, 1661 (2002).

6) S. Xie, Y. Wang, Y. Lei, B. Wang, N. Wu, Y. Gou, and D. Fang, *RSC Adv.*, **5**, 64911 (2015).

7) S. Yajima, T. Shishido, and M. Hamano, *Nature*, **266**, 522 (1997).

8) H. M. Woilliams, E. A. Dawson, P. A. Barnes, B. Rand, R. M. D. Brydson, *Microporous Mesoporous Mater.*, **99**, 261 (2007).

9) L. Li, J. Zhao, H. Li, and T. Zhao, *Appl. Organo. Chem.*, **27**, 723 (2013).

10) S. Yajima, J. Hayashi, and K. Okamura, *Nature*, **266**, 521 (1977).

11) S. Hoshi, and A. Kojima, *J. Mater. Res.*, **11**, 2536 (1996).

12) S. Hoshi, A. Kojima, H. Endou, S. Otani, T. Satou, Y. Nakaido, and Y. Hasegawa, *Tanso*, **161**, 23 (1994).

13) D. Devapal, S. Packirisamy, K. J. Sreejith, P. V. Ravindran, and B. K. George, *J. Inorg. Organomet. Polym.*, **20**, 666 (2010).

14) M. A. Schiavon, N. A. Armelin, and I. V. P. Yoshida, *Mater. Chem. Phys.*, **112**, 1047 (2008).

15) H. W. Bai, G. Wen, X. X. Huang, Z. X. Han, B. Zhong, Z. X. Hu, and X. D. Zhang, *J. Eur. Ceram. Soc.*, **31**, 977 (2011).

16) Z. Wenjun, S. Jian, C. Youcai, W. Xueqin, and Z. Jingli, *CIES J.*, **63**, 3365 (2012).

17) H. W. Bai, G. Wen, X. X. Huang, Z. X. Han, B. Zhong, Z. X. Hu, and X. D. Zhang, *J. Eur. Ceram. Soc.*, **31**, 931 (2011).

18) R. Pena-Alonso and G. D. Soraru, *J. Sol-Gel Sci. Technol.*, **43**, 313 (2007).

19) R. L. Siqueira, I. V. P. Yoshida, L. C. Paradini, and M. A. Schiavon, *Mater. Res.*, **10**, 147 (2007).

20) G. D. Soraru, F. Babonneau, C. Gervais, and N. Dallabona, *J. Sol-Gel Sci.*

Technol., **18**, 11 (2000).

21) B. Ameduri and H. Sawada (Eds.), *Fluorinated polymers: Volume 1, "Synthesis, Properties, Processing and Simulation",* Chembridge, RSC, UK (2016).

22) B. Ameduri and H. Sawada (Eds.), *Fluorinated polymers: Volume 2, "Applications",* Chembridge, RSC, UK (2016).

23) H. Sawada, *Polym. J.*, **39**, 637 (2007).

24) H. Sawada, *Prog. Polym. Sci.*, **32**, 509 (2007).

25) H. Sawada, *Polym. Chem.*, **3**, 46 (2012).

26) H. Takashima, K. Iwaki, R. Furukuwa, K. Takishita, and H. Sawada, *J. Colloid Interface Sci.*, **320**, 436 (2008).

27) T. Kijima, M. Nishida, H. Fukaya, M. Yoshida, and H. Sawada, *J. Polym. Sci. Part A: Polym. Chem.*, **51**, 2555 (2013).

28) M. Mugisawa, K. Ohnishi, and H. Sawada, *Langmuir*, **23**, 5848 (2007).

29) M. Mugisawa and H. Sawada, *Langmuir*, **24**, 9215 (2008).

30) H. Sawada, A. Sasaki, and K. Sasazawa, *Colloid Surf. A: Physicochem. Eng. Asp.,* **337**, 57 (2009).

31) M. Mugisawa, R. Kasai, and H. Sawada, *Langmuir*, **25**, 415 (2009).

32) S. Soma, Y. Mizutani, M. Sugiya, and H. Sawada, *J. Polym. Sci. Part A: Polym. Chem.*, **52**, 1869 (2014).

33) E. Sawada, H. Kakehi, Y. Chounan, M. Miura, Y. Sato, N. Isu, and H. Sawada, *Compos. Part B*, **41**, 498 (2010).

34) S. Guo, H. Yoshioka, H. Kakehi, Y. Kato, M. Miura, N. Isu, B. Ameduri, and H. Sawada, *J. Colloid Interface Sci.*, **387**, 141 (2012).

35) S. Guo, H. Yoshioka, Y. Kato, H. Kakehi, M. Miura, N. Isu, A. Manseri, H. Sawada, and Ameduri, *Eur. Polym. J.*, **58**, 79 (2014).

36) Y. Mulazim, M. V. Kahraman, N. K. Apohan, S. Kiziltas, and A. Gungor, *J. Appl. Polym. Sci.*, **120**, 2112 (2011).

37) Y. Aomi, M. Nishida, and H. Sawada, *J. Polym. Sci. Part A: Polym. Chem.*, **54**, 3835 (2016).

38) H. Sawada and M. Nakayama, *J. Chem. Soc. Chem. Commun.*, 677 (1991).

39) T. Mori, S. Masukawa, T. Kikkawa, A. Fujimori, A. Satoh, K. Matsumoto, M. Jikei, Y. Oishi, and Y. Shibasaki, RSC Adv., **7**, 33812 (2017).

40) M. Jikei, Y. Aikawa, and K. Matsumoto, *High Perform. Polym.*, **28**, 1015 (2016).

41) H. Sawada, T. Suzuki, H. Takashima, and K. Takishita, *Colloid Polym. Sci.*, **286**,

1569 (2008).

42) C. Gervais, F. Babonneau, N. Dallabonna, and G. D. Soraru, *J. Am. Cerm. Soc.*, **84**, 2160 (2001).

43) G. D. Soraru, F. Babonneau, S. Maurina, and J. Vicens, J. Non-Crystallogr. Solids, **224**, 173 (1998).

44) K. Yamada, T. Shimizu, K. Deguchi, S. Ando, H. Kamada, and T. Kobayashi, *Polym. Preprints Jpn.*, **60 (1)**, 2D26 (2011).

45) L. -S. Du and J. F. Stebbins, *J. Non-Cryst. Solids*, **351**, 3508 (2005).

46) S. Sen, Z. Xu, and J. F. Stebbins, *J. Non-Cryst. Solids*, **226**, 29 (1998).

47) G. L. Turner, K. A. Smith, R. J. Kirkpatrick, and E. J. Oldfield, *J. Magn. Res.*, **67**, 544 (1986).

48) H. Sawada, T. Narumi, S. Kodama, M. Kamijo, R. Ebara, M. Sugiya, and Y. Iwasaki, *Colloid Polym. Sci.*, **285**, 977 (2007).

49) H. Sawada, T. Tashima, and S. Kodama, *Polym. Adv. Technol.*, **19**, 739 (2008).

50) H. Sawada, H. Kakehi, T. Tashima, Y. Nishiyama, M. Miura, and N. Isu, *J. Appl. Polym. Sci.*, **112**, 3482 (2009).

51) Y. Goto, Y. Matsuki, M. Nishida, S. Oyama, K. Chikama, and H. Sawada,

Colloid Polym. Sci., **290**, 11 (2011).

52) H. Sawada, T. Tashima, Y. Nishiyama, M. Kikuchi, G. Kostov, Y. Goto, and B. Ameduri, *Macromolecules*, **44**, 1114 (2011).

53) H. Sawada, Y. Matsuki, Y. Goto, S. Kodama, M. Sugiya, and Y. Nishiyama, *Bull. Chem. Soc. Jpn.*, **83**, 75 (2010).

54) H. Sawada, M. Kikuchi, and M. Nishida, *J. Polym. Sci. Part A: Polym. Chem.*, **49**, 1070 (2011).

55) H. Sawada, T. Tashima, H. Kakehi, Y. Nishiyama, M. Kikuchi, M. Miura, Y. Sato, and N. Isu, *Polym. J.*, **42**, 167 (2010).

CHAPTER 3

Preparation of Amphiphobically Modified Poly(vinyl alcohol) Film by Fluoroalkyl End-Capped Vinyltrimethoxysilane Oligomer

3.1. Introduction

There has been great interest in poly(vinyl alcohol) (PVA), due to its application into a wide variety of fields such as membranes, coatings, wood and paper adhesives, fibers, paper sizing agents, textiles, emulsifiers, and dispersants.[1 ~ 6)] This is because of their good biocompatibility, biodegradability, non-toxicity, non-carcinogenicity, and environmental friendness.[7, 8)] It is well known that PVA is also a water-soluble synthetic polymer, which is applicable to numerous industrial fields; however, its application in the wet state and in the moisture sensitive areas is extremely restricted due to its poor resistance toward water.[9)] Therefore, it is deeply desirable to develop the PVA derivatives possessing a good water-resistance ability. In fact, there have been hitherto various reports on the hydrophobically modified PVA composite materials such as PVA/boron nitride[10)], PVA/SiO_2[11, 12)], PVA/boric acid[13, 14)], PVA/graphene[15, 16)], and PVA/cellulose/ trifluoroacetic acid.[17)] However, the exploration of PVA derivatives possessing an amphiphobically characteristic; that is, oleophobic and hydrophobic properties has been very limited, so far. The introduction of longer fluoroalkyl groups into the PVAs enables the corresponding polymers to create the amphiphobic property on their surfaces, In fact, perfluoroacyl chlorides [$CF_3(CF_2)_n$-C(=O)Cl; n = 3, 5, 6 and 7] were applied to the surface modification of PVA through the formation of ester bond [$CF_3(CF_2)_n$-C(=O)-O-CH<] to

provide an amphiphobic surface toward the PVA. These perfluoroalkylated PVA derivatives are unstable toward water to produce the corresponding perfluoroalkanoic acid [$CF_3(CF_2)_n$-C(=O)OH] through the hydrolysis of the ester moiety due to the strong electronegativity of fluorine.[18, 19] Longer fluoroalkyl group-containing monomeric silane coupling agent such as *1H, 1H, 2H, 2H*-perfluorodecyltrichlorosilane [Cl_3Si-$CH_2CH_2(CF_2)_7CF_3$] were also applied to the surface modification of PVA through the formation of siloxane units [$(\sim O)_3Si$-$CH_2CH_2(CF_2)_7CF_3$] to provide the hydrophobic characteristic toward the PVA surface.[20] However, the creation of amphiphobic PVA surface was not unclear and its application scope was limited. During the comprehensive studies on the preparation and applications of two fluoroalkyl end-capped oligomeric nanocomposites[21 ~ 29], it has been already reported that two fluoroalkyl end-capped vinyltrimethoxysilane oligomeric silica nanocomposites [R_F-$(CH_2CHSiO_2)_n$-R_F; R_F = $CF(CF_3)OC_3F_7$; R_F-$(VM\text{-}SiO_2)_n$-R_F], which were prepared by the sol-gel reaction of the corresponding oligomer [R_F-$(CH_2CHSi(OMe)_3)_n$-R_F; R_F-$(VM)_n$-R_F] under alkaline conditions, can afford the oleophobic/superhydrophobic characteristic on the modified glass surface.[30] From this point of view, it is of particular interest to develop the PVA derivatives possessing an amphiphobic characteristic by using R_F-$(VM)_n$-R_F oligomer as a key intermediate. This chapter shows that R_F-$(VM)_n$-R_F oligomer is applicable to the

surface modification of PVA to lead the PVA/R_F-$(VM)_n$-R_F composite film possessing an amphiphobic property on the surface. In addition, it was clarified that R_F-$(VM)_n$-R_F oligomer/boric acid nanocomposites, which were prepared by the reaction of the corresponding oligomer with boric acid, can also afford the PVA/R_F-$(VM)_n$-R_F/boric acid composite film possessing a similar amphiphobic characteristic. Especially, the obtained composite film was found to provide the perfect water-resistance ability, compared to that of the corresponding PVA/R_F-$(VM)_n$-R_F composite film or pristine PVA film. These results will be described in this chapter.

3.2. Experimental

3.2.1 Measurements

Field emission scanning electron micrographs (FE-SEM) were recorded using JEOL JSM-7000F (Tokyo, Japan). Thermal analyses were recorded by raising the temperature around 800 °C (the heating rate: 10 °C/min) under atmospheric conditions by the use of NETZSCH JAPAN TG-DTA2010SEα differential thermobalance (Kanagawa, Japan). X-ray diffraction (XRD) measurements were performed by the use of MiniFlex 600 (Tokyo, Japan). Contact angles were measured using a Kyowa Interface Science Drop Master 300 (Saitama, Japan). Energy dispersive X-ray (EDX) spectra were obtained using JEOL JSM-7000F (Tokyo, Japan).

3.2.2. Materials

Boric acid and hydrochloric acid were purchased from FUJIFILM Wako Pure Chemical Industries (Osaka, Japan). Vinyltrimethoxysilane was used as received from Dow Corning Toray Co., Ltd. (Tokyo, Japan). Fluoroalkyl end-capped vinyltrimethoxysilane

oligomer [R_F-(CH_2-$CHSi(OMe)_3$)$_n$-R_F: the mixture of dimer and trimer; R_F = $CF(CF_3)OC_3F_7$] was synthesized by reaction of fluoroalkanoyl peroxide with the corresponding monomer according to the previously reported method.[31] Poly(vinyl alcohol) (KL-118^{TR}; degree of hydrolysis: 95.0 ~ 99.0 %) was kindly supplied from Kuraray Co., Ltd. (Tokyo, Japan).

3.2.3. Preparation of poly(vinyl alcohol)/fluoroalkyl end-capped vinyltrimethoxysilane oligomer/boric acid composite film

To a methanol solution (10 mL) containing fluoroalkyl end-capped vinyltrimethoxysilane oligomer [R_F-(CH_2-$CHSi(OMe)_3$)$_n$-R_F, n = 2, 3; R_F = $CF(CF_3)OC_3F_7$: R_F-$(VM)_n$-R_F] (100 mg) was added boric acid powder (50 mg). The mixture was stirred at room temperature for 5 min to provide the transparent colorless solution. To this solution were added 10 wt% aqueous poly(vinyl alcohol) solution (5 mL), water (5 mL) and 1 M hydrochloric acid (1.0 mL), and was successively stirred at room temperature for 12 hrs to afford the homogeneous solution. The PVA/R_F-$(VM)_n$-R_F/boric acid composite film was prepared by casting this homogeneous solution on glass plate. The solvent was evaporated at room temperature, and the film formed peeled off and dried at room temperature for 1

day under vacuum to afford the expected composite film. In addition, the PVA/R_F-$(VM)_n$-R_F/boric acid composite film was also prepared in the absence of catalyst (1 M HCl) under similar conditions.

3.2.4. Dodecane and water contact angle measurements of poly(vinyl alcohol)/ fluoroalkyl end-capped vinyltrimethoxysilane oligomer/boric acid composite film

The contact angles of dodecane and water were measured at room temperature by the deposit of each droplet (2 μL) on the PVA/R_F-$(VM)_n$-R_F/boric acid composite film.

3.2.5. Swelling ratio of poly(vinyl alcohol)/fluoroalkyl end-capped vinyltrimethoxy-silane oligomer/boric acid composite film

The PVA/R_F-$(VM)_n$-R_F/boric acid composite film was cut into a square of 20 mm × 20 mm × 71 μm (thickness), and was dried at room temperature for 1 day under vacuum. Swelling ratio of the film was measured after the pre-weight dried film was swollen in water at 25 °C. The swollen film was weighed after being slightly removed from the water surface. The swelling ratio was calculated by the following equation:

swelling ratio (g/g) = (W_s - W_d)/W_d, where W_d is the weight of dried film, and W_s is the weight of swollen film.

3.3. Results and discussion

It is well known that fluoroalkyl end-capped vinyltrimethoxysilane oligomer [R_F-$(VM)_n$-R_F] is applicable to the preparation of the R_F-$(VM)_n$-R_F/$B(OH)_3$ nanocomposites, and organic molecules such as diphenylsilanediol [$Ph_2Si(OH)_2$] can be effectively encapsulated into these fluorinated nanocomposite cores to exhibit no weight loss behavior for the encapsulated molecules even after calcination at 800 °C.[32] This finding suggests that the R_F-$(VM)_n$-R_F/$B(OH)_3$ nanocomposites should interact with the hydroxy segments-containing organic polymers such as poly(vinyl alcohol) (PVA) to afford the corresponding PVA composites. Thus, the PVA/R_F-$(VM)_n$-R_F/$B(OH)_3$ composite film was tried to prepare through the interaction of the R_F-$(VM)_n$-R_F oligomer/$B(OH)_3$ nanocomposites with aqueous PVA solution. The PVA/R_F-$(VM)_n$-R_F composite film and the pristine PVA film were also prepared under similar conditions, for comparison. The results are shown in Scheme 3-1 and Table 3-1.

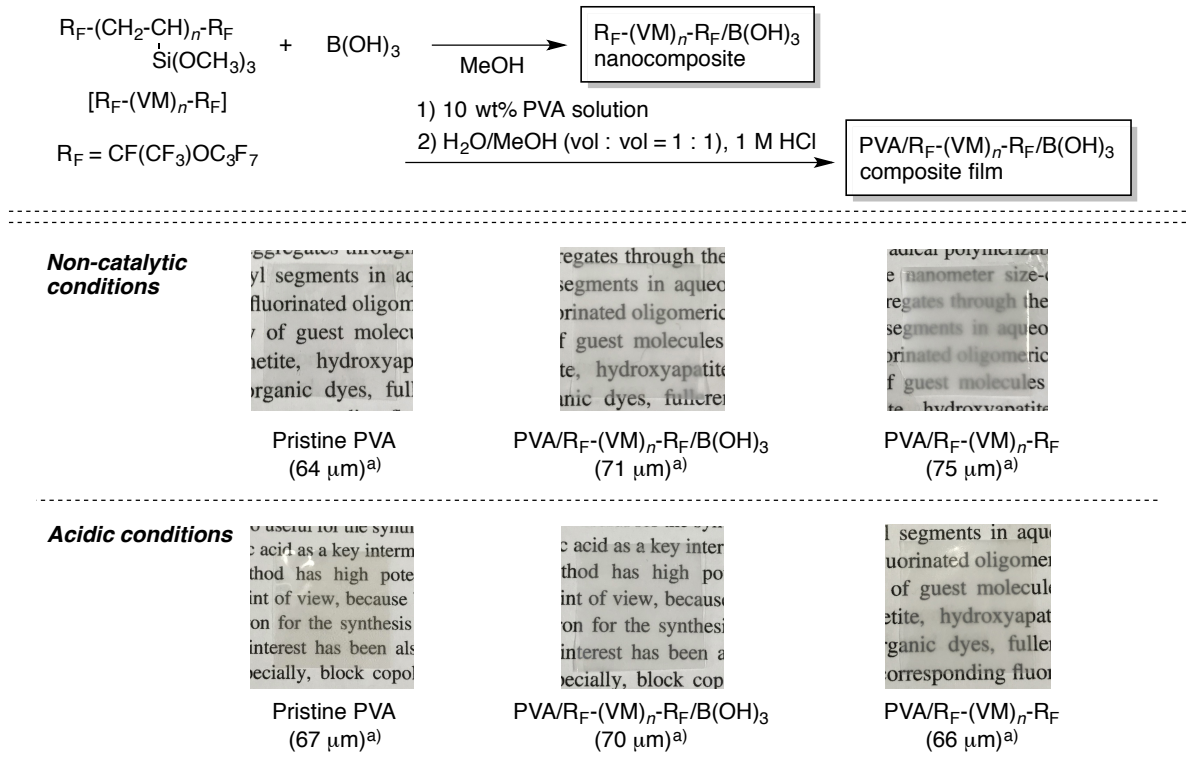

Scheme 3-1 Preparation of PVA/R_F-$(VM)_n$-R_F/$B(OH)_3$ composite film, PVA/R_F-$(VM)_n$-R_F composite film, and pristine PVA film under non-catalytic or acidic conditions, and photograph of these films. (a) Film thicness

Table 3-1 Preparation of the PVA/R_F-$(VM)_n$-R_F/$B(OH)_3$ and PVA/R_F-$(VM)_n$-R_F composite films under non-catalytic or acidic conditions

Run	R_F-$(VM)_n$-R_F (mg)	$B(OH)_3$ (mg)	10 wt% PVA solution (mL)	H_2O/MeOH (vol/vol : 1/1) (mL)	1 M HCl (mL)	Product (composite)	Content (%) of PVA in the composites[a)]
1	100	50	5.0	10	—	PVA/R_F-$(VM)_n$-R_F/$B(OH)_3$	77
2	100	—	5.0	10	—	PVA/R_F-$(VM)_n$-R_F	83
3	100	50	5.0	10	1.0	PVA/R_F-$(VM)_n$-R_F/$B(OH)_3$	77
4	100	—	5.0	10	1.0	PVA/R_F-$(VM)_n$-R_F	83

a) The content (%) of PVA is based on the used R_F-$(VM)_n$-R_F oligomer and PVA (and boric acid).

As shown in Scheme 3-1 and Table 3-1, it was demonstrated that R_F-$(VM)_n$-R_F oligomer is effective for the preparation of the PVA/R_F-$(VM)_n$-R_F/$B(OH)_3$ composite film and the PVA/R_F-$(VM)_n$-R_F composite film, respectively. The composite films thus obtained

(the content of PVA: 77 ~ 83 %) were found to be transparent colorless, similar to that of the pristine PVA film (see Scheme 3-1).

Furthermore, the transparent colorless PVA/R_F-$(VM)_n$-R_F/$B(OH)_3$ composite film and PVA/R_F-$(VM)_n$-R_F composite film were also prepared under acidic conditions, respectively, as illustrated in Scheme 3-1 and Table 3-1.

In order to clarify the formation of the PVA/R_F-$(VM)_n$-R_F/$B(OH)_3$ composite film, the thermogravimetric analyses (TGA), in which the weight loss of the film was measured by raising the temperature at around 800 °C at a 10 °C/min heating rate under air atmospheric conditions, have been studied and the results are shown in Figures 3-1 and 3-2.

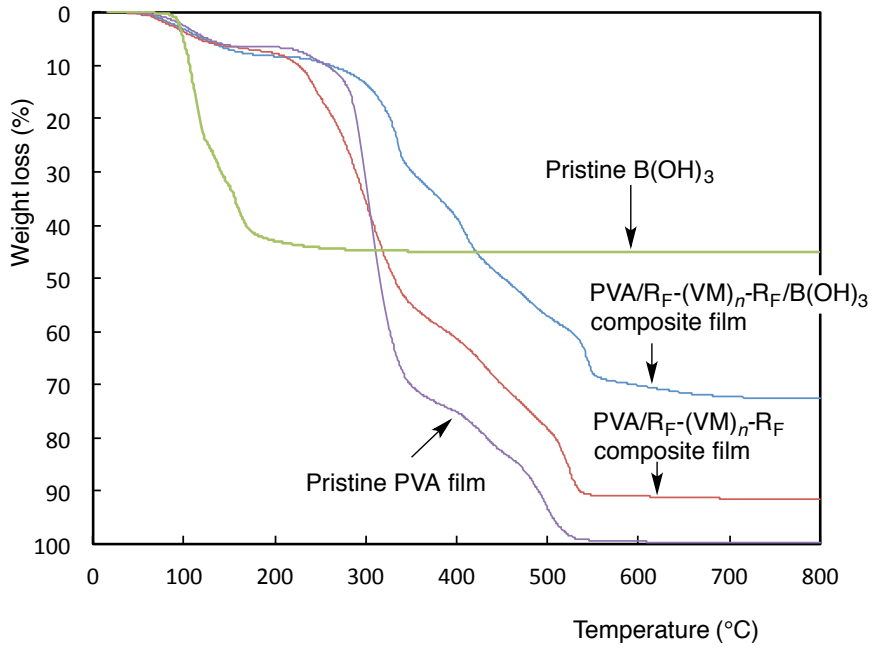

Figure 3-1 Thermogravimetric analyses (TGA) of PVA/R_F-$(VM)_n$-R_F composite film, PVA/R_F-$(VM)_n$-R_F/$B(OH)_3$ composite film, and pristine PVA film, which were prepared under non-catalytic conditions, and pristine $B(OH)_3$.

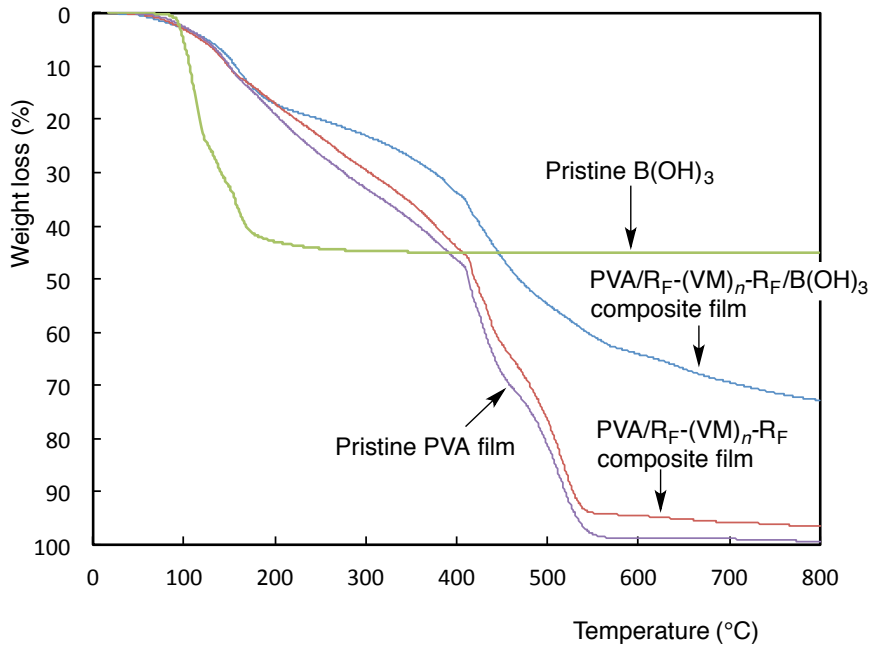

Figure 3-2 Thermogravimetric analyses (TGA) of PVA/R_F-$(VM)_n$-R_F composite film, PVA/R_F-$(VM)_n$-R_F/$B(OH)_3$ composite film, and pristine PVA film, which were prepared under acidic conditions, and pristine $B(OH)_3$.

Figure 3-1 shows the TGA curves of the PVA/R_F-$(VM)_n$-R_F/$B(OH)_3$ composite film (Run 1 in Table 3-1), the PVA/R_F-$(VM)_n$-R_F composite film (Run 2 in Table 3-1), the pristine PVA film and $B(OH)_3$, respectively. The pristine PVA film has the perfect weight loss (100 %) at around 540 °C, and original $B(OH)_3$ shows the clear weight loss related to the formation of the metaboric acid (HBO_2) and boron trioxide (B_2O_3) by the dehydration during the calcination process. DTA (differential thermal analyses) curve shows that this dehydration corresponds to the clear endothermic peaks at around 100 ~ 200 °C depicted in Figure 3-3. The PVA/R_F-$(VM)_n$-R_F/$B(OH)_3$ composite film can exhibit a clear weight loss at 800 °C (73 %), of whose value is lower than that (92 %) of the PVA/R_F-$(VM)_n$-R_F

composite film, indicating that the boric acid moieties can be surely incorporated into the PVA/R_F-$(VM)_n$-R_F composite cores (see Figure 3-1). DTA curve of the pristine PVA film shows a clear exothermic peak at around 500 °C (see Figure 3-3). Of particular interest, the exothermic peak at around 500 °C related to the pristine PVA film was found to shift to 520 ~ 550 °C in the PVA/R_F-$(VM)_n$-R_F composite film and the PVA/R_F-$(VM)_n$-R_F/$B(OH)_3$ composite film as shown in Figure 3-3. Especially, a higher temperature shift was observed in the PVA/R_F-$(VM)_n$-R_F/$B(OH)_3$ composite film. Such higher temperature shift would be due to the effective interaction between the PVA and the R_F-$(VM)_n$-R_F oligomer or boric acid.

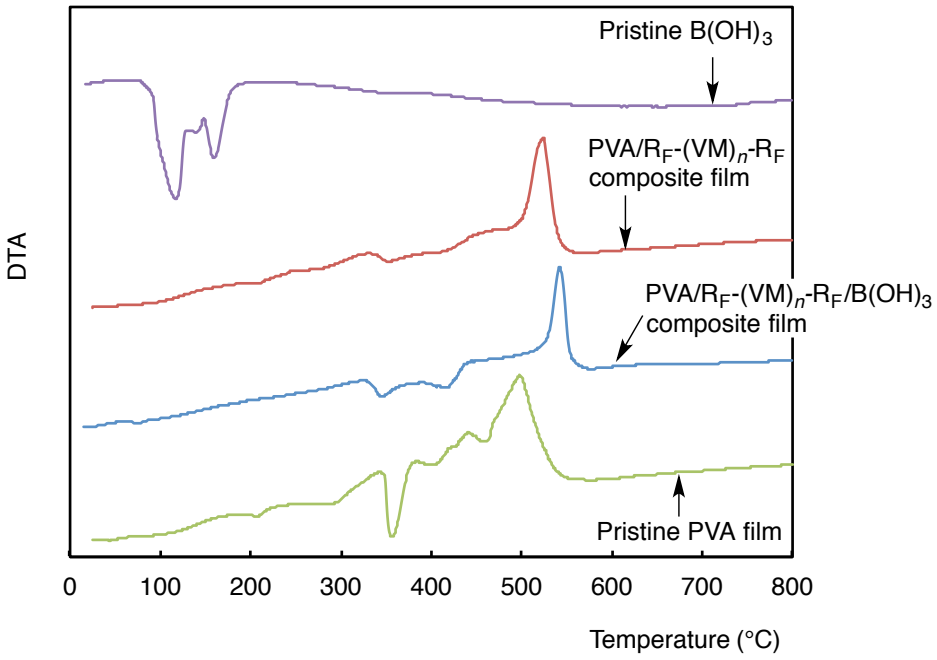

Figure 3-3 Differential thermal analyses (DTA) of PVA/R_F-$(VM)_n$-R_F composite film, PVA/R_F-$(VM)_n$-R_F/$B(OH)_3$ composite film, and pristine PVA film, which were prepared under non-catalytic conditions, and pristine $B(OH)_3$.

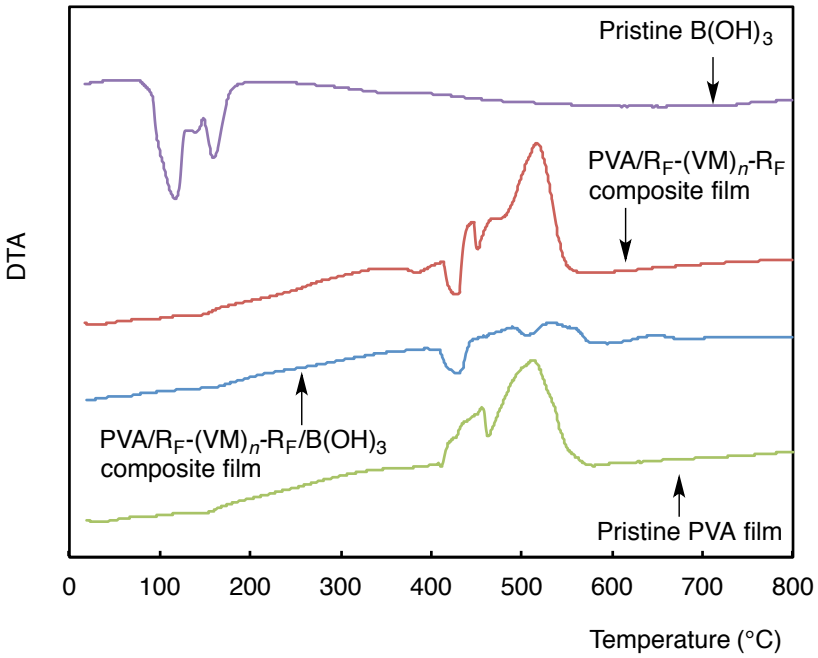

Figure 3-4 Differential thermal analyses (DTA) of PVA/R_F-$(VM)_n$-R_F composite film, PVA/R_F-$(VM)_n$-R_F/$B(OH)_3$ composite film, and pristine PVA film, which were prepared under acidic conditions, and pristine $B(OH)_3$.

Figure 3-2 shows the similar TGA curves of the PVA/R_F-$(VM)_n$-R_F/$B(OH)_3$ composite film (Run 3 in Table 3-1) and PVA/R_F-$(VM)_n$-R_F composite film (Run 4 in Table 3-1) to those of the corresponding films illustrated in Figure 3-1. Figure 3-4 depicts that DTA curve of the PVA/R_F-$(VM)_n$-R_F composite film reveals the slightly higher temperature shifted exothermic peak related to the PVA in the PVA/R_F-$(VM)_n$-R_F/$B(OH)_3$ composite film (see Figure 3-4), quite different from that of the PVA/R_F-$(VM)_n$-R_F/$B(OH)_3$ composite film (Run 1 in Table 3-1) in Figure 3-3. The $T_{dec}50$ or $T_{dec}70$ (defined as the temperature at which 50 % or 70 % of the mass of the film is lost during a 10 °C/min heating rate under atmospheric conditions) of these composites have been summarized to verify this finding.

The results are as follows:

Run No.*	Composite film	T_{dec}50 (°C)	T_{dec}70 (°C)
1	PVA/R_F-$(VM)_n$-R_F/$B(OH)_3$	452	594
2	PVA/R_F-$(VM)_n$-R_F	332	413
	Pristine PVA	315	349
3	PVA/R_F-$(VM)_n$-R_F/$B(OH)_3$**	469	714
4	PVA/R_F-$(VM)_n$-R_F**	421	481
	Pristine PVA**	413	459

*Each Run No. corresponds to that of Table 3-1

**The films were prepared under acidic conditions

As indicated above, the PVA/R_F-$(VM)_n$-R_F/$B(OH)_3$ composite film obtained under acidic conditions can provide the highest thermal stability (T_{dec}70 = 714 °C), compared to that of other composite films. This finding is due to the effective interaction between PVA and the R_F-$(VM)_n$-R_F/$B(OH)_3$ nanocomposites. In fact, it has been already reported that R_F-$(VM)_n$-R_F/$B(OH)_3$ nanocomposites are applicable to the encapsulation of low molecular weight organic compounds such as diphenylsilanediol, 1, 1'-bi-2-naphthol, 4, 4'-biphenol, bisphenol A, bisphenol F, bisphenol AF, biphenyl, dibenzyl, and pentaerythritol into these nanocomposite cores.[32] Moreover, the obtained nanocomposites can exhibit no weight loss behavior corresponding to the contents of these encapsulated organic molecules even after calcination at 800 °C.[32] R_F-$(VM)_n$-R_F/$B(OH)_3$ nanocomposites were also applied to the

interaction with the thermoplastic elastomers such as poly(*N*-methyl benzamide)-*b*-poly(propylene oxide) block copolymers to afford the corresponding R_F-$(VM)_n$-R_F/$B(OH)_3$/ thermoplastic elastomers nanocompoites, providing no weight loss characteristic corresponding to the contents of the block copolymers in the composites even after calcination at 800 °C.[32] From these findings, the R_F-$(VM)_n$-R_F/$B(OH)_3$ nanocomposite should interact with the PVA in the nanocomposite matrices to enhance the thermal stability of the obtained composite film. Especially, R_F-$(VM)_n$-R_F oligomer would cause the sol-gel reaction under acidic conditions to create the siloxane network, which would interact with the PVA or boric acid, giving a higher thermal stability in the composite films. In fact, Uragami et al. reported that a similar siloxane networks between PVA and tetraethoxysilane (TEOS) can be formed under acidic conditions to decrease the swelling ability toward water and to improve the water permselectivity of the obtained PVA/TEOS hybrid film.[9] In addition, PVA/1, 2-bis(triethoxysilyl)ethane composite films were also prepared through the formation of siloxane networks by the sol-gel reactions under acidic conditions to reduce the swelling of the corresponding film in an aqueous solution.[34]

The XRD spectra of these composite films have been studied in order to clarify their physical structure. The results are shown in Figures 3-5 and 3-6.

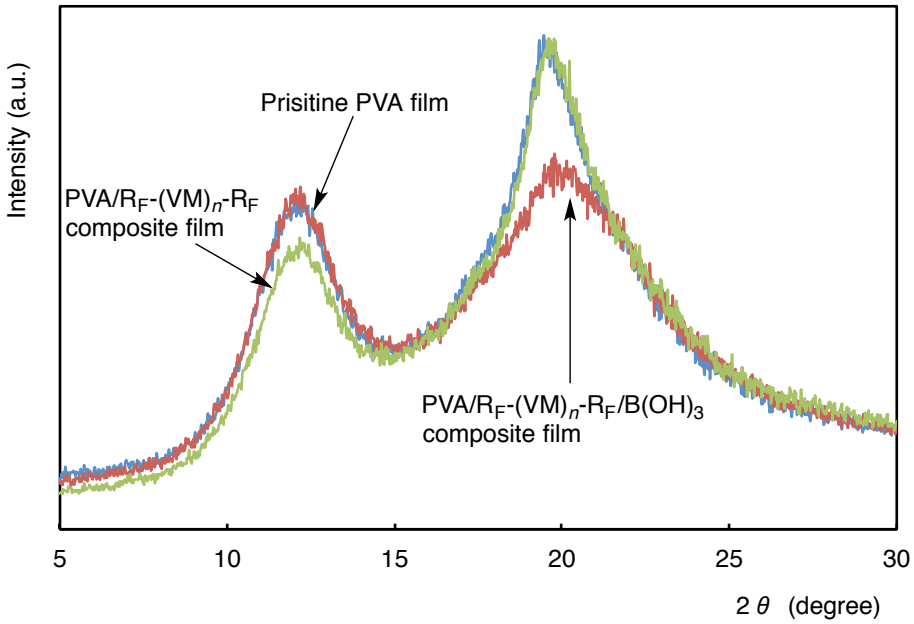

Figure 3-5 X-ray diffraction (XRD) patterns of R_F-(VM)$_n$-R_F/B(OH)$_3$/PVA composite films, PVA/R_F-(VM)$_n$-R_F composite film, and prisitine PVA film, which were prepared under acidic conditions.

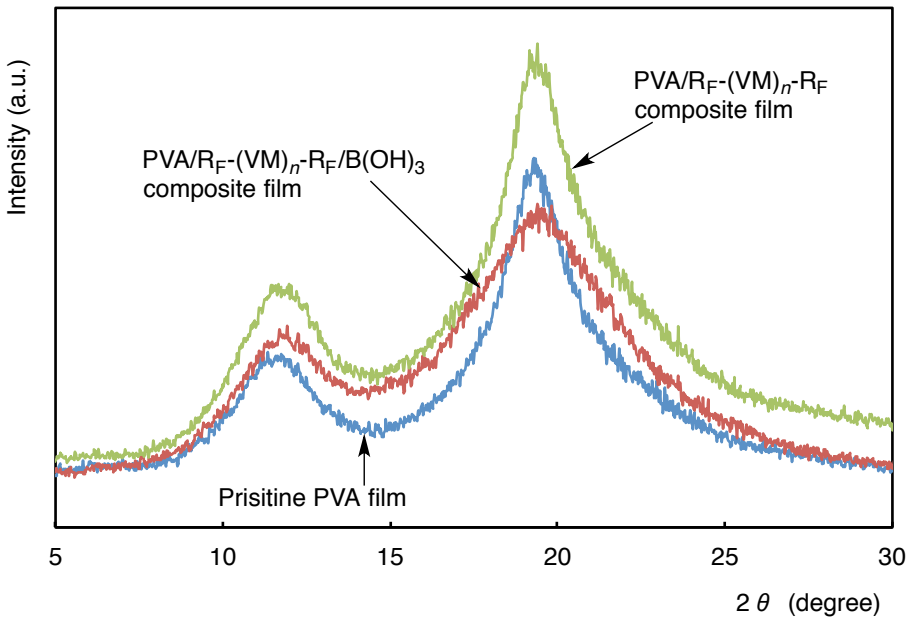

Figure 3-6 X-ray diffraction (XRD) patterns of R_F-(VM)$_n$-R_F/B(OH)$_3$/PVA composite films, PVA/R_F-(VM)$_n$-R_F composite film, and prisitine PVA film, which were prepared under non-catalytic conditions.

Figures 3-5 shows the XRD spectra of the PVA/R_F-$(VM)_n$-R_F composite film, the PVA/R_F-$(VM)_n$-R_F/$B(OH)_3$ composite film, and the pristine PVA film obtained under acidic conditions illustrated in Scheme 3-1 and Table 3-1. A sharp diffraction peak at around $2\theta = 20°$ for the pristine PVA film was observed, and its intensity was quite similar to that of the PVA/R_F-$(VM)_n$-R_F composite film, although the PVA/R_F-$(VM)_n$-R_F/$B(OH)_3$ composite film decreased its intensity. This finding suggests that the PVA/R_F-$(VM)_n$-R_F/$B(OH)_3$ composite film can provide less crystalline domains than that of the pristine PVA film or the PVA/R_F-$(VM)_n$-R_F composite film.

DTA curves in Figure 3-4 show that the exothermic peaks related to the PVA were observed at around 520 °C in the pristine PVA film and the PVA/R_F-$(VM)_n$-R_F composite film; however, such clear peak were unable to detect in the PVA/R_F-$(VM)_n$-R_F/$B(OH)_3$ composite film. The Si-O-C bonds or C-O-B(O-C)O-C bonds[35] formed between the linear PVA chains with R_F-$(VM)_n$-R_F oligomer or $B(OH)_3$ that dispersed in the composite films would afford a size-exclusive effect to prevent the formation of crystalline region, leading to a decrease of the crystalline regions in the composite film. Thus, such effect should increase the amorphous region in the PVA/R_F-$(VM)_n$-R_F/$B(OH)_3$ composite film as shown in Figure 3-5. On the other hand, the PVA/R_F-$(VM)_n$-R_F composite film was found to give the same diffraction peak intensity at around 20° to that of the pristine PVA film, indicating

that R_F-$(VM)_n$-R_F oligomer cannot interact strongly with the hydroxy units in PVA to decrease the crystalline region (see Figure 3-5).

However, of particular interest, a higher diffraction peak intensity was observed at around $2\theta = 20°$ related to the PVA in the PVA/R_F-$(VM)_n$-R_F composite film, which was prepared under non-catalytic conditions, than that of the pristine PVA film or the PVA/R_F-$(VM)_n$-R_F/$B(OH)_3$ composite film, indicating that R_F-$(VM)_n$-R_F oligomer can form the self-assembled aggregate cores through the aggregation of the terminal fluoroalkyl segments under non-catalytic conditions, and such oligomeric aggregate cores should interact with the PVA to accelerate the formation of crystalline region in the composite film as shown in Figure 3-6. In fact, it is well known that the fluoroalkyl end-capped oligomer can form the self-assembled oligomeric aggregates through the aggregation of the end-capped fluoroalkyl segments in aqueous and organic media, and a variety of organic molecules can be effectively encapsulated into these fluorinated aggregate cores to provide the corresponding fluorinated oligomeric aggregates/guest molecules composites.[24, 25] On the other hand, unexpectedly, the PVA/R_F-$(VM)_n$-R_F/$B(OH)_3$ composite film was found to decrease the characteristic peak intensity at around 20°, compared to that of the pristine PVA, indicating that the boric acid in the PVA/R_F-$(VM)_n$-R_F/$B(OH)_3$ composite film should interact with the hydroxy groups in the PVA to prevent the formation of the

crystalline region in the composite film (see Figure 3-6). In fact, DTA curves in Figure 3-4 show that a clear exothermic peak related to the PVA at around 500 °C was disappeared in the PVA/R_F-$(VM)_n$-R_F/$B(OH)_3$ composite film, although the clear exothermic peaks at around 500 °C was observed in the pristine PVA film and the PVA/R_F-$(VM)_n$-R_F composite film, indicating that the boric acid should interact with the PVA to prevent the formation of the crystalline regions in the composite film. A similar decrease of the crystalline region in the PVA hybrids was observed in the PVA/γ-aminopropyltriethoxysilane hybrid[36, 37], PVA/silica hybrid[38], and PVA/vinyltrimethoxysilane hybrid.[39]

The wettability of the PVA/R_F-$(VM)_n$-R_F composite films and the PVA/R_F-$(VM)_n$-R_F/$B(OH)_3$ composite films illustrated in Scheme 3-1 and Table 3-1 was studied in order to clarify the amphiphobic characteristic on the modified PVA film surface. Contact angle values of dodecane and water on these film surface and reverse sides were measured by the deposit of each droplet (2 μL), and the results are shown in Table 3-2.

Table 3-2 Contact angles of dodecane and water on the PVA/R_F-$(VM)_n$-R_F/$B(OH)_3$ composite film, PVA/R_F-$(VM)_n$-R_F composite film, which were prepared under acidic or non-catalytic conditions.

Composite film		Contact angle (degree) Dodecane	Water						
			0	5	10	15	20	25	30 (min)
PVA/R_F-$(VM)_n$-R_F/$B(OH)_3$[a]	surface side	57	110	109	107	105	104	103	100
	reverse side	47	108	101	98	94	87	79	75
PVA/R_F-$(VM)_n$-R_F[a]	surface side	56	106	-[b]					
	reverse side	48	101	-[b]					
PVA/R_F-$(VM)_n$-R_F/$B(OH)_3$[c]	surface side	58	113	103	-[d]				
	reverse side	51	104	99	-[d]				
PVA/R_F-$(VM)_n$-R_F[c]	surface side	57	105	-[d]					
	reverse side	46	97	-[d]					

a) Composite film was prepared under acidic conditions.
b) Composite film surface exhibited swelling behavior.
c) Composite film was prepared under non-catalytic conditions.
d) Composite film exhibited solubility toward water.

Table 3-2 shows that each modified PVA surface can give a higher oleophobic property imparted by fluoroalkyl segments in the composites not only on the surface side but also on the reverse side, because the dodecane contact angle values are 56 ~ 58 degrees on the surface side, and are 46 ~ 51 degrees on the reverse side, respectively, compared to that (33 degrees) of the traditional fluorinated polymer sheet surface such as poly(tetrafluoroethylene).[27] These findings suggest that the PVA/R_F-$(VM)_n$-R_F composite and the PVA/R_F-$(VM)_n$-R_F/$B(OH)_3$ composite, of whose structures consist of the siloxane networks, have a uniformly dispersive characteristic toward the PVA to give the similar oleophobic characteristic related to fluoroalkyl segments in the composites on the surface side and even on the reverse side. To verify such unique dispersibility toward the PVA, the

EDX (Energy Dispersive X-ray) spectra measurements of the PVA film surface and reverse side have been studied, and the results are as following:

	Content of boron (atm. %)		Content of fluorine (atm. %)	
	Surface side	Reverse side	Surface side	Reverse side
PVA/R_F-$(VM)_n$-R_F/$B(OH)_3$[a)]	15.4	17.1	1.3	9.3
PVA/R_F-$(VM)_n$-R_F[a)]	−	−	4.5	15.2

a) Composite film was prepared under acidic conditions.

The PVA/R_F-$(VM)_n$-R_F/$B(OH)_3$ composite film (Run 3 in Table 3-1) can give the similar boron and fluorine values on the surface (the contents of boron and fluorine are 15.4 % and 1.3 %), and even on the reverse side (the contents of boron and fluorine are 17.1 % and 9.3 %). In the PVA/R_F-$(VM)_n$-R_F composite film (Run 4 in Table 3-1), the similar fluorine values were observed even on the reverse side (15.2 %). These findings suggest that R_F-$(VM)_n$-R_F oligomer and R_F-$(VM)_n$-R_F/$B(OH)_3$ nanocomposites can be uniformly dispersed in the PVA film.

In addition, each modified PVA film in Table 3-2 also afforded the hydrophobic characteristic on the surface and even on the reverse sides related to the fluoroalkyl segments in the composites, because the water contact angle values are 105 ~ 113 degrees on the surface side and are 97 ~ 108 degrees on the reverse side, respectively, just after the

deposit of a water droplet on each surface, although it was unable to measure the water contact angle values on the pristine PVA surface under similar conditions, due to the swelling behavior on the highly hydrophilic PVA film surface. However, interestingly, it was clarified that the PVA/R_F-$(VM)_n$-R_F/$B(OH)_3$ composite film obtained under acidic conditions can provide a good hydrophobic characteristic during 30 min after the deposit of a water droplet as shown in Table 3-2, because the water contact angle value can keep 100 degrees even after 30 min on the PVA film surface to exhibit a good hydrophobic property. A similar result was obtained on the reverse side to keep the hydrophobic property even after 30 min, although the water contact angle values decrease slightly from 108 to 75 degrees over 30 min.

The PVA/R_F-$(VM)_n$-R_F composite film obtained under acidic conditions was unable to afford the good hydrophobic characteristic toward the PVA film, showing the swelling behavior on the surface at 5 min after the deposit of a water droplet. On the other hand, the PVA/R_F-$(VM)_n$-R_F/$B(OH)_3$ composite film and the PVA/R_F-$(VM)_n$-R_F composite film, which were prepared under non-catalytic conditions, enabled these composite films to cause not the swelling behavior but the soluble characteristic on these film surfaces at 10 or 5 min, respectively, after the deposit of a water droplet. In this way, the PVA/R_F-$(VM)_n$-R_F/$B(OH)_3$ composite film obtained under acidic conditions was found to

exhibit the good amphiphobic (oleophobic/hydrophobic) characteristic on both the surface and the reverse sides. This finding is due to the higher thermal stability of this modified PVA film, compared to that of the other modified PVA films. Especially, not only the effective interaction of the PVA with the siloxane networks derived from the sol-gel reaction of R_F-$(VM)_n$-R_F oligomer but also the interaction of the PVA with boric acid under acidic conditions are essential to provide an amphiphobic property on the modified PVA surfaces.

The water-resistance ability of the PVA/R_F-$(VM)_n$-R_F/$B(OH)_3$ composite film (Run 3 in Table 3-1) was studied to verify such unique hydrophobic characteristic. The PVA/R_F-$(VM)_n$-R_F composite film and the pristine PVA film were also studied under similar conditions. The results are shown in Figure 3-7.

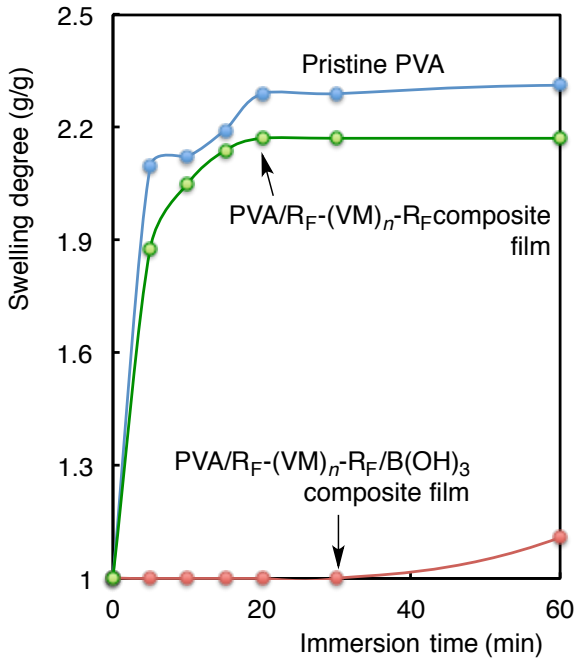

Figure 3-7 Relationship between the immersion time into water and the swelling ration of PVA/R_F-$(VM)_n$-R_F/$B(OH)_3$ composite film, PVA/R_F-$(VM)_n$-R_F composite film, and pristine PVA film, which were prepared under acidic conditions

Figure 3-7 shows the relationship between the immersion time of the film into water at room temperature and the swelling degree of the film. Both the PVA/R_F-$(VM)_n$-R_F composite film and the pristine PVA film obtained under acidic conditions can form the hydrogel after immersion into water, keeping the constant swelling degrees: 2.2 (g/g) and 2.3 (g/g) over 20 min, respectively, although the corresponding films obtained under non-catalytic conditions can give a perfect solubility toward water. On the other hand, of particular interest, it was demonstrated that the present PVA/R_F-$(VM)_n$-R_F/$B(OH)_3$ composite film can give the perfect water-resistance ability after immersion into water for 30 min, and a slightly swelling behavior [swelling degree: 1.1 (g/g)] was observed even

after immersion into water for 60 min to keep the shape of its transparent colorless film as shown in Figure 3-7.

3.4. Conclusion

PVA/R_F-$(VM)_n$-R_F/$B(OH)_3$ composite film was prepared through the interaction of the R_F-$(VM)_n$-R_F/$B(OH)_3$ nanocomposite with PVA under acidic or non-catalytic conditions, respectively. The PVA/R_F-$(VM)_n$-R_F/$B(OH)_3$ composite film, which were prepared under acidic conditions, was found to exhibit an amphiphobic characteristic on both the surface and reverse sides to give a perfect water-resistance ability even after immersion into water, although the corresponding PVA/R_F-$(VM)_n$-R_F composite film and the pristine PVA film, which were prepared under similar conditions, form the hydrogel after immersion into water. On the other hand, the PVA/R_F-$(VM)_n$-R_F/$B(OH)_3$ composite film and the PVA/R_F-$(VM)_n$-R_F composite film, which were prepared under non-catalytic conditions, can give a solubility toward water, as well as the pristine PVA film. In addition, the PVA/R_F-$(VM)_n$-R_F/$B(OH)_3$ composite film obtained under acidic conditions was found to give a higher thermal stability, compared to other composites. In this way, the present fluorinated PVA composite film has high potential for new fluorinated PVA composite materials possessing not only an amphiphobic characteristic but also good thermal stability, and is also expected to be applicable in a wide variety of fields.

References

1) M. Cao, C. Wang, R. Xia, P. Chen, J. Miao, B. Yang, J. Qian, and Y. Tang, *Constr. Build. Mater.*, **168**, 482 (2018).

2) C. Shao, H. -Y. Kim, J. Gong, B. Ding, D. -R. Lee and S. -J. Park, *Mater. Lett.*, **57**, 1579 (2003).

3) M. Nishimura and M. Higa, *Bull. Soc. Sea Water Sci., Jpn.*, **63**, 381 (2009).

4) E. H. Qua, P. R. Hornsby, H. S. S. Sharma, G. Lyons, and R. D. McCall, *J. Appl. Polym. Sci.*, **113**, 2238 (2009).

5) G. Moreno, M. V. de Paz, C. Valenda, and J. M. Franco, *J. Appl. Polym. Sci.*, **125**, 3259 (2012).

6) W. Zhang, M. Chen, and G. Diao, *Carbohydrate Polym.*, **86**, 1410 (2011).

7) M. D. Harun-or-Rashid, M. D. Saifur Rahaman, S. E. Kabir, and M. A. Khan, *J. Appl. Polymer Sci.*, 42870 (1 ~11) (2016); DOI:10.1002/APP.42870.

8) M. Kobayashi, J. Toguchida, and M. Oka, *Biomaterials*, **24**, 639 (2003).

9) T. Uragami, K. Okazaki, H. Matsugi, and T. Miyata, *Macromolecules*, **35**, 9156 (2002).

10) R. Zhang, W. Wan, L. Qiu, Y. Wang, and Y. Zhou, *Appl. Surface Sci.*, **419**, 342

(2017).

11) Q. Wang, Z. Dong, X. Yan, Y. Chang, L. Ren, and J. Zhou, *J. Bionic Eng.*, **14**, 476 (2017).

12) A. Bandyopadhyay, M. De Sarkar, and A. K. Bhowmick, *J. Mater. Sci.*, **40**, 5233 (2005).

13) D. Y. Yoon and J.-C. Kim, *Colloids Surfaces A: Physicochem. Eng. Aspects*, **506**, 678 (2016).

14) M. Lim, H. Kwon, D. Kim, J. Seo, H. Han, and S. B. Khan, *Prog. Org. Coatings*, **85**, 68 (2015).

15) J. Wang, X. Wang, C. Xu, M. Zhang, and X. Shang, *Polym. Int.*, **60**, 816 (2011).

16) S. Xu, W. Yu, X. Yao, Q. Zhang, and Q. Fu, *Compos. Sci. Technol.*, **131**, 67 (2016).

17) S. Guzman-Puyol, L. Ceseracciu, J. A. Heredia-Guerrero, G. C. Anyfantis, R. Cingolani, A. Athanassiou, and I. S. Bayer, *Chem. Eng. J.*, **277**, 242 (2015).

18) K. Ogino, T. Ohtsuka, and N. Ishikawa, *Kobunshi Ronbunshu*, **43**, 377 (1983).

19) T. Nishino, S. Nakahara, and K. Nakamae, *J. Adhesion Soc. Jpn.*, **35**, 138 (1999).

20) T. Nishino, M. Meguro, and K. Nakamae, *Int. J. Adhesion Adhesives*, **19**, 399 (1999).

21) B. Ameduri and H. Sawada (Eds.), *Fluorinated Polymers: Volume 1, "Synthesis, Properties, Processing and Simulation"*, Cambridge, RSC (2016).

22) B. Ameduri and H. Sawada (Eds.), *Fluorinated Polymers: Volume 2, "Applications"*, Cambridge, RSC (2016).

23) H. Sawada, *Chem. Rev.*, **96**, 1779 (1996).

24) H. Sawada, *Prog. Polym. Sci.*, **32**, 509 (2007).

25) H. Sawada, *Polym. Chem.*, **3**, 46 (2012).

26) Y. Oikawa, T. Saito, S. Yamada, M. Sugiya and H. Sawada, *ACS Appl. Mater. Interfaces*, **7**, 13782 (2015).

27) J. Suzuki, Y. Takegahara, Y. Oikawa, M. Chiba, S. Yamada, M. Sugiya, and H. Sawada, *J. Sol-Gel Sci. Technol.*, **81**, 611 (2017).

28) H. Sawada, Y. Suto, T. Saito, Y. Oikawa, K. Yamashita, S. Yamada, M. Sugiya, and J. Suzuki, *Polymers*, **9**, 92 (1 ~ 14) (2017); DOI:10.3390/polym9030092.

29) S. Katayama, S. Fujii, T. Saito, S. Yamazaki, and H. Sawada, *Polymers*, **9**, 292 (1 ~ 17) (2017); DOI:10..3390/polym9070292.

30) H. Sawada, T. Suzuki, H. Takashima, and K. Takishita, *Colloid Polym. Sci.*, **286**, 1569 (2008)

31) H. Sawada and M. Nakayama, *J. Chem. Soc., Chem. Commun.*, 677 (1991).

32) Y. Aomi, M. Nishida, and H. Sawada, *J. Polym. Sci., Part A: Polym. Chem.*, **54**, 3835 (2016).

33) Y. Aomi, Y. Oishi, Y. Shibasaki, Y. Aikawa, M. Jikei, M. Nishida, S. Yamazsaki, and H. Sawada, *J. Sol-Gel Sci. Technol.*, **85**, 318 (2018).

34) Q. G. Zhang, Q. L. Liu, A. M. Zhu, Y. Xiong, and X. H. Zhang, *J. Phys. Chem. B*, **112**, 16559 (2008).

35) S. Mondal and A. K. Banthia, *J. Eur. Ceramic Soc.*, **25**, 287 (2005).

36) Q. G. Zhang, Q. L. Liu, Z. Y. Jiang, and Y. Chen, *J. Membrane Sci.*, **287**, 237 (2007).

37) Q. G. Zhang, Q. L. Liu, X. J. Meng, and I. Broadwell, *J. Appl. Polym. Sci.*, **118**, 1121 (2010).

38) W. W. Hu, X. H. Zhang, Q. G. Zhang, Q. L. Liu, and A. M. Zhu, *J. Appl. Polym. Sci.*, **126**, 778 (2012).

39) M. Lim, D. Kim, J. Seo, and H. Han, *Macromol. Res.*, **22**, 1096 (2014).

Conclusions

The results obtained from this study are summarized as follows.

1. Fluoroalkyl end-capped vinyltrimethoxysilane oligomer [R_F-$(VM)_n$-R_F] reacted with boric acid to afford the corresponding fluorinated oligomeric silica/boric acid nanocomposite [R_F-$(VM\text{-}SiO_2)_n$-$R_F/B(OH)_3$] fine particles with mean diameter: 36 – 105 nm. The obtained R_F-$(VM\text{-}SiO_2)_n$-$R_F/B(OH)_3$ nanocomposites were applied to the encapsulation of low molecular weight organic compounds such as diphenylsilanediol, 1, 1'-bi-2-naphthol, 4, 4'-biphenol, bisphenol A, bisphenol F, bisphenol AF, biphenyl, dibenzyl, and pentaerythritol into these nanocomposite cores to provide the corresponding fluorinated oligomeric silica/boric acid nanocomposites – encapsulated these organic molecules. Interestingly, the obtained nanocomposites were found to exhibit no weight loss behavior corresponding to the contents of these guest molecules even after calcination at 800 °C, although these nanocomposites were isolated through no purification process. The R_F-$(VM\text{-}SiO_2)_n$-R_F nanocomposites – encapsulated these organic guest molecules were prepared under similar conditions. However, it was demonstrated that these nanocomposites can provide the clear weight loss

corresponding to the contents of these guest molecules in the nanocomposites after calcination at 800 °C.

2. Fluoroalkyl end-capped vinyltirimethoxysilane oligomeric silica/boric acid nanocomposites [R_F-(VM-SiO_2)$_n$-R_F/$B(OH)_3$] were prepared by the composite reaction of the corresponding fluorinated oligomer [R_F-($CH_2CHSi(OMe)_3$)$_n$-R_F, n = 2, 3; R_F = $CF(CF_3)OC_3F_7$: R_F-(VM)$_n$-R_F] with boric acid. The nanocomposites thus obtained were tried to interact with the thermoplastic elastomers such as poly(*N*-methyl benzamide)-*b*-poly(propylene oxide) block copolymers [(MAB)$_{m\text{-}m}$-*b*-PPO_{32}: m = 5, 6, 7, and 8] and poly(ethersulfone)-*b*-poly(tetrahydrofuran)-*b*-poly(ethersulfone) triblock copolymer [PES-*b*-PTHF-*b*-PES] under alkaline conditions to afford the corresponding R_F-(VM-SiO_2)$_n$-R_F/$B(OH)_3$/thermoplastic elastomers nanocomposites. The corresponding R_F-(VM-SiO_2)$_n$-R_F/thermoplastic elastomers nanocomposites were also prepared under similar conditions, for comparison. In these thermoplastic elastomers, PES-*b*-PTHF-*b*-PES triblock copolymers cannot interact with the R_F-(VM-SiO_2)$_n$-R_F/ $B(OH)_3$ nanocomposites or the R_F-(VM-SiO_2)$_n$-R_F oligomeric nanoparticles to supply the expected nanocomposite products. However, it was demonstrated that the

$(MAB)_{m\text{-}m}$-*b*-PPO_{32} block copolymers can react with the R_F-$(VM\text{-}SiO_2)_n$-$R_F/B(OH)_3$ nanocomposites under alkaline conditions to afford the R_F-$(VM\text{-}SiO_2)_n$-$R_F/B(OH)_3$/ $(MAB)_{m\text{-}m}$-*b*-PPO_{32} nanocomposites, providing no weight loss characteristic corresponding to the contents of the block copolymers in the composites even after calcination at 800 °C, although these expected nanocomposites were isolated without purification process. The R_F-$(VM\text{-}SiO_2)_n$-$R_F/(MAB)_{5\text{-}5}$-*b*-PPO_{32} nanocomposites, which were isolated under similar process, were also able to supply no weight loss in proportion to the content of the copolymer in the nanocomposites even after calcination at 800 °C.

3. Hydrophilic poly(vinyl alcohol) (PVA) was chemically modified by using fluoralkyl end-capped vinyltrimethoxysilane oligomer [R_F-$(VM)_n$-R_F] to lead the PVA/R_F-$(VM)_n$-R_F composite films. The PVA/R_F-$(VM)_n$-R_F composite film obtained under non-catalytic conditions was found to provide the water-soluble property; however, the acidic conditions enabled the composite film to afford no solubility toward water, giving an amphiphobic property on both the surface and reverse sides just after the deposit of oil or water droplet. R_F-$(VM)_n$-R_F oligomer was also applied to the

fabrication of the PVA/R_F-$(VM)_n$-R_F/$B(OH)_3$ composite film by using the R_F-$(VM)_n$-R_F/$B(OH)_3$ nanocomposites, which were prepared by the composite reaction of R_F-$(VM)_n$-R_F oligomer with boric acid. It was demonstrated that the PVA/R_F-$(VM)_n$-R_F/$B(OH)_3$ composite film obtained by the interaction of the corresponding nanocomposites with PVA under acidic conditions can afford the perfect water-resistance ability even after immersion of this film into water for 30 min to give the amphiphobic property on both the surface and reverse sides, although the corresponding PVA/R_F-$(VM)_n$-R_F composite film and the pristine PVA film provided the swelling behavior toward water, respectively. TGA (thermal gravimetric analyses) and DTA (differential thermal analyses) measurements showed that the PVA/R_F-$(VM)_n$-R_F/$B(OH)_3$ composite film can give a higher thermal stability than that of the PVA/R_F-$(VM)_n$-R_F composite film and the pristine PVA film.

Publications

1) Y. Aomi, M. Nishida, and H. Sawada, "Preparation and Thermal Stability of Fluoroalkyl End-Capped Vinyltrimethoxysilane Oligomeric Silica/Boric Acid Nanocomposites – Encapsulated a Variety of Low Molecular Weight Organic Compounds", *J. Polym. Sci., Part A: Polym. Chem.*, **54**, 3835 ~ 3845 (2016).

2) Y. Aomi, Y. Oishi, Y. Shibasaki, Y. Aikawa, M. Jikei, M. Nishida, S. Yamazaki, and H. Sawada, "Preparation of Fluoroalkyl End-Capped Vinyltrimethoxysilane Oligomeric Silica/Boric Acid/Poly(*N*-methyl benzamide)-*b*-poly(propylene oxide) Block Copolymer Nanocomposites – No Weight Loss Behavior of the Block Copolymer in the Nanocomposites even after Calcination at 800 °C", *J. Sol-Gel Sci. Technol.*, **85**, 318 ~ 329 (2018).

3) Y. Aomi and H. Sawada, "Preparation of Amphiphobically Modified Poly(vinyl alcohol) Film by Fluoroalkyl End-Capped Vinyltrimethoxysilane Oligomer", *J. Coat. Technol. Resl.*, https://doi.org/10.1007/s11998-018-0148-2.

(not described in this thesis)

4) J. Suzuki, Y. Takegahara, Y. Oikawa, Y. Aomi, and H. Sawada, “Preparation of Fluoroalkyl End-Capped Oligomer/Cyclodextrin Polymer Composites: Development of Fluorinated Composite Material Having a Higher Adsorption Ability toward Organic Molecules”, *J. Encap. Adsorp. Sci.*, **8**, 117 ~ 138 (2018).

Acknowledgements

The author would like to express his deepest gratitude to Prof. Hideo Sawada for his guidance and valuable discussions on this study.

He deeply thanks to Prof. Shunji Ito, Associate Prof. Jun Kawakami, Associate Prof. Fumihiko Kitagawa, and Associate Prof. Masanobu Sagisaka, for their kind advice and discussions. He would also deeply thank to Dr. Masakazu Nishida and Mrs. Tomoko Tanaka of National Institution of Advanced Industrial Science and Technology, for their kind advice and discussions. Prof. Yoshiyuki Oishi and Associate Prof. Yuji Shibasaki of Department of Chemistry and Bioengineering, Graduate School of Engineering, Iwate University, and Prof. Mitsutoshi Jikei of Department of Applied Chemistry, Graduate School of Engineering and Resource Science, Akita University, Mr. Yusei Tsushima of Hirosaki University, Mr. Hidetaka Takahashi, Mr. Hiroshi Sakama, Mr. Wataru Sakurai, Mr. Takashi Nishimura, Dr. Takafumi Erami, and Mrs. Rika Takahashi of Fujikura Composites Co., Ltd. for their kind advice and discussions, respectively.

He wishes to extend his thanks to all students of a laboratory for their cooperation and great advice.

Finally, he would like to specially thank to his parents.